

Classification of Full-waveform Airborne Laser Scanning Data and Extraction of Attributes of Vegetation for Topographic Mapping

Thesis submitted for the degree of Doctor of Philosophy
at the University of Leicester. September 2009

Cicimol Alexander

Department of Geography
University of Leicester

Classification of Full-waveform Airborne Laser Scanning Data and Extraction of Attributes of Vegetation for Topographic Mapping

Cicimol Alexander

ABSTRACT

There is an increasing demand for urban vegetation mapping, and airborne laser scanning (ALS) has the unique ability to provide geo-referenced three-dimensional data useful for mapping of surface features. This thesis examines the ability of full-waveform and discrete return ALS point data to distinguish urban surface features, and represent the three-dimensional attributes of vegetation at different scales in a vector-based GIS environment. Two full-waveform datasets, at a wavelength of 1550 nm, and a discrete return dataset, at 1064 nm, are used. Points extracted from the first full-waveform dataset are classified with k-means clustering and decision tree into vegetation, buildings and roads, based on the attributes of individual points and the relationships between neighbouring points. A decision tree is shown to perform significantly better (74.62%) than k-means clustering (51.59%) based on the overall accuracies. Grass and paved areas could be distinguished better using intensity from discrete return data than amplitude from full-waveform data, both values proportional to the strength of the return signal. The differences in the signatures of surfaces could be related to the wavelengths of the lasers, and need to be explored further. Calibration of intensity is currently possible only with full-waveform data. When the decision tree is applied on the second full-waveform dataset, the backscatter coefficient proves to be a more useful attribute than amplitude, pointing to the need for calibration if a classification method using intensity is to be applied on datasets with different scanning geometries. A vector-based approach for delineating tree crowns is developed and implemented at three scales. The first scale provides a good estimation of the tree crown area and structure, suitable for estimating biomass and canopy gaps. The third scale identifies the number of trees and their locations and can be used for modelling individual trees.

Acknowledgements

I am indebted to those who made it possible for me to work on and complete this thesis.

I am grateful to:

Ordnance Survey, for providing valuable data – Ordnance Survey (OS) products and the LiDAR datasets – and for partial funding;

The University of Leicester, for the Open PhD scholarship;

Dr. Kevin Tansey, for supervision, support and comments on the earlier drafts of this thesis;

Dr. Jörg Kaduk, for introducing me to Matlab, for supervision, and for the many useful discussions;

Dr. David Holland (OS), for encouragement and helpful comments;

Dr. Nicholas Tate, for supervision in the initial stages;

Dr. Sarah Smith-Voysey (OS), for her support and role in initiating the project;

Mr. Hubert Lehner (Vienna University of Technology), for helpful discussions;

Dr. Ross Hill (Bournemouth University) and Prof. Heiko Balzter, for comments and suggestions for improving this thesis;

3D Laser Mapping (UK), for acquisition of data;

RIEGL GmbH (Austria), for the provision of software for processing the data;

Arun, for constant support, and suggestions for improving the format of this thesis;

Isabel, Keith, Dénes and Michael, for fun, friendship and interesting conversations;

Keith, also for proofreading this thesis, and Michael and Cutberto for particular chapters;

My friends in the Department of Geography, for support and encouragement;

Auroville, for memories of a better world; and

My family, for their unconditional support and prayers.

CONTENTS

ABSTRACT	II
ACKNOWLEDGEMENTS	III
CONTENTS	IV
1. INTRODUCTION	1
1.1. INTRODUCTION	2
1.1.1. Discrete Return and Full-waveform ALS.....	3
1.1.2. Classification using ALS Data	4
1.1.3. Mapping of Urban Vegetation	4
1.2. RATIONALE	5
1.3. AIM AND OBJECTIVES	6
1.4. THESIS OUTLINE	7
1.5. SUMMARY.....	7
2. AIRBORNE LASER SCANNING	9
2.1. INTRODUCTION	10
2.2. LASER SCANNING SYSTEMS	10
2.2.1. System Components.....	10
2.2.2. The Measurement Principle	12
2.2.3. Laser Beam Footprint	12
2.2.4. Full-waveform Laser Scanning Systems.....	14
2.3. THE RETURN SIGNAL	14
2.3.1. Amplitude and Intensity	16
2.3.2. Backscatter Cross Section.....	18
2.3.3. Gaussian Decomposition	21
2.4. APPROACHES TO CLASSIFICATION.....	23
2.4.1. From Points to Surfaces.....	23
2.4.2. Classification of ALS Data	24
2.4.3. Accuracy Assessment	26
2.5. LASER SCANNING FOR VEGETATION APPLICATIONS	28
2.5.1. Classification of Vegetation	29
2.5.2. Height Metrics and Profiles	30
2.5.3. Delineation of Trees	31
2.6. SUMMARY.....	32
3. DATASETS AND METHODOLOGY	34
3.1. INTRODUCTION	35
3.2. STUDY AREAS AND DATASETS.....	35
3.2.1. Study Areas.....	35
3.2.2. Full-waveform ALS Datasets	36
3.2.3. Discrete ALS Dataset.....	47
3.2.4. Data Exchange Format for ALS Datasets	49
3.2.5. Other Datasets.....	49
3.3. BROAD METHODOLOGY	50
3.4. SUMMARY.....	51
4. CLASSIFICATION OF AIRBORNE LASER SCANNING POINTS	52

4.1. INTRODUCTION	53
4.2. METHODOLOGY	54
4.2.1. Pre-processing	54
4.2.2. Exploratory Data Analysis	55
4.2.3. Deriving Additional Attributes of Points from Elevation	60
4.2.4. Creation and Analysis of Training Data	64
4.2.5. Classification of Points by Clustering	65
4.2.6. Classification of Points using a Decision Tree	67
4.2.7. Assessment of Classification Accuracy	68
4.3. RESULTS	71
4.4. DISCUSSION	75
4.4.1. Analysis of the Attributes	79
4.4.2. Classification by Clustering	82
4.4.3. Classification using Decision Tree	84
4.5. SUMMARY	87
5. COMPARISON BETWEEN FULL-WAVEFORM AND DISCRETE RETURN DATA	88
5.1. INTRODUCTION	89
5.2. METHODOLOGY	89
5.2.1. Classification of Bristol_Optech Data	89
5.2.2. Influence of Point Density on the Attributes	90
5.3. RESULTS	91
5.3.1. Comparison of the accuracies of classification using Bristol_Riegl and Bristol_Optech Data	91
5.3.2. Influence of Point Density on the Attributes	93
5.4. DISCUSSION	94
5.4.1. Comparison of Thinned Bristol_Optech and Bristol_Riegl Data	95
5.4.2. Decision tree from the Bristol_Optech Data	97
5.4.3. Pruning level of a decision tree	98
5.4.4. Influence of Point Density on the Attributes	98
5.5. SUMMARY	101
6. BACKSCATTER COEFFICIENT AS AN ATTRIBUTE IN THE DECISION TREE CLASSIFIER	103
6.1. INTRODUCTION	104
6.2. METHODOLOGY	105
6.2.1. Calculation of the Calibration Constant	105
6.2.2. Derivation of Attribute Values Based on Backscatter Cross section	106
6.2.3. Generation of Additional Decision Trees for Classification	108
6.2.4. Pre-processing of the ALS Data from Bournemouth	108
6.2.5. Classification of Points using Decision Trees	108
6.2.6. Assessment of Accuracies	109
6.3. RESULTS	112
6.4. DISCUSSION	116
6.4.1. Comparison of the Calibration Constants	116
6.4.2. Accuracies of Classification	118
6.4.3. Analysis of the Attributes	126
6.5. SUMMARY	129
7. ATTRIBUTES OF VEGETATION FOR A DIGITAL TOPOGRAPHIC DATABASE	130
7.1. INTRODUCTION	131

7.2. METHODOLOGY	131
7.2.1. Delineation of Tree Crowns	132
7.2.2. Aggregation at the landscape scale	134
7.2.3. Aggregation at the Land Parcel Scale	135
7.2.4. Aggregation at the Single Tree Scale	136
7.2.5. Applications of the Additional Attributes	137
7.3. RESULTS.....	138
7.3.1. Delineation of Tree Crowns	138
7.3.2. Aggregation at Different Scales	142
7.3.3. Representation of Vegetation in Topographic Maps	142
7.4. DISCUSSION.....	147
7.5. SUMMARY.....	159
8. CONCLUSION.....	160
8.1. INTRODUCTION	161
8.2. CONTRIBUTIONS OF THIS RESEARCH.....	162
8.3. FUTURE WORK.....	163
APPENDIX 1	165
APPENDIX 2	166
APPENDIX 3	167
REFERENCES.....	172

List of Tables

Table 1: Technical specifications for full-waveform lidar systems (Mallet and Bretar, 2009).....	15
Table 2: Summary of studies on land cover classification using ALS data	27
Table 3: The attributes of points extracted from the waveform by RiAnalyze.....	40
Table 4: The standard deviation of each echo derived from the echo width	41
Table 5: The locations of the echoes derived from the distances between the points.....	41
Table 6: Comparison of the three datasets used for the study – Full-waveform datasets from Bristol and Bournemouth, and discrete return dataset from Bristol.....	47
Table 7: Matrix showing correlation coefficients of the eight attributes used for classification	66
Table 8: Kappa coefficient, overall accuracy, average producer’s and user’s accuracies of the classifications using k-means clustering and decision tree. k-means 1: k-means clustering; k-means 2: k-means clustering using the means of the attributes of the classes from the training data; k-means 3: k-means clustering using Principal Components; k-means 4: k-means clustering using Canonical Components.....	75
Table 9: Coefficients of principal components of the variables and the variance attributed to each principal component.....	81
Table 10: Coefficients of canonical components of the variables and the variance attributed to each canonical component	81
Table 11: Error Matrix for k-means clustering of the attributes of full-waveform data.....	82
Table 12: Error Matrix for k-means clustering, with the mean of the attribute values for the various classes in the training dataset as the seed points	83
Table 13: Error Matrix for k-means clustering using Principal Components	83
Table 14: Error Matrix for k-means clustering using Canonical Components	84
Table 15: Error matrix for classification using the pruned decision tree on the full-waveform data.....	84
Table 16: Kappa coefficient, overall accuracy, average producer’s and user’s accuracies of the classifications using the decision trees generated from Bristol_Optech and Bristol_Riegl data.....	91
Table 17: Comparison of classifications from Bristol_Riegl and Bristol_Optech data. The underlined numbers highlight the major misclassifications, above 10% of the total, in each column.....	91
Table 18: Error matrix for classification using the pruned decision tree on the Bristol_Optech data	93
Table 19: Number of points from road polygons correctly classified in ALS data, separated into roads and other paved surfaces	93
Table 20: Number of points in the training data for Bristol_Riegl and Bristol_Optech data.....	95
Table 21: Kappa coefficients, overall accuracies, average user’s accuracies and average producer’s accuracies of the classifications for the six decision trees using amplitude, σ , γ_{ci} , γ_{cs} , γ_{ei} and γ_{es} as attributes	112
Table 22: (Column 1) The six decision trees are based on amplitude, backscatter cross section (Chilton et al.) and the four backscatter coefficients (γ_{ci} , γ_{cs} , γ_{ei} and γ_{es}); (Column 2) The number of nodes in	

the unpruned decision tree generated using the six attributes; (Column 3) The initial pruning level; (Column 4) The number of nodes resulting from pruning level 1; (Column 5) The pruning level selected to have no more than 31 nodes, the number of nodes in the pruned decision tree using amplitude as an attribute in pruning level 1; (Column 6) The final number of nodes using pruning level 2. 118

Table 23: Error matrix showing points in each class in the reference data and from the decision tree classifications using amplitude, backscatter cross section (Chilton et al.) and backscatter coefficients (γ_{ci} , γ_{cs} , γ_{ei} and γ_{es}). 120

Table 24: User’s and producer’s accuracies of classifications for the six decision trees – using amplitude, backscatter cross section (Chilton et al.) and backscatter coefficients (γ_{ci} , γ_{cs} , γ_{ei} and γ_{es}). 122

Table 25: Kappa coefficients of the agreements between the classifications from the six decision trees using amplitude, σ , γ_{ci} , γ_{cs} , γ_{ei} and γ_{es} as attributes 122

Table 26: Comparison of classifications using decision trees with amplitude and γ_{ci} as attributes 123

Table 27: Attributes for classifying each leaf node in the decision tree using γ_{ci} as an attribute, and the percentage of correctly classified points in each class in the training data 124

Table 28: The deviations of location, height and crown base height of trees from the reference data. The tree with ID 7 is difficult to locate, ID 10 looks like part of a building, ID 13 is a lamppost and the tree with ID 17 is not clear enough to estimate the values. 146

Table 29: Attributes of the six trees shown in Figure 70 152

List of Figures

Figure 1: A typical airborne laser scanning system. The laser beams sent downwards by the transmitter is deflected, by the scanner across the swath width, to cover large areas required for surveying (Adapted from Hyyppä et al. (2000) and Wehr and Lohr (1999)) 13

Figure 2: The measurement principle of laser ranging 13

Figure 3: Conceptual differences between full-waveform and discrete return ALS systems (Adapted from Ullrich (2006)) 17

Figure 4: Intensity of the return signal from multiple echoes (Adapted from Rohrbach (2007)). The distribution of laser energy is not uniform within the footprint of the laser beam. 17

Figure 5: (A) Point data displayed by elevation. (B) Point data can be interpolated to a grid with regular (square) tessellations, at different resolutions, (B) 1 m and (C) 0.5 m resolutions are shown here. (D) A Triangulated Irregular Network (TIN) with irregular tessellations can be created from the points. (E) Thiessen polygons are complementary to a TIN; both of them retain the original values at the point locations, and (F) Figure showing the relation between TIN and Thiessen polygons..... 24

Figure 6: Location of Bristol and Bournemouth in the United Kingdom (Ordnance Survey © Crown Copyright. All Rights Reserved)..... 36

Figure 7: (A) An aerial image of the study area in Bristol. The subset of the study area is used for detailed analysis; (B) OS 1:10,000 scale raster of the subset (Ordnance Survey © Crown Copyright. All Rights Reserved) 37

Figure 8: (A) An aerial image and (B) OS 1:10,000 scale raster of the study area in Bournemouth (Ordnance Survey © Crown Copyright. All Rights Reserved) 38

Figure 9: RiAnalyze and RiWorld convert the laser scanner raw data, the flight data and the calibration data into data in WGS84 (RIEGL, 2007) 40

Figure 10: The echoes representing the (A) first, (B) second, (C) third and (D) fourth echoes of a return waveform, (E) the individual echoes shown separately and (F) the waveform obtained when they are added together. (G) The sampled raw waveform is very similar to the reconstructed waveform in (F). (Note: The red lines in the figures connect the data points for better clarity.)..... 43

Figure 11: Examples of the raw waveforms (left) and the waveforms reconstructed from the attributes of the return echoes (right). A fifth echo of the lowest intensity seems to be ignored in the examples. (Note: There are slight offsets between the locations of the echoes in the reconstructed and raw waveforms, due to the value given for the position of the first echo in the reconstructed waveform.) .. 45

Figure 12: Examples of the raw waveforms (left) and the waveforms reconstructed from the attributes of the return echoes (right). The majority of the waveforms, reconstructed from the points, seem to be good approximations of the sampled raw waveforms. (Note: There are slight offsets between the locations of the echoes in the reconstructed and raw waveforms, due to the value given for the position of the first echo in the reconstructed waveform.) 46

Figure 13: (A) Point data from four flight lines were used for the study in Bristol. The scan angles ranged from 67.5° to 112.5°. (B) In Bournemouth, point data from seven flight lines were used for the study. The scan angles ranged from 60° to 120°	48
Figure 14: Workflow for achieving the objectives of the thesis	51
Figure 15: (A) Amplitude and width of the first echo from a return with two echoes. (B) Multiple echoes from a single pulse emitted at an angle of 13° from vertical represented as separate points on the horizontal plane, having x, y and z coordinates.....	55
Figure 16: Samples of raw waveforms from trees, buildings, grass and roads	56
Figure 17: ALS Points displayed by (A) elevation in metres, (B) amplitude, (C) echo width in nanoseconds and (D) number of echoes for a subset of the study area (Ordnance Survey © Crown Copyright. All Rights Reserved)	58
Figure 18: (A) Amplitude, (B) echo width and (C) echo number of the points within the rectangle marked in (D) (Ordnance Survey © Crown Copyright. All Rights Reserved).....	59
Figure 19: The Triangulated Irregular Network (TIN) created from the ALS points displayed by (A) elevation, (B) slope and (C) aspect	62
Figure 20: TIN triangles connected to the point with ID 100. The elevations of each point connected to it by the TIN triangles, the slopes and aspects of the attached TIN triangles and the derived attributes of the point are shown in the tables.....	62
Figure 21: An aerial image of the area (A); ALS points from Flightline 1 (B) and Flightline 2 (C); Slope of TIN from the points from both the flightlines (D); Slope of TIN from the points in Flightline 1 (E) and Flightline 2 (F); Aspect of TIN from the points from both the flightlines (G); Aspect of TIN from the points in Flightline 1 (H) and Flightline 2 (I).	63
Figure 22: Workflow for the derivation of additional attributes for the full-waveform ALS data to be used in the classification process as shown in Figure 25.	64
Figure 23: Polygons used for selecting the points within them to be used as the training data in Bristol	69
Figure 24: Polygons used for selecting the points within them to be used as the reference data in Bristol	69
Figure 25: Workflow for the classification of full-waveform ALS data, and comparison of the k-means clustering and decision tree methods	70
Figure 26: Box-and-whisker plots of the attributes grouped by land cover classes	71
Figure 27: Derived attributes of the ALS points (A) Average Slope, mean of the slopes of attached TIN triangles; (B) Standard Deviation of slopes of attached TIN triangles; (C) Standard Deviation of aspects of attached TIN triangles; (D) Height Variation, range of the elevations of points attached to each ALS point and (E) Normalised Elevation, elevation of each point from the estimated DTM.....	74
Figure 28A: ALS points classified into flat roofs, pitched roofs, grass, shrubs, trees and road using k-means clustering for (A) option 1; (B) option 2, using the means of the attributes of the classes from the training data; (C) option 3, using Principal Components; and (D) option 4, using Canonical Components.	

Figure 28B: The pruned decision tree used for classifying the ALS point cloud data. The boxes below the leaf nodes indicate the percentage of correctly classified points of a particular land cover class.	78
Figure 29: ALS points classified into flat roofs, pitched roofs, grass, shrubs, trees and road using the Decision Tree classifier.	78
Figure 30: Amplitude values plotted against (A) echo width; (B) normalised elevation; (C) average slope; (D) standard deviation of slope; (E) standard deviation of aspect and (F) height variation grouped by class.....	80
Figure 31: (A) The roof edges and features such as chimneys on the roof classified as trees; the roof edges and the edges of height variations within the with flat roofs classified as either pitched roofs or trees; a few smaller structures not detected and classified as shrubs; medians on roads, marked in white classified as grass; some points on trees, possibly with dense foliage, classified as building roofs; (B) An aerial image of the area is shown for comparison (Ordnance Survey © Crown Copyright. All Rights Reserved)	86
Figure 32: The pruned decision tree used for classification. The percentages of points classified at each leaf node are also shown.	92
Figure 33: Box-and-whisker plots of the six attributes grouped by categories for the Bristol_Optech dataset. The median values for the processed Bristol_Riegl data and the thinned Bristol_Optech data are also shown.	94
Figure 34: (A) Points classified as grass in Bristol_Riegl data and road in Bristol_Optech data; (B) MasterMap polygons showing the ‘man-made’ features in grey; and (C) features seen to be correctly identified as paved areas in the Bristol_Optech data marked in the aerial image (Ordnance Survey © Crown Copyright. All Rights Reserved)	96
Figure 35: Comparison of the intensities and amplitudes of the Bristol_Optech and Bristol_Riegl data for points from grass, road and other paved surfaces	97
Figure 36: The decision tree using the Bristol_Optech data pruned to have similar number of nodes as that of the Bristol_Riegl data. The nodes pruned at each pruning level are also shown.	100
Figure 37: The decision tree for the un-thinned Bristol_Optech data pruned to 31 nodes for a better comparison with the earlier decision trees	101
Figure 38: Workflow for the classification of full-waveform ALS data using additional attributes derived from intensity in decision tree classifiers	110
Figure 39: The workflow for thinning the data; (A) A subset of the original un-thinned ALS point cloud; (B) Grid points at 1 m spacing; (C) First echo points closest to the grid points; (D) The thinned dataset obtained by including the second, third, fourth and fifth echo points if the selected points in (C) are the first from multiple echoes	110
Figure 40: Polygons used for selecting the points within them to be used as the reference data in Bournemouth.....	113

Figure 41: Points classified using the decision tree with amplitude as an attribute, converted to polygons by merging Thiessen polygons based on class. The section line through the misclassified road is shown in black.....	113
Figure 42: Section through the misclassified road (A). The section line is shown in Figure 41.	114
Figure 43: Nodes of the decision tree dependent on amplitude values for classification (within the rectangles)	114
Figure 44: Decision tree with γ_{ci} as an attribute.	115
Figure 45: Points classified using the decision tree with the backscatter coefficient (γ_{ci}) as an attribute, converted to polygons by merging Thiessen polygons based on class.....	115
Figure 46: (A) Mean of the calibration constants for the nine road sections and (B) the frequencies for all the points in Bristol.....	117
Figure 47: (A) Mean of the calibration constants for the ten road sections and (B) the frequencies for all the points in Bournemouth	117
Figure 48: (A) Points classified as pitched roofs using amplitude, and trees using γ_{ci} . Polygons classified as buildings in MasterMap are shown for comparison; (B) Points classified as grass using amplitude, and road using γ_{ci} . Polygons classified as road or track, roadside or path in MasterMap are also shown for comparison.	125
Figure 49: (A) The three sections of road were incorrectly classified as shrubs due to their estimated elevations from the ground; (B) Water having low reflectance in the infrared wavelength, an inland water body was incorrectly classified as road. These classifications are from the decision tree using γ_{ci} as an attribute.	125
Figure 50: Frequency distribution of the amplitudes of echoes from grass, road, trees and pitched roofs in Bristol_Riegl and Bournemouth_Riegl.....	126
Figure 51: Frequency distribution of the amplitudes, backscatter cross sections and backscatter coefficients of echoes from grass and road in Bristol_Riegl and Bournemouth_Riegl. The values of the attributes used for separating grass and road in the decision tree classifiers are also shown.	127
Figure 52: Frequency distribution of the amplitudes and backscatter cross sections of echoes from pitched roofs and trees in Bristol_Riegl and Bournemouth_Riegl.....	128
Figure 53: Frequency distribution of the backscatter coefficients of echoes from pitched roofs and trees in Bristol_Riegl and Bournemouth_Riegl.....	128
Figure 54: Backscatter coefficients of pitched roofs and trees in Bournemouth. The single and multiple echoes from trees are shown separately. The values of the attributes used for separating trees and pitched roofs in the decision tree classifiers are also shown.	129
Figure 55: (A) Aerial image of a tree; (B) ALS point cloud; (C) Triangulated Irregular Network (TIN) generated from the points by Delaunay triangulation; (D) TIN displayed by elevation showing the estimated treetops at scale 1; (E) Seed point at scale 1 higher than one tier of points joined by TIN edges; (F) Seed point at scale 2 higher than two tiers of points; (G) Seed point at scale 3 higher than	

three tiers of points; (H) Points belonging to the tree at scale 3; (I) Voronoi diagram or Thiessen polygons generated from the points belonging to the tree dissolved to form the tree polygon.....	133
Figure 56: 95 th percentile of elevation gives a more representative canopy height than maximum elevation by avoiding the outliers	135
Figure 57: (A) An aerial photograph of a subset of the study area with the seed points, or estimated treetops displayed at (B) scale 1 (C), scale 2 and (D) scale 3	139
Figure 58: (A) An aerial photograph of a subset of the study area in Bournemouth with the seed points, or estimated treetops displayed at (B) scale 1 (C), scale 2 and (D) scale 3.....	141
Figure 59: Attributes of ALS points aggregated at the landscape scale.....	143
Figure 60: Attributes of ALS points aggregated at the land parcel scale	143
Figure 61: Attributes of ALS points aggregated at the single tree scale	144
Figure 62: Single trees represented in MasterMap	144
Figure 63: A three-dimensional view of the study area with trees represented as points	145
Figure 64: (A) Natural permeable surface from MasterMap and (B) from the classification	145
Figure 65: Estimated heights of trees plotted against the reference heights from Street Mapper.	147
Figure 66: Thiessen polygons generated from the tree crown points at scales (B) 1, (C) 2 and (D) 3 (A) overlaid on the aerial photograph	150
Figure 67: All the tree segments at (B) scale 1 are not detected at scales (C) 2 and (D) 3; (A) The aerial photograph is shown for reference.	150
Figure 68: Compact tree crowns are not over-segmented at (B) scale 1 and they are also detected at the scales (C) 2 and (D) 3; (A) The aerial photograph is shown for reference.	150
Figure 69: Classified polygons (A) before and (B) after the reclassification	150
Figure 70: Examples of isolated single trees (A-F) in the study area showing the first echoes (Congalton and Green), second echoes (orange) and third echoes (black). The histograms of elevations are also shown for each tree.....	153
Figure 71: (A) Aerial image of a subset of the study area in Bournemouth containing the tree with ID 18; (B) the Thiessen polygons classified as tree crowns at the first scale, (C) second scale and (D) third scale; (E) points from the full-waveform data displayed in the x-z axis as viewed from the South and (F) in the y-z axis as viewed from the East (G) the reference data from StreetMapper displayed in the x-z axis and (H) in the y-z axis.....	155
Figure 72: (A) Aerial image of a subset of the study area in Bournemouth containing the tree with ID 6; (B) the Thiessen polygons classified as tree crowns at the first scale, (C) second scale and (D) third scale; (E) points from the full-waveform data displayed in the x-z axis as viewed from the South and (F) in the y-z axis as viewed from the East (G) the reference data from StreetMapper displayed in the x-z axis and (H) in the y-z axis.....	157
Figure 73: StreetMapper data for isolated single trees displayed in the x-z and y-z axes. Views from the South and East of trees with (A) ID 1, (B) ID 8, (C) ID 16 and (D) ID 19.....	159

Abbreviations

ALS	Airborne Laser Scanning
LiDAR	Light Detection and Ranging
DTM	Digital Terrain Model
DEM	Digital Elevation Model
TIN	Triangulated Irregular Network
LASER	Light Amplification by Stimulated Emission of Radiation
RADAR	Radio Detection and Ranging
GPS	Global Positioning System
dGPS	differential Global Positioning System
IMU	Inertial Measurement Unit
POS	Position and Orientation System
COG	Centre Of Gravity
GPE	Gaussian Pulse Estimation
GPF	Gaussian Pulse Fitting

1. Introduction

Full-waveform airborne laser scanning data can provide more information about the objects in the path of the laser beam than discrete return data. This thesis aims to develop a method to classify laser scanning data in urban environments, and extract attributes of vegetation for topographic mapping.

1.1. Introduction

The measurement of distances using lasers is fast becoming a standard tool in the fields of remote sensing, surveying and mapping. This technique, used in airborne laser scanning (ALS), is known as Light Detection and Ranging, or LiDAR (hereafter referred to as lidar). The distance between an airborne, spaceborne or terrestrial sensor and a target surface is calculated from the travel time of laser pulses to the surface and back (Lillesand et al., 2004; Wagner et al., 2004). Laser scanning can provide dense, accurate and fast digital models of the topography, and vertical structures of target surfaces at much lower field-operation costs point-for-point, and reduced post-processing time and effort compared to traditional survey methods (Flood, 2001).

ALS data have been used for creating digital terrain models (DTMs) by many countries, including the Netherlands and Switzerland, on a national level, and many states in Germany and the USA. The recent developments in the use of ALS data in forest inventory, building detection and 3D modelling of urban areas have made it possible to plan nation-wide surveys for use in multiple applications. Such data have also been utilised for creating and updating topographic maps (Hyypä et al., 2007).

ALS was initially considered to be highly suitable for the generation of DTMs, as laser beams can penetrate vegetation to collect information from below the canopy (Flood, 2001). The generation of DTMs in woodlands and under vegetation was one of the first applications of ALS, which has a distinct advantage over photogrammetry in this area, as shadows and difficulty in seeing the ground make it difficult to generate a DTM from aerial photographs in areas with dense vegetation cover. ALS is also comparable to photogrammetry in many aspects, since both methods generate terrain models by digitally processing image data, can produce highly accurate DTMs and can cover large areas.

The ALS system is considered 'blind' in that it cannot be directed to a certain point in contrast to photogrammetry, which can. However, laser scanning is an active system and hence can be used even at night and the scanning pattern is determined by the system design. In the case of buildings, although the laser system can generate high density of points, it cannot directly capture break-lines or roof ridges, which could be provided by photogrammetry. In the case of vegetation, laser scanning has a distinct advantage in that the echoes may be from the top, within or below the vegetation cover, whereas photogrammetric points would lie on the canopy. ALS provides geo-referenced elevation data giving it a clear advantage over

photogrammetry in this respect. It is also not affected by shadows or illumination conditions (Ackermann, 1999; Baltsavias, 1999b).

Many algorithms have been developed to extract the terrain points from ALS and create a terrain model in the form of a Triangular Irregular Network (TIN) or interpolated to a grid (Axelsson, 1999; Elmqvist, 2001; Tovari and Vogtle, 2004). The concepts of TIN and grid are explained in section 2.4.1. More recently, it was also found to be useful for other applications such as 3D modelling of buildings, forestry and for land cover mapping (Alharthy and Bethel, 2002; Brennan and Webster, 2006; Hyypä et al., 2004; Vosselman and Dijkman, 2001). ALS data are often integrated with other remote sensing data to distinguish between vegetation and other surfaces (Charaniya et al., 2004; Chust et al., 2008; Haala and Brenner, 1999; Straub, 2003).

1.1.1. Discrete Return and Full-waveform ALS

There are two distinct techniques used in ALS systems based on how the return signal is recorded. The more commonly used discrete return ALS systems record single (first or last), or multiple (first and last, or sometimes up to five) echoes for every transmitted pulse. The other emerging technique is waveform-digitising ALS which samples and records the full return waveform to capture a complete elevation profile within the target footprint, or the area illuminated by the laser beam (Flood, 2001). The objects that scatter back the emitted beam are often referred to as targets or scatterers.

ALS data provide the three-dimensional location of data points and in many cases, the intensity of the return pulse. However, the analysis of discrete return ALS data has been based mainly on the spatial relationship of the points. The full-waveform ALS data provide additional information about the objects in the path of the laser pulse in comparison to discrete return data, such as width of the echo from a target surface (Wagner et al., 2006). They also give more control to the user over the processing and extraction of points. This could lead to the development of improved classification methods based on the information from each point as well as their spatial relationships. Gaussian decomposition methods (Hofton et al., 2000; Wagner et al., 2006) give estimates of the location and scattering properties of the targets in full-waveform data. The attributes extracted from the waveform include echo width, echo amplitude, range and scan angle, which can be used to calibrate the intensity data (Wagner et al., 2008a). Some of these attributes have been used for distinguishing vegetation and non-vegetation points from full-waveform data. The classification of vegetation points from ALS

point clouds is considered to be a challenge, especially in the case of low vegetation (Ducic et al., 2006; Wagner et al., 2008a).

1.1.2. Classification using ALS Data

The main methods used by the classification studies using ALS data are parametric classification (Charaniya et al., 2004), k-means clustering (Miliaresis and Kokkas, 2007), object-oriented methods (Brennan and Webster, 2006), decision trees (Ducic et al., 2006; Hyypä et al., 2007; Matikainen et al., 2007; Rutzinger et al., 2008) and support vector machines (Koetz et al., 2008; Mallet et al., 2008). The studies on classification using ALS data alone can also be divided into those using discrete return (Brennan and Webster, 2006; Miliaresis and Kokkas, 2007) and full-waveform data (Ducic et al., 2006; Mallet et al., 2008; Rutzinger et al., 2008). In many classification approaches, points were first converted to grids before classification. Additional attributes of the surface derived from ALS data such as roughness and mean slope have also been used for classification.

Much of the past research in the applications of laser scanning has concentrated on the information about elevation, which was initially considered the single most important attribute obtained from laser scanning data. Intensity from ALS data can be considered to be an image in a very narrow wavelength band (Axelsson, 1999). Ackermann (1999) pointed out that the results could be dramatic if intensity image data could directly be combined with spatial position data. There are problems with using intensity without calibration, as it is dependent on various factors including spherical loss and topographic and atmospheric effects. This is especially true for large ALS datasets containing strong elevation differences (Höfle, 2007). Although some recent studies have looked into using intensity as an attribute for classification of land cover, research is still going on to understand the waveform response for different targets (Mallet and Bretar, 2009; Wagner et al., 2006).

1.1.3. Mapping of Urban Vegetation

Urban areas pose a challenge in land cover mapping due to the difficulty in segmenting and classifying the variety of objects present in the landscape (Rutzinger et al., 2008). Urban vegetation is a critical component in understanding the complex relationship between land surface characteristics and other properties of urban systems. The spatial distribution and abundance of urban vegetation influence air and water quality, temperature, humidity and wind flow, whereas impervious surfaces cause urban heat island effects. There is therefore an

increasing demand for urban vegetation mapping and classification techniques (Aubrecht et al., 2009; Hecht et al., 2008; Tooke et al., 2008).

Remotely sensed images have been widely used for the identification of vegetation (Liang, 2004). The focus has been on classifying and mapping the extent of vegetation from multi-spectral satellite and airborne imagery for two-dimensional land cover mapping. Conventional sensors however have limitations in fully representing the three-dimensional structure of vegetation. These images are two-dimensional representations of the recorded radiation, where each grid cell of the image represents an area on the ground. In vegetated terrain, even with high-resolution images, each grid cell of the image would be made up of different vegetation elements such as leaves and branches at different heights above the ground. The recorded image thus depends strongly on the geometric arrangement of these elements, in addition to the illumination conditions. This makes it difficult to classify vegetation since the geometric composition of elements can vary strongly even within one vegetation class (Wagner et al., 2008b).

Multi-spectral images provide useful information about vegetation. They have been used for identifying the species and assessing the health of vegetation, and estimating the shape and size of tree crowns. The significant advantage of ALS over imagery is its ability to provide information about elevation in addition to estimating the shape and size of crowns. However, studies indicate that tree growth differs in isolation and in woodlands due to the competition for space, and multi-spectral imagery may be better at outlining crowns and extracting specific information in woodlands (Leckie et al., 2003).

Active remote sensing techniques such as radar (radio detection and ranging) are able to resolve the vertical structure of vegetation. Spaceborne Synthetic Aperture Radar (Cunningham et al.) systems can be used for three-dimensional (3DLM) mapping of large areas, making use of two SAR images and the technique of interferometry. Although it depends on the resolutions, achievable accuracies are higher with lidar than with radar. SAR models provide a more generalised, less detailed characterisation. The top height estimates of forest stands from lidar data are found to be more accurate than from SAR data (Andersen et al., 2003; Balzter et al., 2007; Wagner et al., 2008a).

1.2. Rationale

The importance of classifying the urban landscape has already been noted. Classification routines could be made more effective by integrating object information from intensity data

with the elevation data (Flood, 2001; Lim et al., 2003). The studies using full-waveform data for classification have given importance to vegetation due to the advantages full-waveform data have over discrete return data in describing the properties of vegetation. However, roads and buildings are also an integral part of the urban landscape, and the attributes of full-waveform ALS data could be used along with the spatial relationships of points for classifying vegetation, road and buildings in an urban environment.

The full-waveform ALS data contain more information than discrete return data, such as echo width, which could be used for classification. However, in spite of the advantages, the costs of full-waveform ALS are considerably higher than discrete return ALS data, both in financial and data processing terms (Bretar et al., 2008). The classifications using full-waveform and discrete return data for the same study area therefore need to be compared to estimate the advantages of full-waveform data, if any, over discrete return data for land cover classification.

Much of the research on vegetation using ALS has been in forestry, and can be divided into stand-based and individual tree-based studies. Stand-based studies have focussed on extracting characteristics such as canopy height, canopy openness and tree-species composition and derived information such as average stem diameter, forest biomass, leaf area index and canopy volume (Harding et al., 2001; Hollaus et al., 2006). Individual tree-based studies mainly look at location, crown delineation, height and species identification (Holmgren and Persson, 2004; St-Onge, 1999; Suárez et al., 2004). These studies were based on ALS data alone, or ALS data integrated with other imagery (Bork and Su, 2007; Hill et al., 2002; Hill and Thomson, 2005; Hyde et al., 2005). Mapping of urban vegetation is required for sustainable management of urban areas (Van de Voorde et al., 2008), and can be useful for realistic 3D reconstruction of city models (Vosselman, 2003). However, there are few studies on representing the information about vegetation, which can be extracted from ALS data, in topographic maps.

1.3. Aim and Objectives

The aim of this study is to classify full-waveform ALS data and extract attributes of vegetation for topographic mapping.

The main objectives are:

- to explore different techniques for the classification of features in an urban environment using full-waveform ALS data;

- to determine whether the additional attributes from full-waveform data give a significant advantage over discrete return data with reference to the classification of urban features;
- to determine whether the method is transferable by applying it on full-waveform ALS data with a different scanning geometry, using calibrated intensity as an attribute; and
- to identify the three-dimensional attributes of vegetation, for topographic mapping, using a vector-based approach for delineating tree crowns.

1.4. Thesis Outline

Chapter 2 provides a review of relevant literature, including an overview of the full-waveform ALS technique. Chapter 3 gives a description of the study area, datasets and the broad methodology. Full-waveform ALS datasets were collected from Bristol and Bournemouth. The dataset from Bristol is used to develop a method to classify the ALS points into six categories – vegetation with trees, shrubs and grass as subclasses, road, and flat and pitched roofs. This classification method is then applied to the dataset from Bournemouth. A discrete return dataset is also available for the study area in Bristol. The four objectives are addressed in chapters 4, 5, 6 and 7, including the detailed methodology, results and discussion for each objective. Chapter 4 describes the development of the classification method using the full-waveform dataset from Bristol. Chapter 5 compares the accuracies of the classifications from the full-waveform and discrete return datasets from Bristol. Chapter 6 describes the application of the classifier on the full-waveform dataset from Bournemouth. The classifier is also refined to make it useful for classifying full-waveform datasets from different areas and flight conditions. Chapter 7 examines the attributes of vegetation that could be extracted from ALS data, and could potentially be used in digital topographic maps. The conclusions from the study and scope for future work are discussed in Chapter 8.

1.5. Summary

ALS data are increasingly being used in land cover classification. They provide information about the elevation of surfaces, which provides a significant advantage over many other remote sensing data. Digitisation of the full return waveform is a recent development in ALS. Full-waveform ALS data give more information about the objects in the path of the laser beam, albeit at an increased cost. It is therefore important to compare full-waveform and the more

traditional discrete return ALS data. The intensity of the return signal, available in both discrete return and full-waveform data, is an attribute that has been less explored than the elevation attribute. In this study, the full-waveform and discrete return ALS data are compared with reference to the classification of urban land cover, incorporating the intensity attribute in the classification methods. There is an increasing demand for urban vegetation mapping, and ALS data are considered highly useful for extracting the three-dimensional attributes of vegetation. Therefore, the study also looks at the representation of vegetation within a digital topographic map. This chapter provided an introduction to the thesis and rationale of the study. It also provided an outline of the thesis. The next chapter reviews the relevant literature related to the topic.

2. Airborne Laser Scanning

This chapter provides a review of relevant literature, and is divided into four sections. The first section gives an introduction to laser scanning systems. The second section describes the characteristics of the return signal. The third section describes the approaches to classification and accuracy assessment, with reference to ALS data. The fourth section looks at the applications of laser scanning in vegetation studies.

2.1. Introduction

Laser, or light amplification by stimulated emission of radiation, generates a powerful, directional, optical light beam that is often highly coherent in space and time. It can be controlled so that only light in a particular wavelength is released (Wehr and Lohr, 1999). The theory of laser was put forward in 1958 and the first laser was demonstrated in 1960. However, it was only in the 1970s and 1980s that laser altimetry, the measurement of distances using laser, was developed and used in airborne instruments by NASA. Laser altimetry is considered to contribute significantly to information from remote sensing, either independently or in conjunction with other sensor systems (Flood, 2001).

Lidar is often referred to as laser radar since it is a direct extension of conventional radar techniques to very short wavelengths, in the region from ultraviolet to far infrared (10 nm-1 mm). Although laser radars are active systems, and operate on the same basic principle as microwave radars (1 mm-1 m), they are capable of higher accuracy and resolution (Jelalian, 1991).

2.2. Laser Scanning Systems

ALS systems may broadly be classified into discrete return and full-waveform based on the method of recording the return signal. In a system, that records the first and last pulses, for an impervious surface such as a road or a flat building roof, only one echo is recorded, or we get the same first and last echoes. In the case of a tree, echoes may be obtained from a leaf, branches, and then the ground, but only echoes from the leaf and ground are recorded, being the first and last echoes. This leads to loss of available information, especially from vegetation. On the other hand, full-waveform laser scanners record the full waveform of the return pulse. This will be described in more detail in section 2.3. ALS systems are also distinguished based on the sampling rate, maximum scanning angle and scanning pattern (Dubayah et al., 2000).

2.2.1. System Components

An ALS system consists of a laser scanning unit and a Position and Orientation System (POS). The laser scanning unit contains a laser ranging unit, a scanner and control, monitoring and recording units. The ranging unit consists of the laser emitter and the receiver (Figure 1). The transmitting and receiving apertures are mounted so that they are in the same optical path. This is to make sure that the points illuminated by the laser are always in the field of view of the receiver. The laser beam has a narrow divergence angle, in the range from 0.3 milliradians

(mrad) to 2 mrad, which defines the instantaneous field of view (IFOV) of the receiver. The laser beam, sent downwards by the transmitter, is deflected by the scanner to cover large areas required for surveying. This makes the modern scanning systems different from the earlier profiling sensors that recorded echoes only from the nadir (Kager, 2006; Lim et al., 2003; Wehr and Lohr, 1999).

The scanning pattern on the ground is dependent on the scanning mechanism in the sensor. A Palmer scanner uses a mirror, rotating about its axis to deflect the beam in an elliptical pattern. This system was used in laser scanning in the 90s. An oscillating mirror directs the laser pulse across the swath perpendicular to the flight direction. It produces a zigzag pattern on the ground, with points towards the end of the swath closer together due to the decrease in speed of the oscillating mirror. The slowing down, stopping, reversing of direction and speeding up again, of the mirror add strain to the mechanics, and could affect the positional accuracy of the system. A polygon scanner uses a rotating multi-faceted mirror (four facets in the case of Riegl scanners) to direct laser pulses along parallel lines across the swath, in a single direction. The polygon scanner is faster, but requires timing for when data is to be collected. Mirror scanners can cause deflection errors due to the mechanics, and require regular calibration. A fibre scanner, on the other hand, has stiff mounting of all components on a rigid carbon fibre plate. This ensures that the factory calibration remains valid over the period of operation. The laser fibre scanner consists of two arrays of 128 light guiding glass fibres, the transmitting and the receiving arrays. The pulses travelling through 127 of the fibres are sent to the ground, while one is used for reference (Burtch, 2002; Lohani, 2007; Schnadt and Katzenbeisser, 2004; Wehr, 2008).

The laser scanning unit measures and records the polar coordinates of points on the target surface in its own local coordinate system. The position of the points on the ground can be calculated only if the position and orientation of the laser system is known with respect to a geographic coordinate system. The POS provides this information. It consists of an Inertial Measurement Unit (IMU) and a differential Global Positioning System (dGPS). The IMU measures the roll, pitch and heading of the sensor. Two GPS receivers are usually used to locate the position of the aircraft at the time of emission of each laser pulse. One GPS receiver is installed in the aircraft, and the other at a known ground location. The ground receiver is used to identify and correct the errors in the aircraft's position (Flood and Gutelius, 1997; Kager, 2006; Lim et al., 2003; Wehr and Lohr, 1999).

2.2.2. The Measurement Principle

The location of the target points can be determined from their distances from the flying platform and the scan angle, since the location of the flying platform is recorded (Flood, 2001). The distances to targets can be estimated from the time lag between the transmitted and received pulses, and the speed of light (Figure 2). The travel time can be calculated using pulse ranging or continuous wave ranging. In pulse ranging, the travel time of a laser pulse from the sensor to the object and back is recorded, whereas in continuous wave ranging, the phase change in a transmitted continuous sinusoidal signal is converted into travel time (Wehr and Lohr, 1999). The travel time, when multiplied by the speed of light, gives the round-trip distance travelled by the beam. When this value is divided by two, it gives the distance between the sensor and the target (Burtch, 2002; Lefsky, 2002). The majority of the commercially available laser scanners make use of pulse ranging and all references in this thesis are to pulse ranging.

2.2.3. Laser Beam Footprint

The laser beam footprint is the sampling area of the sensor on the ground, which receives the individual laser beam and reflects energy to the sensor. The size of the footprint, usually given as the diameter, is an important parameter in laser remote sensing, and varies with the scanning geometry and the local topography. The generalised equation for the area of the laser beam footprint is given by (Yongwei, 2008) as:

$$A = \pi \cdot R^2 \cdot \frac{\cos(\theta - \alpha) \cdot (1 - \cos \beta)}{(\cos(2\theta - 2\alpha) + \cos \beta) \cdot \cos^2 \theta} \quad [1]$$

where θ is the instantaneous scan angle, α is the inclination angle of the intersection line between the vertical view plane and the terrain surface, and β is the laser-beam divergence angle.

The beam footprint on the target surface is proportional to the square of the range. It is also considered proportional to the square of the divergence angle of the transmitter beam, at very low laser-beam divergence angles, as is the case with most commercial laser scanners. The footprint at nadir on flat ground is circular. The distribution of laser energy is not uniform within the footprint of the laser, but has a radial Gaussian distribution of laser energy (Harding et al., 2001) as shown in Figure 1.

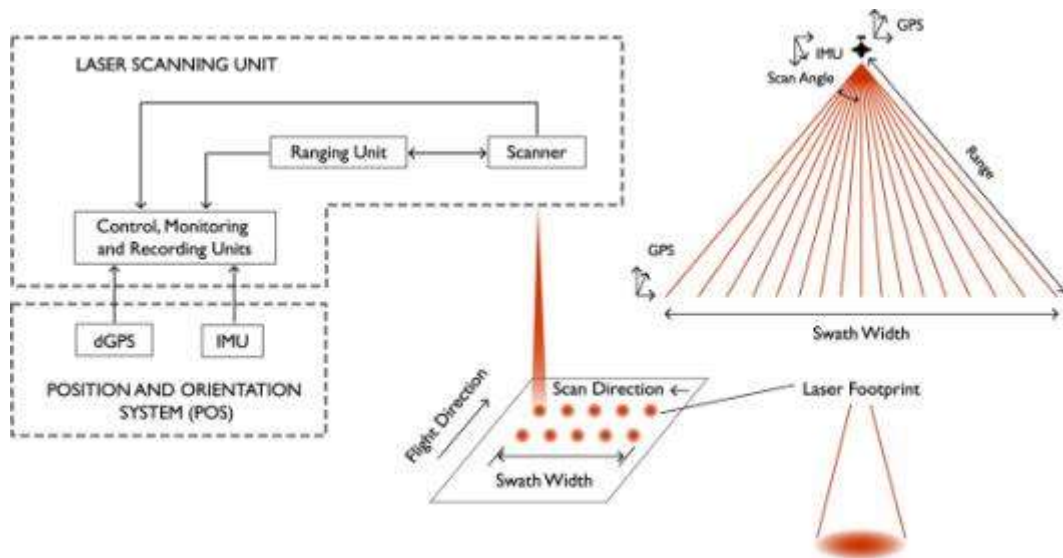


Figure 1: A typical airborne laser scanning system. The laser beams sent downwards by the transmitter is deflected, by the scanner across the swath width, to cover large areas required for surveying (Adapted from Hyypä et al. (2000) and Wehr and Lohr (1999))

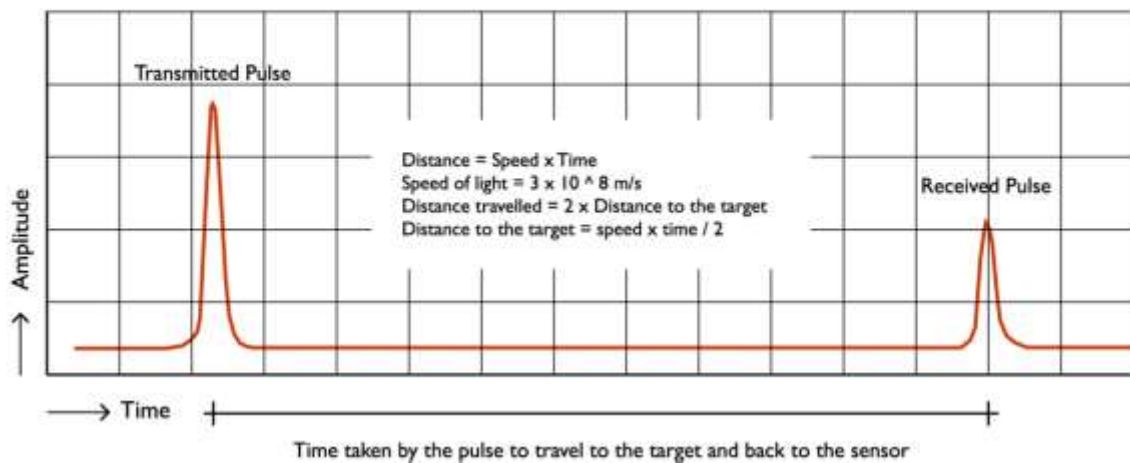


Figure 2: The measurement principle of laser ranging

2.2.4. Full-waveform Laser Scanning Systems

Full-waveform systems can be divided into three: Bathymetric, Experimental and Commercial (Table 1). They differ mainly in footprint size, pulse energy and pulse repetition frequency. Bathymetric lidar systems use two beams, a green (532 nm) and an infrared one (1064 nm). They are used for accurately determining the sea depth. The green beam reaches the bottom of the sea, whereas the infrared beam is reflected by water. The Experimental lidar systems were developed by NASA to study the feasibility of using them for satellite missions. Most Commercial systems are small-footprint, with diameters from 0.2 to 3 m depending on flying height and beam divergence. They can provide a high point density and an accurate description of the altitude. However, they could also miss treetops, and it also becomes difficult to determine whether ground has been reached under dense vegetation (Dubayah and Drake, 2000). Large-footprint systems increase the probability of hitting both the ground and the top of the canopy, since they collect data from a larger footprint, usually from 10 to 70 m (Lefsky, 2002; Mallet and Bretar, 2009).

2.3. The Return Signal

The electromagnetic fields can be considered to travel sometimes in a wave train, and sometimes as discrete packets of energy. In the microwave region, as in radar, they may behave as waves, while at the laser wavelengths; they behave more as packets of energy, or photons. So, the received signal power can be considered to be equivalent to the number of photons arriving per second at a specific wavelength (Jelalian, 1991).

The return signal is the product of the transmitted laser pulse and the scattering function of the target or targets. The temporal shape of the return signal is often referred to as waveform. In the case of a single flat target perpendicular to the incident laser beam, the waveform is a smaller version of the transmitted signal in terms of shape. The full-waveform recording ALS systems record the entire time-varying power of the return signal from all illuminated surfaces (Figure 3). This makes it capable of collecting more information about canopy structure than most discrete return ALS systems. The waveform from multiple targets is more complex, and represents the sum of the signals from the individual targets. It is often decomposed into components representing the individual targets (Mallet and Bretar, 2009; Wagner et al., 2006). Figure 3 shows the conceptual differences between the full-waveform and discrete return systems.

Table 1: Technical specifications for full-waveform lidar systems (Mallet and Bretar, 2009)

System	Manufacturer	Platform	Beam Deflection	Wavelength (nm)	Flying Height (km)	Echo Width (ns)	Beam Divergence (mrad)	Footprint Size (m)	Range Accuracy (cm)	Digitiser (ns)
Bathymetric										
LARSEN 500	Terra Surveys Optech	Airborne	Rotating Mirror	1064/532	0.5	12	4	2@500 m	30	1
Mark II	LADS TopEye	Airborne	Fibres	1064/532	0.37-0.5	-	-	-	15	2
Hawk Eye	Saab Optech	Airborne	Osc. Mirror	1064/532	0.05-0.8	2/15	2-15	1-7.5@500 m	30	1
SHOALS 1000T	US army Optech	Airborne	Osc. Mirror	1064/532	0.2-0.4	2/15	2-15	0.8-6@400 m	15	1
EAARL	NASA	Airborne	Osc. Mirror	1064/532	0.3	0.07	0.03	0.15@300 m	3	1
Experimental										
SLICER	NASA	Airborne	Osc. Mirror	1064	<8	-	2	10@5 km	11	1.35
SLA-02	NASA	Satellite	None	1064	285	40	0.3	85@285 km	150	4
LVIS	NASA	Airborne	Osc. Mirror	1064	<10	5	8	40@ 5km	30	2
GLAS	NASA	Satellite	None	1064/532	600	75/35	0.11-0.17	66@60 km	5-20	1
MBLA	NASA/University of Maryland	Satellite	Osc. Mirror	1064	400	10	0.06	24@400 km	100	4
Commercial										
LMS Q-560	Riegl	Airborne	Polygon	1550	<1.5	0.008	0.5	0.5@1 km	2	1
Falcon III	TopoSys	Airborne	Fibres	1560	<2.5	-	0.7	0.7@1 km	-	-
Mark II	TopEye	Airborne	Palmer	1064	<1	-	1	1@1 km	2-3	1
ALTM 3100	Optech	Airborne	Osc. Mirror	1064	<=3.5	<0.2	0.3/0.8	0.3/0.8@1 km	1	1
ALS 60	Leica	Airborne	Osc. Mirror	1064	0.2-6	<0.2	0.22	0.22@1 km	2	1

2.3.1. Amplitude and Intensity

The term intensity is still neither clearly defined in the field of laser scanning, nor well specified by the laser scanner manufacturers. Intensity of the return signal is defined as the ratio of strength of reflected light to that of emitted light (Song et al., 2002). The terms signal intensity, reflectance intensity and pulse reflectance are also used to refer to the return amplitude or energy of a single echo (Figure 4). The intensity data provided by the commercial discrete return systems are based on proprietary echo detection algorithms. The intensity could therefore correspond to a specific, such as maximum, amplitude of the detected echo. It could also be the integral of the returned signal over the echo width (Höfle and Pfeifer, 2007; Mallet and Bretar, 2009; Wagner et al., 2008b).

The main problem with using intensity, whether it corresponds to the amplitude or the integral of the echo, as an attribute in classification methods is that it is dependent on various factors. The main factors that make the direct use of intensity values in classification difficult are spherical loss and topographic and atmospheric effects. Spherical loss refers to the decrease in the received power with increasing distance between the sensor and the target.

The topographic effect is caused by the angle of incidence of the laser beam. The atmospheric effects are due to the varying flying heights, and atmospheric conditions. Höfle and Pfeifer (2007) suggest methods for correcting these effects on the intensity. However, the effective reflecting areas of surfaces for multiple echoes and the scattering characteristics of the individual targets still cause uncertainties (Coren and Sterzai, 2006; Höfle and Pfeifer, 2007).

The intensity values vary for a given target depending on the flying height or elevation differences, even within a single dataset. Multi-temporal analysis using intensity values, from different ALS systems, scan geometry and atmospheric conditions, would require the values to be calibrated to comparable measurements. The additional information provided by the decomposition of full-waveform ALS data is suitable for calibration, whereby the intensity values are converted to values proportional to the surface reflectance of the target (Höfle and Pfeifer, 2007).

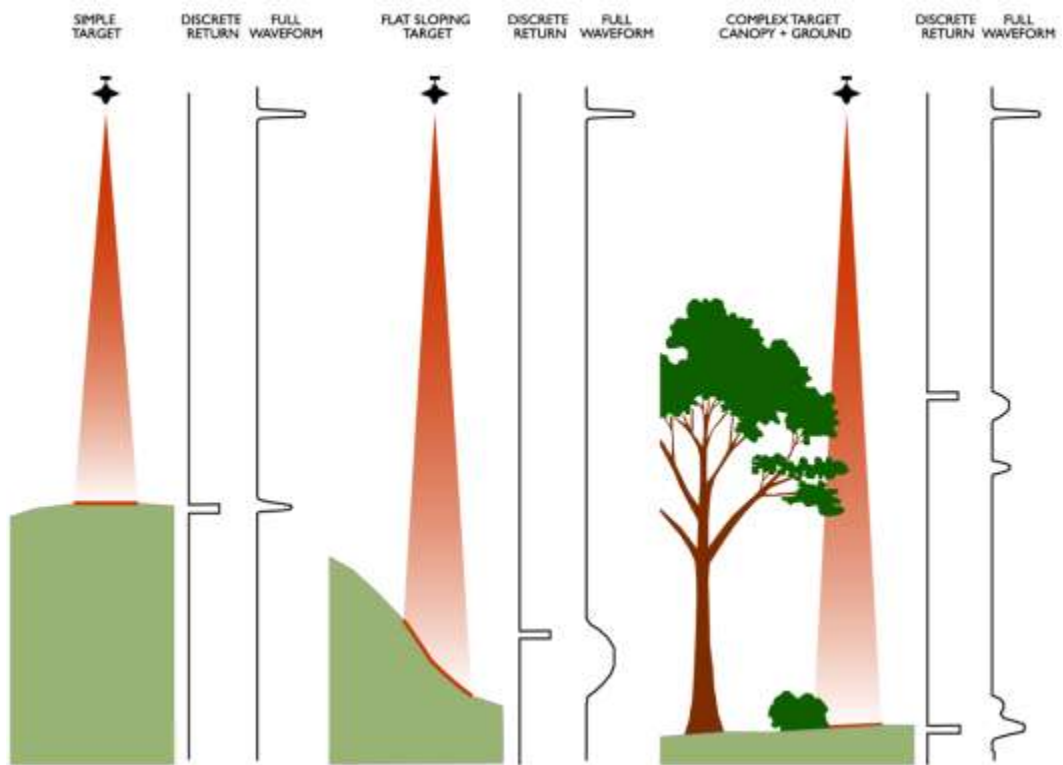


Figure 3: Conceptual differences between full-waveform and discrete return ALS systems (Adapted from Ullrich (2006))

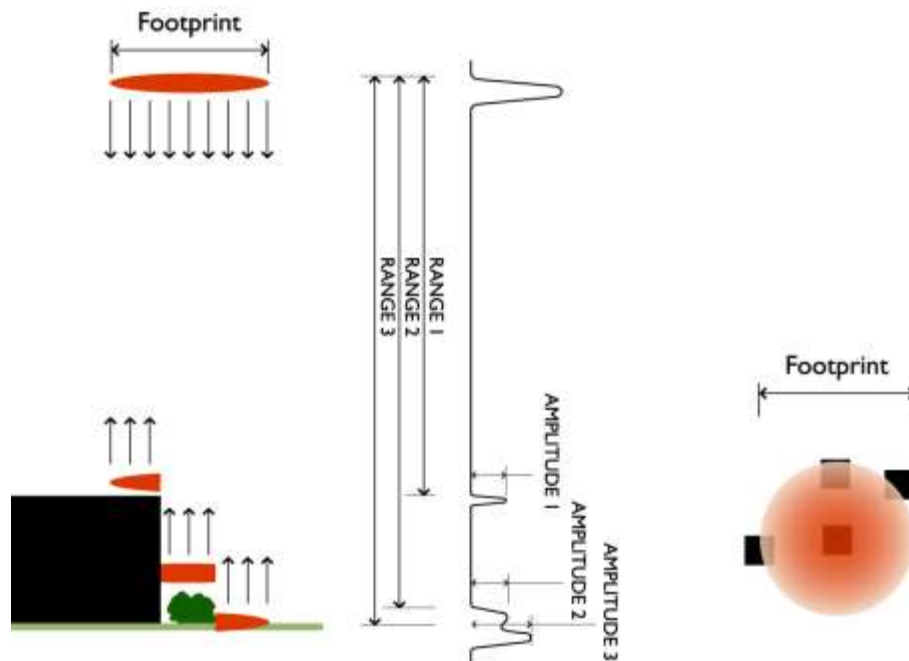


Figure 4: Intensity of the return signal from multiple echoes (Adapted from Rohrbach (2007)). The distribution of laser energy is not uniform within the footprint of the laser beam.

2.3.2. Backscatter Cross Section

The redirection of incident electromagnetic energy by an object is referred to as scattering. In radar remote sensing, the energy that is scattered back to the instrument, called backscattering, is of more interest than what is absorbed or scattered in the same direction as the incident wave. The effectiveness of a scatterer is often quantified by a term called the scattering cross section. Therefore, in radar remote sensing, the backscattering or backscatter cross section, also referred to as radar cross section is of most interest (Woodhouse, 2006). Since lidar is considered to be an extension of radar to shorter wavelengths, the radar cross section is often used to understand the characteristics of the return signal from laser scanning (Wagner et al., 2006).

An isotropic target scatters the incident energy equally in all directions. The backscatter cross section of a target, usually represented by the Greek letter sigma, σ , is equal to the physical cross sectional area of an idealised isotropic target, which has the same intensity as the selected target. It has dimensions of area, in m^2 . This need not correspond to the actual cross sectional area of the target. The backscatter cross section, even for a target with a large physical area, would approach zero if very little energy were scattered back to the receiver. This could occur if the target is too small, absorbs the incident energy, or scatters the energy in a different direction. On the other hand, the backscatter cross section could be more than the physical area, if the energy scattered back is more than that of an idealised isotropic scatterer (Woodhouse, 2006).

The backscatter cross section of a small discrete target would remain the same with a decrease or increase in the illuminated area. However, for an extended target, such as bare ground, the backscatter cross section would increase or decrease in proportion to the illuminated area. This makes it difficult to compare the cross sections of targets, with similar scattering properties, but different physical areas. The backscatter coefficient is a normalised measure of the backscatter cross section irrespective of the area of the footprint. It is estimated by dividing the backscatter cross section by the physical area of the target. When the actual geometric area of the target is used in the calculation, the backscatter cross section is referred to as sigma nought, σ^0 . It is unit-less as the cross-sectional area of the idealised target is divided by the area of the target (m^2m^{-2}).

The radar equation has been used to explain the strength of the return signal in ALS, and to derive the backscatter cross section. If we assume that the radiation is scattered by the target

in the form of a cone, a signal is registered only where this cone overlaps the field of view of the receiver. The power entering the receiver is (Wagner et al., 2006):

$$P_r = \frac{P_e}{A_f} \rho A_s \frac{1}{\Omega R^2} A_r \quad [2]$$

where P_r is the power entering the receiver, P_e is the emitted power, A_f is the footprint area of the beam, ρ is the reflectivity of the scatterer, A_s is the receiving area of the scatterer, Ω is solid angle of the scattering cone, R is the distance from the sensor to the target, A_r is the area of the aperture at the receiver. By expanding A_f and A_r in the above equation, P_r becomes:

$$P_r = \frac{4P_e}{\pi R^2 \beta^2} \rho A_s \frac{1}{\Omega R^2} \frac{\pi D^2}{4} \quad [3]$$

Separating the system and target parameters gives the following equation, where all the target parameters are combined into σ , the backscatter cross section. The backscatter cross section is a complex combination of multiple factors including size, shape, material, edges and wavelength, and has contributions from each scattering source in the case of complex objects (Toomay and Hannen, 2004).

$$P_r = \frac{P_e D^2}{4\pi R^4 \beta^2} \frac{4\pi}{\Omega} \rho A_s = \frac{P_e D^2}{4\pi R^4 \beta^2} \sigma \quad [4]$$

where D is the aperture diameter of the receiver, β is the divergence angle of the transmitter beam and σ is the backscatter cross section of the target.

In the case of multiple targets within the footprint of the laser beam, the second and higher order pulses can be partly shaded by the scatterers closer to the sensor. The shaded areas do not contribute to the return signal, which represents only the illuminated areas within the range interval. The cross section of an echo from a return signal with multiple echoes is therefore referred to as 'apparent cross section' and denoted as σ'_i , which represents the 'apparent' backscatter cross section representing the illuminated area within range interval i .

The receiver has an impact on the waveform, and the effect can be introduced as the receiver impulse function, τ in the above equation. The equation can also be modified taking into consideration the temporal nature of the waveform. Therefore, the power entering the receiver at time t (Wagner et al., 2006):

$$P_r(t) = \sum_{i=1}^N \frac{D^2}{4\pi R_i^4 \beta^2} P_e(t) * \sigma'_i(t) * \tau(t)$$

[5]

where $P_r(t)$ is the power entering the receiver at time t , N is the number of targets, D is the aperture diameter of the receiver, R_i is the distance from the sensor to the target at range interval i , β is the transmitter beam divergence angle, $P_e(t)$ is the transmitted power at time t , $\sigma'_i(t)$ is the 'apparent' backscatter cross section representing illuminated area at time t and $\tau(t)$ is the receiver impulse function at time t .

It is not easy to determine the values of the transmitted power and the receiver impulse function independently. Therefore, their product is taken as the system waveform $S(t)$.

$$P_r(t) = \sum_{i=1}^N \frac{D^2}{4\pi R_i^4 \beta^2} S(t) * \sigma'_i(t)$$

[6]

In some scanners, for example, Riegl LMS-Q560, the system waveform can be described by a Gaussian function (Wagner et al., 2006). It is also assumed that the scattering properties of a cluster of targets can be described by a Gaussian function. Multiple targets within the footprint could be described by a series of Gaussian functions, where each echo represents a cluster of targets too close to be differentiated. This method gives estimates of the location and scattering properties of the targets. The return waveform is the sum of the individual Gaussian pulses. By replacing the system and target waveforms by Gaussian functions, Wagner et al. (2006) arrived at the following form of the radar equation. The additional power losses that occur in the instrument and in the atmosphere were also considered.

$$M_i s_i = \eta_{sys} \eta_{atm} \frac{D^2}{4\pi R_i^4 \beta^2} M_s s_s \sigma_i$$

[7]

where M_i and s_i are the amplitude and standard deviation of the echo pulse, η_{sys} and η_{atm} are the system and atmospheric transmission factors, M_s and s_s are the amplitude and standard deviation of the system waveform and σ_i is the backscatter cross section of the target.

The transmitted and received powers in equation [4] are replaced by the products of the amplitude and standard deviation of the system waveform and the received echo. This is an expression of the fact that the echo energy is proportional to the area below the curve. When measurements from different flight conditions and instruments are to be compared, the measured receiver power has to be converted into backscatter cross section. This is referred to as calibration. The constant and variable terms in equation [7] are separated to obtain:

$$\sigma_i = \frac{4\pi\beta^2}{\eta_{sys} \eta_{atm} D^2 M_s s_s} R_i^4 M_i s_i = C_{cal} R_i^4 M_i s_i \quad [8]$$

where C_{cal} is the calibration constant.

The individual echoes representing the targets have to be extracted from the full waveform for further analysis. Gutierrez et al. (2005) noted that many of the waveforms reflected from ground or dense canopy layers can be described as near-Gaussian shapes with single or multiple modes, whereas those from canopy gaps, undergrowth or branches of trees are more complex and non-Gaussian. Hofton et al. (2000) considered two exponential curves with different decay times to be a better approximation of the shape of the return signal. Extensions of Gaussians such as Lognormal and generalised Gaussian functions can also be used to improve signal fitting for complex waveforms (Chauve et al., 2007). However, the majority (98%) of the return waveforms, from scanners such as Riegl LMS-Q560, could be fitted with a sum of Gaussian functions (Wagner et al., 2006).

2.3.3. Gaussian Decomposition

Many analytical waveform solutions are based on Gaussian decomposition, as it provides the number of echoes and the time, amplitude and width of each echo (Gutierrez et al., 2005; Hofton et al., 2000; Persson et al., 2005; Wagner et al., 2006). The waveform $w(t)$ can be modelled as a sum of Gaussian distribution functions (Chauve et al., 2007; Reitberger et al., 2006)

$$w(t) = \varepsilon + \sum_{i=1}^N M_i e^{-\left[\frac{(t-t_i)^2}{2s_i^2}\right]} \quad [9]$$

where ε is the bias, or noise level, N is the number of pulses, M_i is the amplitude, t_i is the time position, and s_i is the standard deviation of the echo at range interval i .

Hofton et al. (2000) demonstrated the Gaussian decomposition method on data collected by the airborne laser vegetation imaging sensor (LVIS). The number of Gaussian components was estimated to be half the number of inflection points. The half-width of each component was taken to be half the difference of the inflection points, and the position as half the sum of the inflection points. The components were ranked as 'important' if their half-widths were equal to or more than the half-width of the transmitted pulse, and the initial estimates of the amplitude were greater than three times the standard deviation of the mean noise level. The initial non-negative amplitudes were estimated using a least squares method. The initial

parameter estimates of all the 'important' Gaussians were optimised using the Levenburg-Marquardt method. If this initial sum of Gaussians did not approximate the return waveform within an accuracy limit, additional less 'important' Gaussians were included in the optimisation procedure (Blair et al., 1999; Hofton et al., 2000).

In the estimation of the number of Gaussian components, if two neighbouring Gaussians were close together, only two inflection points were detected instead of four. Therefore, it was not possible to isolate the Gaussian pair. False detection of Gaussians also occurred because of the random amplitude changes within the waveform background noise. However, smoothing the waveform prior to estimating the Gaussians minimised this problem.

Persson et al. (2005) fitted Gaussian distribution to the return waveform from a TopEye Mark II System. A threshold was calculated and all the samples below this were set to zero. For each waveform, a range of components, from one to nine, was fitted to the waveform. For each component, the mean, standard deviation and relative weight were estimated using the expectation maximisation (EM) algorithm. The models were then compared, and the one with minimum error, was chosen. The minimum distance between two components was set to avoid estimating too many components. The amplitude of the components were normalised by the area of the waveform.

Wagner et al. (2006) applied the Gaussian decomposition to the return waveform from Riegl LMS-Q560. The number of Gaussians and their respective positions and amplitudes were estimated by using two 'traditional' echo detection methods, the centre of gravity and zero-crossing of the first derivative. The fitting was done only if these two detectors agreed within a given tolerance. They note that two scatterers from a cluster, if they are at a distance comparable to or smaller than the range resolution, were merged into one mode. Two other identified problems were the amplitude of a fitted pulse being negative, and the fitting procedure not finding any solution.

As seen from the above examples, the estimates of the number of targets, the distances to the targets and the initial parameters have to be determined before fitting of the Gaussian model to the observed waveform. This is referred to as echo detection, and it involves the extraction of discrete time-stamped echoes from the continuous waveform. These echoes represent the positions of the individual targets. Some of the standard echo detection methods are threshold, centre of gravity, maximum, zero crossing of the second derivative and constant fraction. Different algorithms for echo detection produce slightly different results. full-

waveform data give the freedom to use different detection methods, or even a combination of methods to extract the required information for a specific application (Wagner et al., 2004).

2.4. Approaches to Classification

ALS point data themselves can be used for classification. They can also be converted to a surface for further analysis. The methods for converting points to surfaces are discussed. The second sub-section describes some of the past research using ALS data for classification. The classification is often followed by an assessment of accuracy, which is discussed in section 2.4.3.

2.4.1. From Points to Surfaces

A surface can be divided into discrete spatial units using regular or irregular tessellation. A raster model, with square grid cells, is an example of a regular tessellation. Interpolation, the prediction of values at locations from the measurements made at point locations (Figure 5A) within the surface, can be used to convert data from point observations to continuous surfaces (Figure 5 B&C). Nearest neighbour, inverse distance weighting and spline are a few functions used for interpolation. The regular grid system has some disadvantages which include data redundancy and inability to adapt to areas with differing relief complexity without changing the grid size (Burrough and McDonnell, 1998).

A TIN, a vector model designed by Peucker and Chrisman (1975), is an example of an irregular tessellation (Figure 5D). A TIN model consists of connected triangles based on Delaunay triangulation, with the irregularly spaced observation points as nodes. Thiessen, also known as Voronoi or Dirichlet, polygons can be used to describe the area of influence of a point in a set of points (Figure 5E). It is based on a nearest neighbour algorithm, as the values are predicted from the nearest data point. A Thiessen polygon is complementary to TIN (Figure 5F). If each TIN edge is bisected at right angle, and closed polygons are created from these perpendicular bisectors, the result would be a set of Thiessen polygons. A circle circumscribed about a Delaunay triangle has its centre at the vertex of a Thiessen polygon and no data points are contained in the circumscribed circle of any triangle (Burrough and McDonnell, 1998).

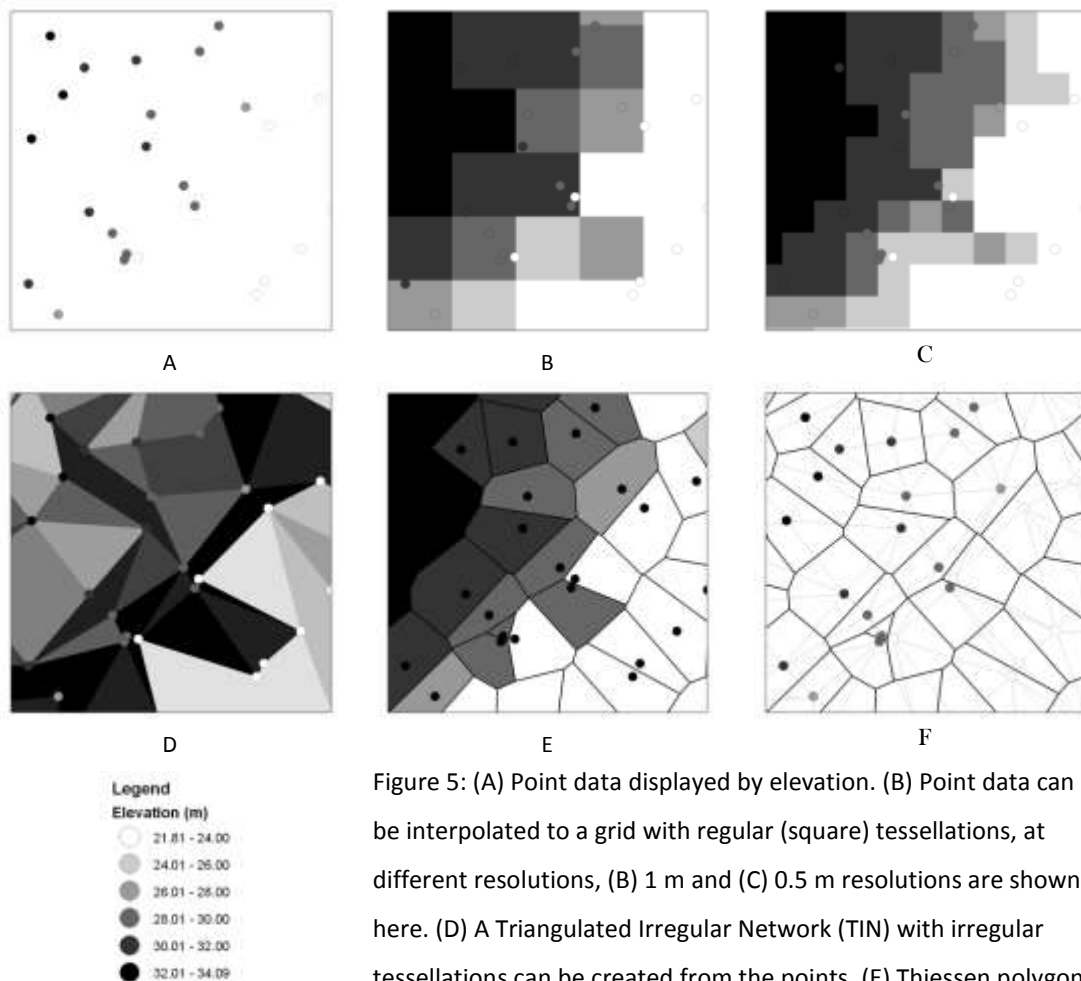


Figure 5: (A) Point data displayed by elevation. (B) Point data can be interpolated to a grid with regular (square) tessellations, at different resolutions, (B) 1 m and (C) 0.5 m resolutions are shown here. (D) A Triangulated Irregular Network (TIN) with irregular tessellations can be created from the points. (E) Thiessen polygons are complementary to a TIN; both of them retain the original values at the point locations, and (F) Figure showing the relation between TIN and Thiessen polygons.

2.4.2. Classification of ALS Data

It was noted by Schreier et al. (1985) that the ability of laser scanning to measure terrain heights as well as infrared reflection provides a new dimension in remote sensing analysis. They made use of a pulsed near infrared laser system at a wavelength of 904 nm to study the ability of the height and reflection measurements to distinguish surfaces. It was seen that clear water, very dark rocks and asphalt-covered roads absorbed the infrared laser signal, although some echoes were observed from water in the presence of sediments, floating vegetation, debris and waves.

Filtering of ALS point clouds and classification into terrain and objects is considered to be a pre-requisite in any class-based modelling (Tovari and Vogtle, 2004). Charaniya et al. (2004) have been able to classify ALS data into trees, grass and building roofs with a classification accuracy of 66% - 84%. In their study, the ALS data were interpolated to a regular grid, and

classification was based on normalised height, height variation, multiple echoes, luminance and intensity. The luminance values were obtained from an additional grey scale aerial image. Miliareisis and Kokkas (2007) employed parametric classification and k-means clustering for the extraction of building and vegetation classes from lidar DEMs based on elevation, roughness, mean slope and standard deviation of the slope of grid cells belonging to a region. Antonarakis et al. (2008) used elevation and intensity data in a method based on point distribution frequency to classify forest types and ages in flood plains.

The object-oriented rule based approach implemented in eCognitionTM has been used for classification of ALS data. Brennan and Webster (2006) classified ALS points interpolated to a 1 m grid to generate as many classes as possible using arithmetic means of intensity, elevation of digital surface model, number of echoes and normalised height, and standard deviation of intensity. They were able to generate ten classes including water, roads, two classes for structures, and four classes for vegetation. They could obtain up to 98% accuracy when the classes were aggregated to seven. Hyypä et al. (2007) segmented ALS data into homogeneous regions, and used selected segments as training data to construct decision trees for classifying all the segments. They used an aerial image in addition to ALS data, and the producer's and user's accuracies of building detection were 95% and 84% respectively (Hyypä et al., 2007).

Gridding of ALS data involves loss of data and precision, and a few studies have looked at segmenting the ALS point cloud. Ducic et al. (2006) used a decision tree to classify ALS points into vegetation (trees and shrubs) and non-vegetation (grass, roof and road) using attributes from full-waveform ALS data. In this study, although the points from grass and road could be separated based on amplitude, grass had a similar range of amplitudes to building roofs. Since their aim was to classify points without using elevation or relationship to adjacent points, grass was grouped with non-vegetation for generating the decision tree. Rutzinger et al. (2008) used a decision tree to classify points from full-waveform ALS data to detect tall vegetation – trees and shrubs. They segmented all the echoes using a seeded region growing procedure, based on the homogeneity of echo width. Segment statistics were calculated by aggregating attributes such as amplitude and surface roughness for a training area. This was used to construct a decision tree to classify the ALS data. They achieved accuracies above 90% for the validation sites. A summary of the studies on the classification of ALS data is given in Table 2.

2.4.3. Accuracy Assessment

The quality of the information derived from the classification of data is usually determined by an accuracy assessment. Error matrices are often used to represent map accuracy. An error matrix is a square array of numbers that denote the number of sample units assigned to a particular category in one classification relative to the number assigned to that particular category in another classification. One of the classifications is usually the reference data, which are considered correct. The reference data can be generated from aerial photography, ground observation or ground measurement. A general guideline for the sample size is a minimum of 50 samples from each category, which should be increased to 75 or 100 samples, for a large area or a large number of categories (Congalton and Green, 1999).

In an error matrix, the individual accuracies of each category are described along with the errors of inclusion (commission errors), and the errors of exclusion (omission errors), in the classification. A commission error is including an area in a category to which it does not belong (related to user's accuracy), while an omission error is excluding an area from a category to which it belongs (related to producer's accuracy). The error matrix can also be used to compute other accuracy measures (Congalton and Green, 1999).

Overall accuracy, producer's accuracy and user's accuracy can be calculated from the error matrix. Overall accuracy is the sum of the major diagonal of the matrix, representing the correctly classified samples, divided by the total number of samples in the entire matrix [10]. Producer's accuracy is calculated by dividing the number of samples that have been classified correctly by the total number of reference samples in that category [11]. User's accuracy is calculated by dividing the number of correctly classified samples by the total number of samples that were classified as belonging to that category [12]. The producers of spatial data are interested in how well a particular area on the Earth's surface can be mapped. The users of spatial data are mainly interested in knowing how well spatial data represent the ground reality. Both the producer's and user's accuracies are therefore important (Story and Congalton, 1986).

Table 2: Summary of studies on land cover classification using ALS data

No.	ALS System	Datasets	Data Model	Attributes	Method	Classes	Source
1.	Discrete	ALS, Colour-infrared image	Raster	Elevation, NDVI	Hierarchical structured generic model	Trees and buildings	(Straub, 2003)
2.	Discrete	ALS, Aerial image	Raster	Elevation, Intensity, Luminance, Multiple echoes	Supervised Parametric Classification	Trees, grass, roads, roofs	(Charaniya et al., 2004)
3.	Discrete	ALS	Raster	Elevation, Intensity, Multiple echoes	Object-oriented (eCognition)	Ten classes (Water, vegetation – bright and dark, roads, structures – bright and dark, trees – coniferous and deciduous, salt marsh – saturated and not saturated)	(Brennan and Webster, 2006)
4.	Full-waveform	ALS	Vector	Amplitude, Echo width, Multiple echoes	Decision Tree	Vegetation, non-vegetation	(Ducic et al., 2006)
5.	Discrete	ALS	Raster	Elevation	Region growing segmentation, k-means clustering	Buildings and non-buildings	(Miliareisis and Kokkas, 2007)
6.	Discrete	ALS, Aerial image		Elevation, colour, shape	Decision Tree	Ground, buildings, trees	(Matikainen et al., 2007)
7.	Discrete	ALS, Aerial image	Raster, Vector	Elevation, intensity, colour	Segmentation, Decision Tree	Buildings, trees	(Hyypä et al., 2007)
8.	Discrete	ALS, Imaging Spectrometer	Raster	Elevation, reflectance	Support Vector Machines	Built-up areas, vegetation, non-urban bare surfaces, water bodies	(Koetz et al., 2008)
9.	Full-waveform	ALS	Vector	Elevation, Amplitude, Echo width, Multiple echoes	Decision Tree	Vegetation, non-vegetation	(Rutzinger et al., 2008)
10.	Full-waveform	ALS	Vector	Elevation, Amplitude, Echo width, Shape of generalised Gaussian pulse, Multiple echoes	Support Vector Machines	Building, vegetation, artificial ground, natural ground	(Mallet et al., 2008)

In an error matrix, n samples are distributed into k^2 cells, where k is the number of categories. Each sample is assigned to one of the k categories in the classified data, and to one of the k categories in the reference data independent of the first. If the classified data are represented in the columns and reference data in the rows, the accuracies can be computed as:

$$\text{Overall Accuracy} = \sum_{i=1}^k \frac{n_{ii}}{n} \quad [10]$$

$$\text{Producer's Accuracy} = \frac{n_{ii}}{n_{i+}} \quad [11]$$

$$\text{User's Accuracy} = \frac{n_{ii}}{n_{+i}} \quad [12]$$

where n_{ii} denotes the numbers along the diagonal of the matrix, n_{i+} denotes the row totals and n_{+i} denotes the column totals. It is possible to determine statistically whether one error matrix is significantly different from another using a technique called Kappa analysis [13]. The resulting KHAT statistic is an estimate of Kappa, and is a measure of agreement based on the actual agreement, represented by the major diagonal and the chance agreement indicated by the row and column totals. It is similar to the more commonly used Chi square analysis, and is calculated as:

$$\kappa = \frac{n \sum_{i=1}^k n_{ii} - \sum_{i=1}^k n_{i+} n_{+i}}{n^2 - \sum_{i=1}^k n_{i+} n_{+i}} \quad [13]$$

A rough guideline for interpreting the KHAT statistic, often referred to as kappa coefficient (κ), was provided by Landis and Koch (1977). They considered values less than 0 to have no agreement, 0.0-0.2 to have slight agreement, 0.21-0.40 to have fair agreement, 0.41-0.60 to have moderate agreement, 0.61-0.80 to have substantial agreement and 0.81-1.00 to have almost perfect agreement.

2.5. Laser Scanning for Vegetation Applications

The visible ground surface and objects on it are directly measured by the laser footprints, but a pulse hitting objects without a well-defined surface, such as trees or cornfields may produce many separately recordable reflections. A laser pulse is therefore able to penetrate partly through vegetation.

This potential of the laser pulse led to studies on generating DTMs in forests. It was found that ground penetration rates of 20-40% could be expected in European coniferous and deciduous

forests. This increased to nearly 70% in deciduous forests in winter (Flood, 2001). Extracting ground points from the point clouds or from the waveform is often seen as a first step in processing. The focus of laser scanning applications had been on generating bare earth DTMs. These were used for ortho-rectification of imagery, generation of contour maps and hydrological modelling for risk assessment. With the development of waveform capture, new applications are being explored. These include topographic mapping beneath dense canopy and large area topographic mapping (Flood, 2001).

2.5.1. Classification of Vegetation

Schreier et al. (1985) showed that pure broadleaf forests show relative reflectance values that are significantly higher than pure coniferous stands. Mixed forests, grass and shrub could not be distinguished from their mean reflection values. Reflection variability, or percentage coefficient of variation, was considerably lower for terrain with low vegetation cover compared to forested terrain, and for pure broadleaf forests compared to coniferous forests. However, many parameters such as the time of observation, tree structure, tree density and type of under-storey cover, influence the reflection measurements. The temporal changes in coniferous forests were seen to be significantly smaller than that over grassland and broadleaf forests, although young coniferous trees were seen to have similar reflectance as those of broadleaf forests. Differences in tree species affect reflection measurements, but increased density of trees of the same species led to an increase in reflectance values. Mean height, mean reflection and reflection variability of stands were used to distinguish surfaces, and it was seen that coniferous forests occurred in a unique space separate from broadleaf forests and low vegetation (Schreier et al., 1985). Hug (1997) made use of reflectance image along with range data for the detection of trees. Laser pulses with a wavelength of 904 nm have been used to differentiate between coniferous forests and other vegetation (Wehr and Lohr, 1999).

Reitberger et al. (2008) extracted 3D points from the return waveform from a TopEye Mark II system, using Gaussian decomposition, for the classification of deciduous and coniferous trees. An intensity related parameter was derived from the integral of the Gaussian function and was approximated as the product of echo width and amplitude, equivalent to the echo energy of the reflection. The echo width was taken as twice the estimated standard deviation. The intensity was corrected using the amplitude and echo width of the emitted pulse, and a specified range as:

$$I_i^c = \frac{2s_i \cdot M_i \cdot R_i^2}{2s_s \cdot M_s \cdot R_0^2} \quad [14]$$

where I_i^c is the corrected intensity, s_i and M_i are the standard deviation and amplitude of the echo at range interval i , s_s and M_s are the standard deviation and amplitude of the emitted pulse, R_i is the distance from the sensor to the target at range interval i and R_0 is the specified distance for normalisation. The corrected intensity, along with parameters related to geometry, was seen to be very useful in the classification. The mean of the intensity values of all points belonging to an individual tree was better at classifying deciduous trees than the outer and internal geometrical tree structure (Reitberger et al., 2006).

The vertical distribution of laser echoes provides a new means to classify vegetation. It can be used for estimating other characteristics such as canopy cover and crown volume. It can also be used to predict the age of a stand as older stands are characterised by canopy gaps and trees of multiple ages and sizes. Crown volume is calculated as the product of the canopy height and spatial extent of the waveforms. Biomass is a useful predictor of carbon in terrestrial carbon pools. Taller trees usually support more foliage and roots and contain more wood than shorter trees of the same species. Stem diameter also usually increases with height. The above ground biomass can therefore be reasonably estimated from the height of trees (Dubayah et al., 2000).

The canopy cover can be estimated from the fraction of the ALS measurement returned from the ground surface. This could be from the number of discrete echoes or the integrated power of a waveform. The relative reflectance of ground and canopy surfaces are often corrected using a scaling factor depending on the wavelength of the laser. The definition of the ground surface is a critical factor in measurements of both canopy height and cover (Lefsky, 2002).

2.5.2. Height Metrics and Profiles

Canopy, or vegetation height and the vertical distribution of surfaces within the canopy are the two basic measurements derived from ALS. All other attributes are modelled or inferred from these direct measurements, or inferred from the horizontal structures revealed from the spatial information. Height is the most important measurement of the ALS system. Canopy height is usually calculated as the difference between the first and last echoes, assuming that the last echo is from the ground. This may be true for large footprint systems, but not necessarily for small footprint ones. Vegetation height is a function of species composition, climate and soil quality, and is useful for classification of land cover.

Large-footprint waveform laser scanning sensors such as LVIS and Scanning Lidar Imager of Canopies by Echo Recovery (SLICER) can provide vertical and volumetric profiles of forest vegetation, thereby characterising the structural complexity and functional properties relevant to ecological investigations (Anderson et al., 2006; Harding et al., 2001). The location at which the signal initially increases above the threshold, or mean noise level is taken as the canopy top. The centre of the last Gaussian pulse is taken as the ground echo. The distance between these two locations is used to derive the height metrics. The distance between the median location of the entire signal and the ground echo gives the height of median energy. This value, which gives the height at which 50% of the waveform energy occur, taken alone or in combination with the canopy height, has been shown to have a significant correlation to the above ground biomass (Anderson et al., 2006). Canopy height profiles have been derived from waveforms by transforming the raw backscatter record using a method that accounts for the occlusion effect inherent to the laser range measurements. Although these techniques were used on large-footprint waveform digitisers, they are applicable to any wave-form recording laser systems (Harding et al., 2001).

2.5.3. Delineation of Trees

As noted by Bortolot and Wynne (2005), individual tree-based approaches have some advantages over stand-based ones. In biomass predictions in forests, for example, non-forested areas may contaminate the measurements and cause inaccuracies in the prediction. Individual tree-based approaches permit estimation of parameters at the tree scale and more detailed evaluation of silviculture techniques. This could lead to more efficient management of resources.

The majority of the algorithms for delineating trees from ALS data are grid-based region growing methods. A commonly used procedure for creating a vegetation model, especially in a forested area, is to subtract the DTM from a digital surface model (DSM). A DTM is either obtained from other sources, or generated from the ALS data using different techniques. Many algorithms have been developed to extract the terrain points from ALS data and create a terrain model in the form of a triangulated irregular network (TIN) or terrain points interpolated to a grid (Axelsson, 1999; Elmqvist, 2001; Tovari and Vogtle, 2004).

A DSM is obtained by interpolating the ALS points to a grid at a suitable scale depending on the ALS point density. The DTM is then subtracted from the DSM to create a Canopy Height Model or Digital Crown Model (DCM) (Evans et al., 2006; Heurich, 2008; Popescu et al., 2003; Tiede et al., 2005; Tiede and Hoffmann, 2006; Zhao and Popescu 2007).

Interpolation of ALS points to a raster surface is useful for creating a smoother surface for detecting the tree crowns. However, this leads to under or over-estimation of tree heights (Tiede et al., 2005). In addition, during segmentation, spaces between trees, especially for conifers, are allocated to the surrounding trees leading to over-estimation of the crown diameters. For deciduous trees, the branches of trees often overlap leading to under-estimation of the tree crowns (Heurich, 2008). In Tiede and Hoffman (2006), the former problem is avoided by first classifying the surface into tree and non-tree objects. Tiede et al. (2005) make use of pseudo-grids where the maximum elevation of points within each grid cell is taken as the value of the grid cell to avoid errors due to interpolation.

Identifying the seed points for region growing is an important step in the tree delineation algorithms. The grid cells with local maxima within a square or circular search window are taken as the seed points for growing the regions. From this seed point, the algorithms search for neighbouring grid cells that are at a lower elevation than the seed points. The region belonging to an individual tree is allowed to grow until certain stopping criteria are reached, similar to the watershed algorithm.

Smaller window sizes for determining the seed points result in fragmentation of trees and larger window sizes lead to small trees not being detected. Variable window sizes are often used for locating the local maxima for grid-based methods. The search windows can be adjusted according to the height of the treetops based on the assumption that a taller tree has a larger crown radius. This height is estimated by deducting the terrain height from the top height of the tree. This is again based on the estimated terrain height.

In Popescu et al. (2003), two perpendicular profiles of the Canopy Height Model centred on the tree-top were extracted and a fourth degree polynomial was fitted on each profile. The crown diameter was calculated as the average of crown widths along the two profiles. The filtering window size was based on tree species, extracted from optical data, and height.

2.6. Summary

An ALS system consists of a laser scanning unit and a position and orientation system. The distances to target surfaces are estimated from the time lag between the transmitted and received pulses. The sampling area within the laser beam footprint receives the individual laser beam and scatters energy back to the sensor. ALS systems can broadly be classified into discrete and full-waveform based on the method of recording the return signal. Full-waveform

systems record the entire waveform of the energy scattered back to the sensor from the footprint of the laser beam.

The return signal is the product of the transmitted laser pulse and the scattering function of the target or targets within the footprint. Backscatter cross section is often used to understand the characteristics of the return signal from laser scanning. In many studies, Gaussian decomposition is used to extract the individual targets from the waveform.

ALS point data themselves, or surfaces interpolated from them, have been used for land cover classification. The ability of the laser pulses to penetrate partly through vegetation make it especially useful in vegetation studies. Although intensity data have proved to be useful in these studies, height is still considered the most important information from ALS data. Individual tree-based studies, rather than stand-based studies, could lead to more efficient management of resources.

This chapter provided an overview of airborne laser scanning, and its application in classification and vegetation studies. The next chapter looks at the datasets used for the study and describes the broad methodology.

3. Datasets and Methodology

Points extracted from full-waveform laser scanning data over a 1 sq. km area from Avonmouth in Bristol are the main data used for the study. A discrete return dataset over part of this area is used for comparing the classifications. Another full-waveform dataset collected from Bournemouth with a different point density and flying height is used for comparison. The study area and datasets are described in this chapter. It also provides a broad methodology to show how the different objectives fit together to achieve the aim of the research.

3.1. Introduction

Full-waveform data were collected from Bristol and Bournemouth using the LiteMapper™ system. A discrete return dataset was also available for the study area in Bristol. The datasets from Bristol were used for estimating the advantages, if any, of using full-waveform data over discrete return data for classification in urban areas. The wavelengths of the sensors, the altitude of capturing data and scan angles were different for the two full-waveform datasets from Bristol and Bournemouth. The raw waveform data from the Riegl LMS-Q560 recorder were also available in binary format.

The raw waveforms were at first analysed to understand the data generated by the commercial software provided by the scanner manufacturer. It should be noted that the waveforms do not contain any information about the actual position of the detected echoes on or above the earth's surface. The information contained in the waveforms is limited to the location of the detected echoes with respect to the scanner. These have to be combined with the data from the GPS and IMU units to derive any meaningful information, which can be directly used for further analysis or applications. The points generated by the commercial software were used for all further analyses. In this study, ArcMap™ and MATLAB® were used for data processing, analysis and visualisation.

3.2. Study Areas and Datasets

3.2.1. Study Areas

The two study areas were located in Bristol and Bournemouth (Figure 6). A 1 km x 1 km area was chosen from British National Grid Easting 354000 to 355000 (longitude 2°39'50" W to 2°38'59" W) and Northing 178000 to 179000 (latitude 51°29'56" N to 51°30'29" N) in Bristol (Figure 7), which includes a range of land use and land cover types. In addition to stands of trees, there are trees along the road, shrubs in gardens in the residential areas as well as grassland. The land use includes residential and institutional areas and agricultural land.



Figure 6: Location of Bristol and Bournemouth in the United Kingdom (Ordnance Survey © Crown Copyright. All Rights Reserved)

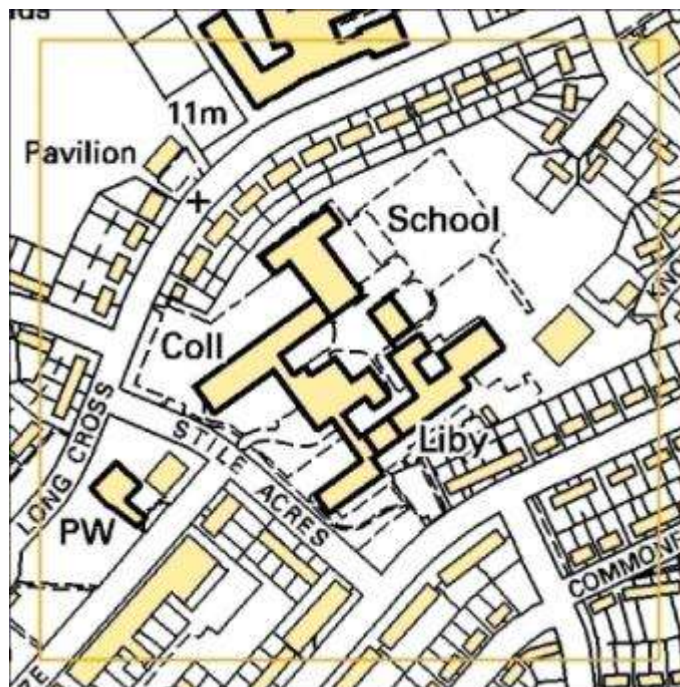
The second study area is in Bournemouth (Figure 8). A 0.5 km x 0.5 km area was chosen in an urban area from Easting 408750 to 409250 (longitude 1°52'38" W to 1°52'13" W) and Northing 91500 to 92000 (latitude 50°43'23" N to 50°43'39" N). It is a more complex site than the one in Bristol. Horseshoe common, in the middle of the study area, has a variety of trees on a sloping terrain. The road network is also complex with bridges and flyovers.

3.2.2. Full-waveform ALS Datasets

In the LiteMapper system, a Riegl LMS-Q560 laser scanner is combined with a DR 560 Digital Recorder, a 256Hz Inertial Measurement Unit, a NovAtel OEM4-G2 GPS, and a Hasselblad digital camera. The laser scanner, Riegl LMS-Q560, was one of the first commercially available waveform digitising airborne laser scanners. The two other scanners which became available around the same time were the TopEye Mark II System and Optech ALTM 3100 System (Wagner et al., 2006). The manufacturers of Riegl LMS-Q560 claim a range accuracy of 2 cm for the instrument.



A

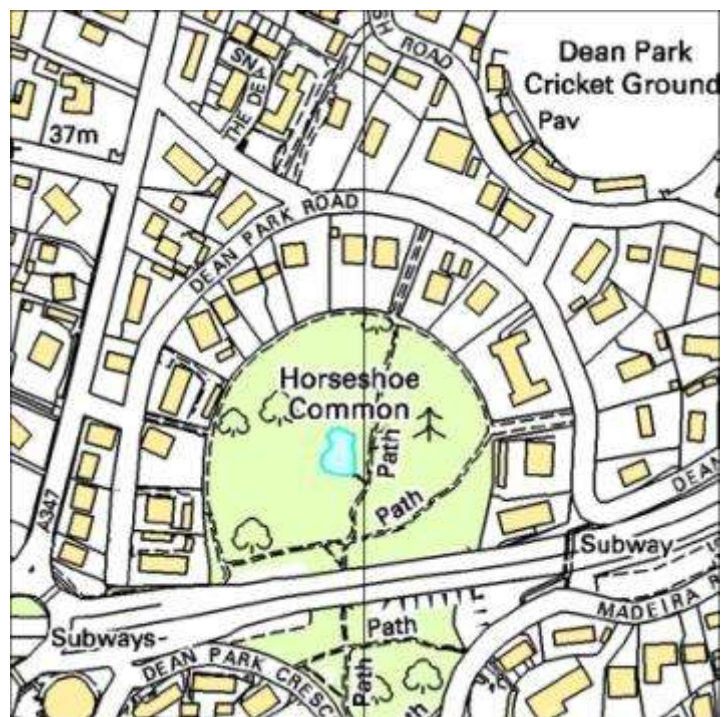


B

Figure 7: (A) An aerial image of the study area in Bristol. The subset of the study area is used for detailed analysis; (B) OS 1:10,000 scale raster of the subset (Ordnance Survey © Crown Copyright. All Rights Reserved)



A



B

Figure 8: (A) An aerial image and (B) OS 1:10,000 scale raster of the study area in Bournemouth (Ordnance Survey © Crown Copyright. All Rights Reserved)

As described in section 2.2.1, an airborne laser scanner system comprises a laser scanner for acquiring the three-dimensional information of the scanned objects and a subsystem for acquiring the position and orientation of the platform within a global coordinate system. These provide two datasets: the scan data and the flight data. RiAnalyze560™ and RiWorld560™ are used to extract the points from the waveforms (Figure 9). RiAnalyze analyses the full-waveform from the digitised echo signals provided by the laser scanner and transforms the range and scan angle into Cartesian coordinates. The output is in the form of a point cloud in the Scanner's Own Coordinate System (SOCS) with additional descriptors for every point, for example, precise time stamp, echo signal intensity, echo width and echo number. RiAnalyze uses three different algorithms: centre of gravity (COG), Gaussian pulse estimation (GPE) and Gaussian Pulse Fitting (GPF).

The COG estimation is very fast, and estimates the target range by calculating the centre of gravity of the echo. The accuracy of this method is slightly lower than that of GPF as there is the possibility of missing points that are close together. The GPF method is the most accurate of the three, but the computation time is about five times that of the COG method. The GPE method combines the high accuracy of the GPF method with the fast execution of the COG method. The difference between the two is that the GPF method is iterative while the GPE method is based on solving a linearised set of equations. The output from RiAnalyze is the input for RiWorld (RIEGL, 2007).

RiWorld transforms the output from RiAnalyze into points on the surface of the earth, using the flight data (RIEGL, 2007). RiWorld requires an accurate geometrical system description as an input for accurate transformation of the scan data. These include the transformations from the scanner system, to the POS coordinate system, and to the body (aircraft) coordinate system. The output data from RiWorld is a point cloud in the World Geodetic System (WGS84) Cartesian coordinates (RIEGL, 2007). The digitised echo signal data are thus converted into data compatible with conventional airborne laser data processing packages for further processing.

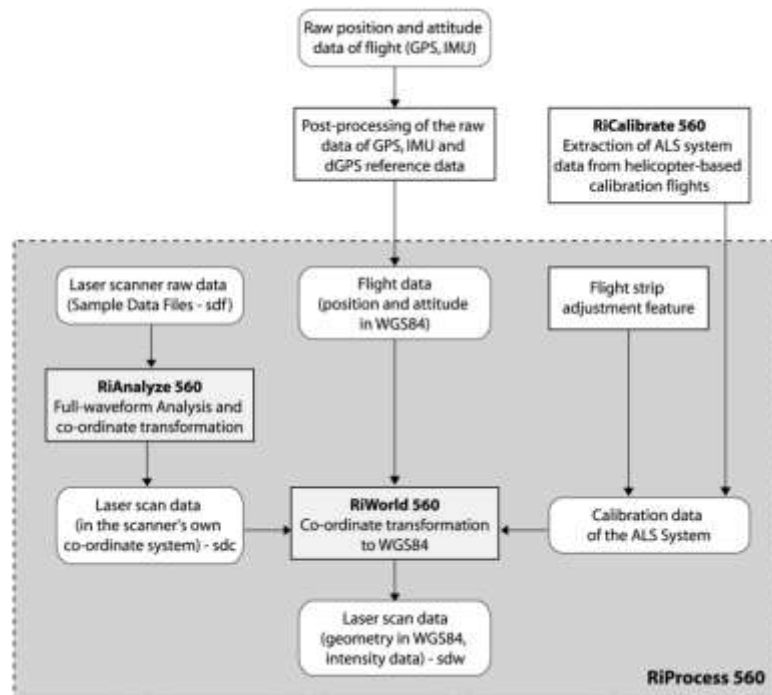


Figure 9: RiAnalyze and RiWorld convert the laser scanner raw data, the flight data and the calibration data into data in WGS84 (RIEGL, 2007)

THE RAW WAVEFORMS

The following analysis was undertaken to understand the data generated by Riegl’s software, and to determine whether the points extracted by the software could be considered to represent the raw waveforms. The raw waveforms were visualised using the description of the format provided by Riegl. The emitted and received pulses had been sampled every nanosecond (ns) and recorded in blocks of 60 ns. The attributes of points, generated by Riegl’s software, were used to reconstruct the waveforms representing the points. The time stamp and scan angle of each emitted pulse, number of detected echoes from each received waveform, and the location, number, amplitude and width of each detected echo were extracted using the software. In the example shown below, there were four echoes detected in the return waveform (Table 3).

Table 3: The attributes of points extracted from the waveform by RiAnalyze

Time	Elevation	Amplitude	Echo width	Scan angle	Echo number	Number of echoes
303659.53909	60.243	11	4.5	22.118	1	4
303659.53909	57.949	13	4.4	22.118	2	4
303659.53909	56.853	19	4.0	22.118	3	4
303659.53909	55.522	14	4.4	22.118	4	4

The echo width provided by the software is the full width at half maximum (FWHM). This can be converted to the standard deviation of the Gaussian using the formula (Weisstein, 2009):

$$s = \frac{FWHM}{2\sqrt{2\ln 2}} \quad [15]$$

The derivation of the above equation is as shown in Appendix 2.

Table 4 shows the standard deviation of each echo in the return waveform.

Table 4: The standard deviation of each echo derived from the echo width

Echo number	Echo width	Standard Deviation
1	4.5	1.9110
2	4.4	1.8685
3	4.0	1.6986
4	4.4	1.8685

The distances between the points were calculated from the elevations and scan angle by dividing the elevations by the cosine of the scan angle, or using the x, y and z coordinates of the points. Taking the speed of light as $3 \cdot 10^8 \text{ m s}^{-1}$, the distance, in metres, was converted to time in nanoseconds [16]. Since the pulse had to hit the target and return to the receiver of the sensor, the total distance was taken as twice the distance between the sensor and the target.

$$t = \frac{2d}{3 \times 10^8 \times 10^{-9}} = \frac{d}{0.15} \quad [16]$$

where t is time in nanoseconds (ns) and d is distance in metres.

The initial time location was chosen arbitrarily for representation as 11. The cumulative distances of the targets from the initial time position were calculated (Table 5).

Table 5: The locations of the echoes derived from the distances between the points

Echo number	Elevation	Difference in elevation	Difference in time (corrected for scan angle)	Time position
1	60.243	0	0	11
2	57.949	2.2940	16.5082	27.5082
3	56.853	1.0960	7.8871	35.3952
4	55.522	1.3310	9.5782	44.9734

The waveform could then be approximated as:

$$\sum_{i=1}^n a_n * e^{-\frac{(t-t_i)^2}{2*s_i^2}}$$
[17]

Figure 10A-D show the echoes representing the first, second, third and fourth echoes of the waveform. Figure 10E shows the individual echoes separately and Figure 10F shows the waveform obtained when they were added together. The sampled raw waveform is shown in Figure 10G. In the decomposition process in RiAnalyze, a fifth echo of the lowest intensity seemed to be ignored in some cases (Figure 11A-C). There were also instances where two adjacent echoes very close to each other were merged into one (Figure 11D). In the majority of the cases, the waveform, reconstructed from the points, seemed to be a good approximation of the sampled raw waveform (Figure 12).

Only up to four echoes seem to be extracted from the waveforms. This leads to some loss of information. In one case, two narrow echoes were extracted as one echo (Figure 11D). Studies have shown that the majority of the waveforms with more than three echoes are usually from vegetation and, in some cases, it is possible to extract approximately 50% more points from the waveform than using proprietary software in forested areas (Chauve et al., 2007; Reitberger et al., 2008). However, this represents the variability within vegetation, than between vegetation and other land cover. Since the aim of the thesis is to classify the points into vegetation, road and buildings, the points, extracted using Riegl's software, are considered accurate enough for further analysis.

FULL-WAVEFORM DATASET FROM BRISTOL

The laser scanning data from eight flight paths were collected from the Avonmouth area in Bristol, using LiteMapper 5600 Airborne Lidar Terrain Mapping System in August 2006. The full-waveform ALS data were captured at a height of approximately 950 m above ground level, at a speed of 65 ms⁻¹ with a laser scanning pulse rate of 50 kHz. The average footprint size on the target at a height of 950 m at nadir with a laser beam divergence of 0.5 mrad is approximately 0.475 m (950 x 0.5 x 10⁻³). This varies with the range and incidence angle. For a flat surface at the maximum scan angle, the footprint might be elliptical with a major diameter of 55.64 cm (Baltsavias, 1999a). The study area was covered by the swath widths of four flight lines (Figure 13 A). The swath width for each scan line at 950 m height and scan angle range of 22.5° is about 787 m.

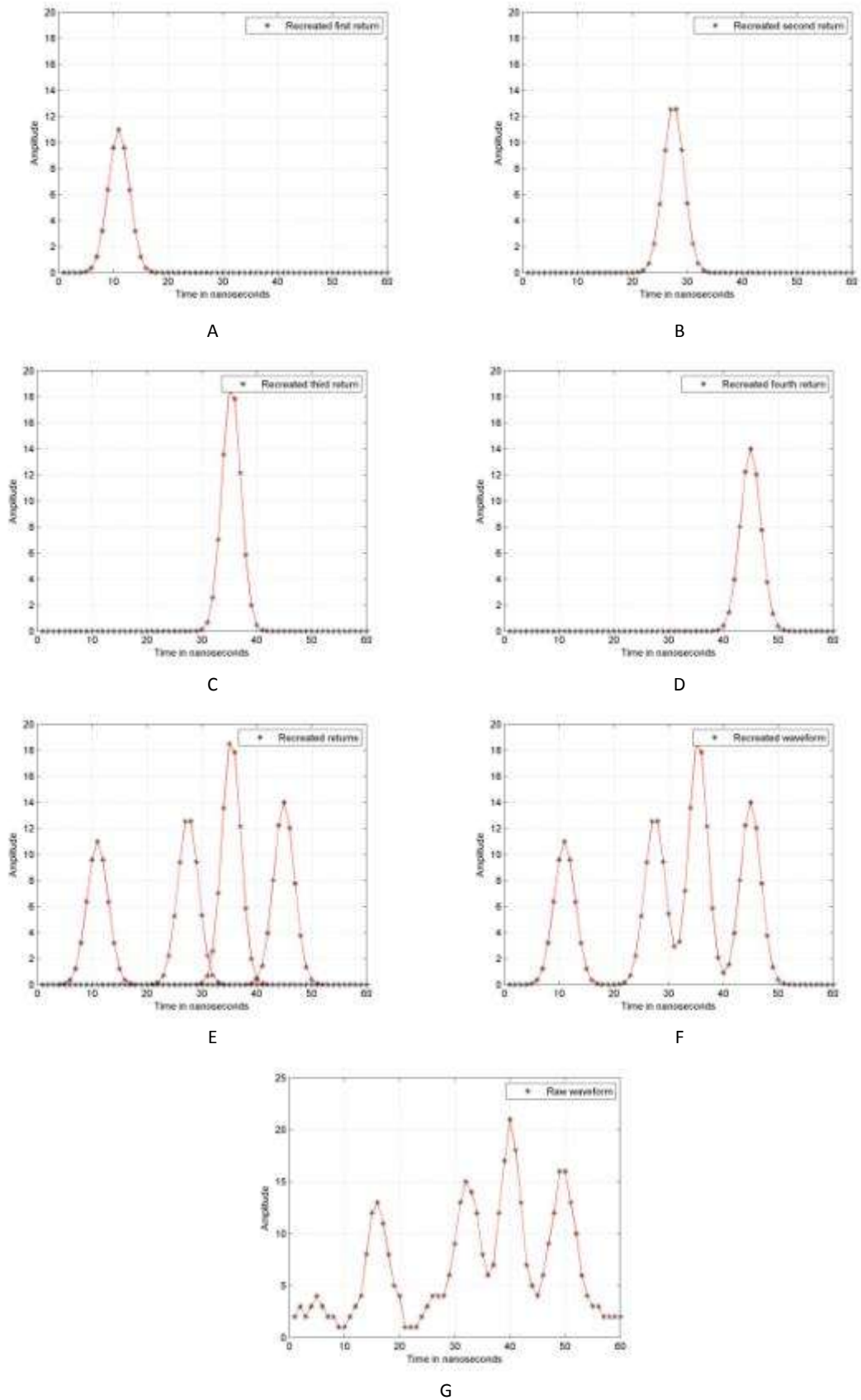
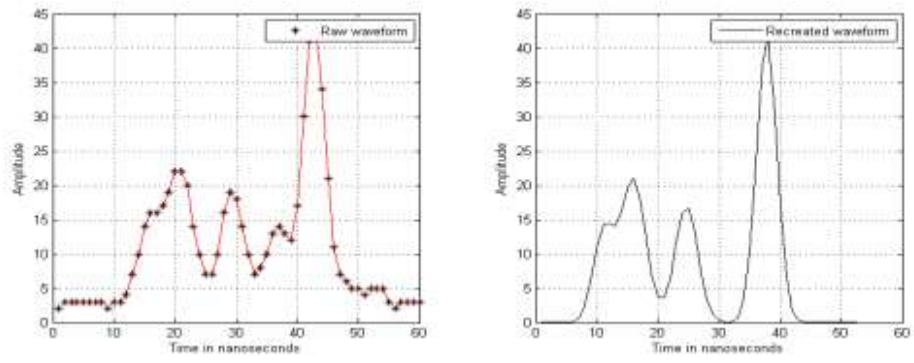
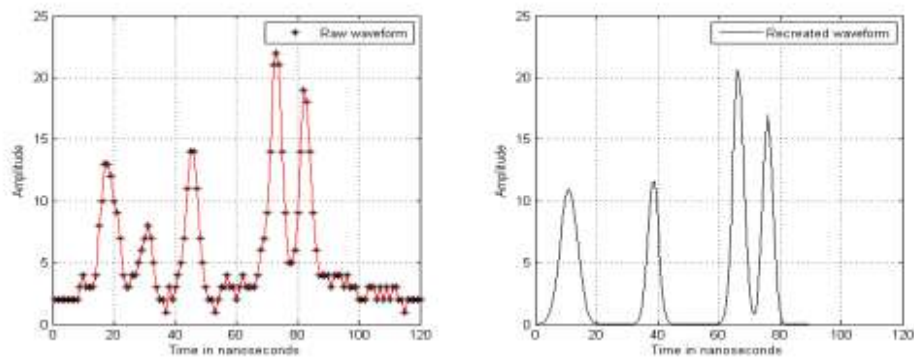


Figure 10: The echoes representing the (A) first, (B) second, (C) third and (D) fourth echoes of a return waveform, (E) the individual echoes shown separately and (F) the waveform obtained when they are

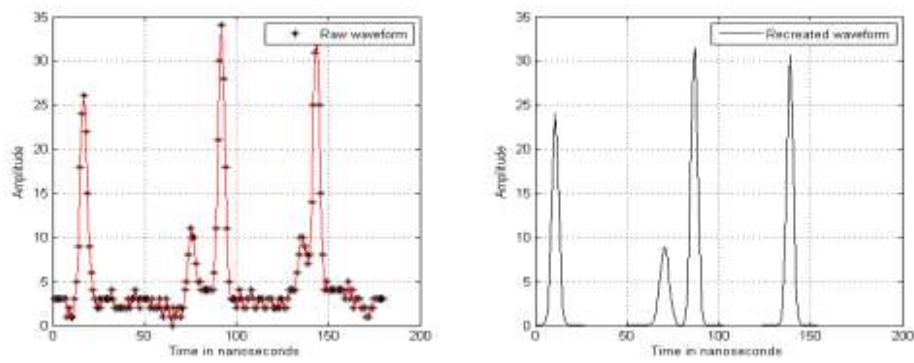
added together. (G) The sampled raw waveform is very similar to the reconstructed waveform in (F).
 (Note: The red lines in the figures connect the data points for better clarity.)



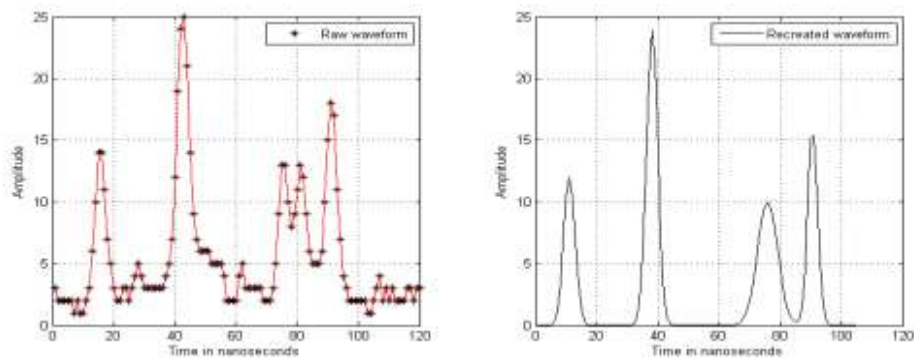
A



B



C



D

Figure 11: Examples of the raw waveforms (left) and the waveforms reconstructed from the attributes of the return echoes (right). A fifth echo of the lowest intensity seems to be ignored in the examples. (Note: There are slight offsets between the locations of the echoes in the reconstructed and raw waveforms, due to the value given for the position of the first echo in the reconstructed waveform.)

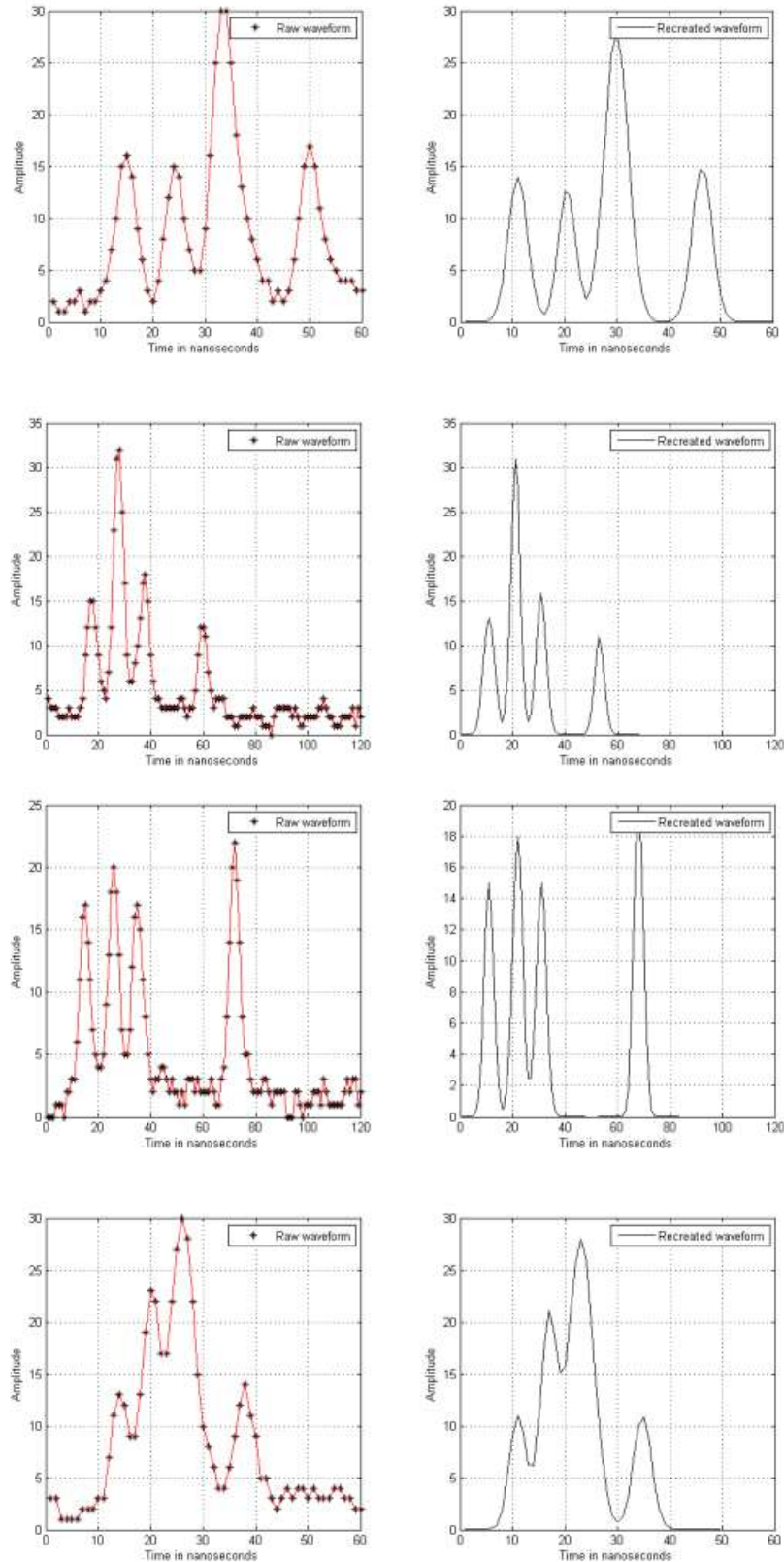


Figure 12: Examples of the raw waveforms (left) and the waveforms reconstructed from the attributes of the return echoes (right). The majority of the waveforms, reconstructed from the points, seem to be good approximations of the sampled raw waveforms. (Note: There are slight offsets between the locations of the echoes in the reconstructed and raw waveforms, due to the value given for the position of the first echo in the reconstructed waveform.)

FULL-WAVEFORM DATASET FROM BOURNEMOUTH

In Bournemouth, the full-waveform data were collected from a height of approximately 300 m and a maximum scan angle of 30°, in June 2008. The study area was covered by the swath widths of seven flight lines (Figure 13 B). The footprint diameter on the target collected from a flying height of 300 m at nadir is 0.15 m ($300 \times 0.5 \times 10^{-3}$). The major axis of the elliptical footprint at the maximum scan angle of 30° is about 15% longer, and the area is about 54% larger.

3.2.3. Discrete ALS Dataset

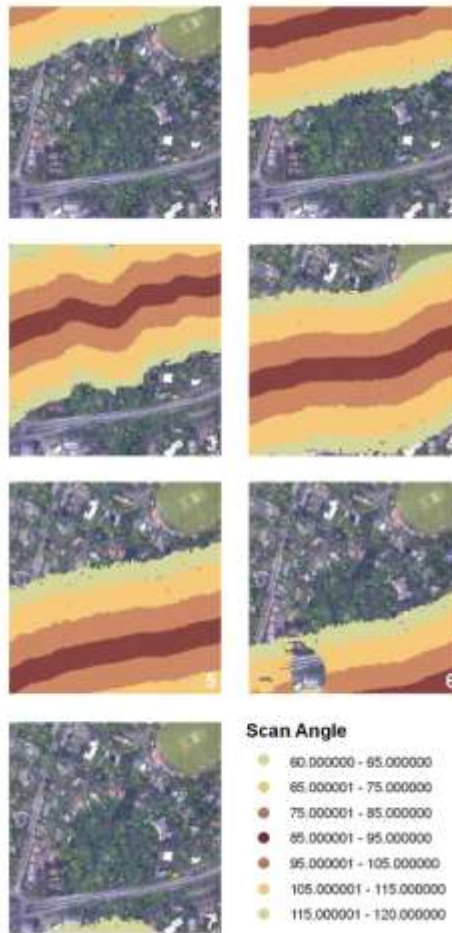
The discrete return data were collected in November 2004 using an Optech 2050 system that emits laser pulses of wavelength 1064 nm. The average flying height was 200 m and the maximum scan angle was 15°. There were 25,476,798 points, including first and last echoes, in the study area providing a point density of a little more than 25 points m^{-2} . For each point, information about the location – X, Y and Z – and intensity were available. The value referred to as intensity in discrete return data is often not well specified by the scanner manufacturers. Therefore, this could either be a specific amplitude of the return pulse, or the integral of the returned signal over the echo width (Höfle and Pfeifer, 2007). Hence, the term ‘amplitude’ is used in this study as an attribute for both full-waveform and discrete return data. A comparison of the above datasets is given in Table 6.

Table 6: Comparison of the three datasets used for the study – Full-waveform datasets from Bristol and Bournemouth, and discrete return dataset from Bristol

Datasets	1	2	3
Location	Bristol	Bournemouth	Bristol
Scanner	Riegl LMS-Q560	Riegl LMS-Q560	Optech 2050
Wavelength	1.55 μm	1.55 μm	1.064 μm
Technique	Full-waveform	Full-waveform	Discrete
Date of Collection	August 2006 (Leaf-on)	June 2008 (Leaf-on)	November 2004 (Leaf-off)
Average Flying Height	950 m	300 m	200 m
Footprint Diameter at nadir	0.475 m	0.15 m	
Maximum Scan Angle	22.5°	30°	15°
Approximate Point Density/ m^2	0.5 – 0.8	25	16



A



B

Figure 13: (A) Point data from four flight lines were used for the study in Bristol. The scan angles ranged from 67.5° to 112.5°. (B) In Bournemouth, point data from seven flight lines were used for the study.

The scan angles ranged from 60° to 120° (Aerial image and ALS data - Ordnance Survey © Crown Copyright. All Rights Reserved)

3.2.4. Data Exchange Format for ALS Datasets

Manufacturers of scanners have their own proprietary formats for recording data, and it is not easy for data to be transferred between systems and workflows. The LAS file format for exchange of lidar data between vendors and customers was proposed by the American Society for Photogrammetry and Remote Sensing (ASPRS). This is a binary format, and is an alternative to ASCII and proprietary file formats. The file sizes of LAS files are 35% to 80% smaller than ASCII files. The binary data format consists of a public header block, variable length records and point data with X, Y, Z, Intensity, etc. as attributes (Chen, 2007; Spatial Resources). The description of the data format is given in Appendix 1.

3.2.5. Other Datasets

The other datasets used in this study include aerial photographs, OS MasterMap® and StreetMapper data. Aerial photographs of the study area in Bristol are at a spatial resolution 0.2 m, while those of Bournemouth are at 0.05 m resolution. These were used in the visual analysis for generating the training and reference data.

OS MasterMap, hereafter referred to as MasterMap, is a digital geographic database product of Ordnance Survey (OS), the national mapping agency for Great Britain. MasterMap is organised in layers and provides topographic information on every landscape feature including buildings, roads, landmarks and vegetation. The positional accuracy requirement for MasterMap in urban areas is 1 m at a confidence level of 99% (Holland et al., 2006). MasterMap was used in this study for generating training and reference data, and for analysing the results.

In the study area in Bournemouth, data were collected using StreetMapper, a mobile vehicle-mounted laser scanner, in February 2008, to be used as reference data. StreetMapper uses laser scanning technology, along with an Inertial Navigation System, to scan roads, buildings and trees from a moving vehicle. It has the ability to capture up to 40,000 3D points per second while the vehicle is in motion. The manufacturer claims a positional accuracy better than 1 m, typically 5 mm for good GPS conditions (3DLM, 2009).

3.3. Broad Methodology

The points extracted from the full-waveform data from Bristol are classified into vegetation, buildings and roads, based on the attributes of individual points and the relationships between neighbouring points. The accuracy of the classification is assessed using reference data. This is described in detail in Chapter 4.

The discrete return data points from Bristol are classified using methods similar to the one used for full-waveform data. The classifications from the two datasets are compared to estimate whether there are any advantages of using full-waveform data for land cover classification, which is described in Chapter 5.

The points extracted from the full-waveform dataset in Bournemouth are classified using the classifier developed using the dataset from Bristol. The accuracy of the classification in Bournemouth is assessed. The classifier is refined to make it more useful when used in different areas. This objective of the research is addressed in Chapter 6.

The first three objectives deal with the classification of ALS points. However, the point cloud data have limited use in a topographic database. Although urban environments contain a variety of elements in complicated spatial patterns, man-made features such as buildings and roads have clear edges. They are therefore easier to represent in GIS-based topographic databases than vegetation that is often fragmented, with unclear boundaries. The points are aggregated at different scales to extract meaningful information from the data, which could be represented within a database. This is described in detail in Chapter 7. The broad methodology for achieving the four objectives is shown in the flow chart (Figure 14).

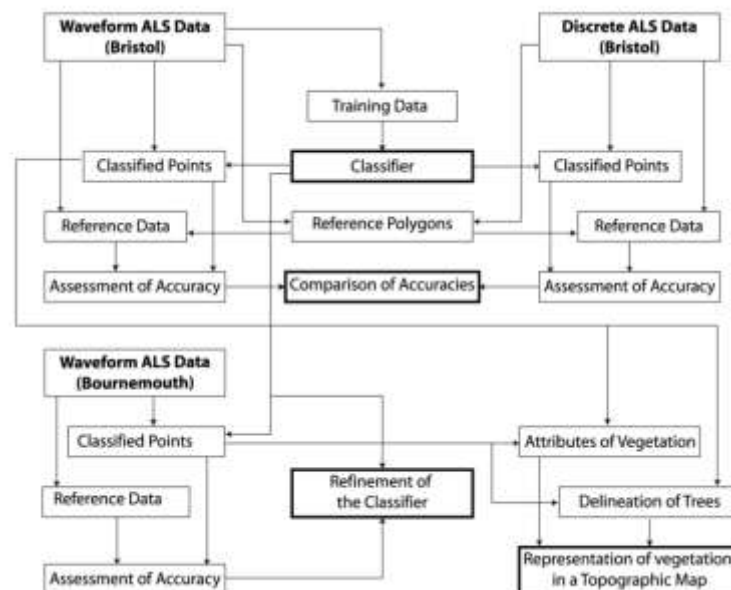


Figure 14: Workflow for achieving the objectives of the thesis

3.4. Summary

Full-waveform datasets from Bristol and Bournemouth, and a discrete return dataset from Bristol are used for this research. The full-waveform datasets are converted to point clouds, using commercial software, for analysis and classification. The classification method is developed using the full-waveform dataset from Bristol, and applied on the discrete return dataset from the same area for comparison of the accuracies. The method is also applied on the full-waveform dataset from Bournemouth to refine the classifier for increasing the transferability of the method.

This chapter gave a brief description of the datasets, software and broad methodology. The methodology used and the results obtained for achieving the four objectives are described in the next four chapters. The first objective, classification of laser scanning points, is addressed in the next chapter.

4. Classification of Airborne Laser Scanning Points

This chapter addresses the first objective - to explore techniques for the classification of features in an urban environment using full-waveform ALS data. The points, extracted from full-waveform data, are classified into vegetation, buildings and roads. A decision tree classifier is shown to perform significantly better than k-means clustering.

4.1. Introduction

Data mining techniques are used to uncover interesting patterns that are often hidden in large datasets. Classification, a predictive data mining task, can be defined as the process of finding a model that describes data classes so that it can be used to predict the class of objects whose class label is not known. The model can be derived from the analysis of data objects whose class label is known, namely the training data. Classification rules, decision trees, neural networks and support vector machines are a few of the ways in which the model can be represented (Han and Kamber, 2006).

The majority of the classification algorithms for ALS data work in the raster domain. The conversion of the points to raster format could introduce errors due to interpolation, or reduce the information content. Hence, the original point data themselves are used in this research for classification.

From the studies listed in Table 2, it can be seen that decision trees have been successfully used in the classification using full-waveform ALS data in urban areas. However, their emphasis was more on vegetation than roads and buildings, which are also an integral part of the urban landscape (Ducic et al., 2006; Rutzinger et al., 2008). Parametric methods have also been used for classification using discrete ALS data (Charaniya et al., 2004; Miliareisis and Kokkas, 2007). Many studies use aerial imagery in addition to ALS data (Charaniya et al., 2004; Matikainen et al., 2007). In this study, k-means clustering, a statistical method, and decision trees, a logical method, are used for classification using ALS data alone (Kotsiantis, 2007). The k-means clustering is based on the assumption that the populations of each group are normally distributed. Decision trees offer a non-parametric alternative and do not require such assumptions or simplifications.

The selected categories for classification are based on those used in Charaniya et al. (2004). They classified the data into trees (coniferous and deciduous), grass (green and dry), roads (asphalt roads, concrete pathways and soil) and roofs. In this study, building roofs are subdivided into flat and pitched, as the slope of the roof surface can be derived from the elevation data in ALS (Alexander et al., 2009). A height value of 2.5 m has been used to distinguish trees and building roofs from other classes (Matikainen et al., 2007). Artificial or natural ground surface, road and grass, should be almost at the same height as the DTM. However, a height of 0.5 m was selected to account for the inaccuracies, which could be introduced by the coarse DTM with a 10 m resolution. Based on the estimated height from the terrain, vegetation was sub-divided into low (< 0.5 m), medium (0.5 - 2.5 m) and high (> 2.5

m), hereafter referred to as grass, shrubs and trees. In the decision tree classifier, the normalised elevation in the training data was also classified into three, based on the above.

4.2. Methodology

Attributes of individual points as well as attributes based on the spatial relationship of direct neighbour points were used in the classification process. Local statistical variation of grid cells has been used for separating buildings from other surfaces (Alharthy and Bethel, 2002). It might be possible to obtain similar results from variation of attributes of TIN triangles attached to a point. TIN was used for deriving the spatial attributes, as they honour the values of elevation at point locations, and are therefore more precise than a grid.

The points were initially classified by k-means clustering using all the attributes. Principal components and canonical components analyses were then used to reduce the number of attributes, and clustering was performed on these transformed data. A decision tree was constructed using points from training polygons, and used for classifying all the points. The accuracies of the two methods – clustering and decision tree - were then compared.

Variation of slopes and aspects of attached TIN triangles were used to analyse whether the different surfaces could be separated. The parameters considered were average and standard deviation of slopes and aspects. Out of these, the average aspect was found to be of little use since even flat surfaces could have minor differences in their aspects. Height variation was another attribute derived from the elevation, which is a measure of the roughness of the surface. This attribute was seen to be more useful than standard deviation and absolute deviation from the mean of elevations within a window in the case of rasterised data by Charaniya et al. (2004). The height variation was calculated as the range of elevations, of nodes of the TIN triangles attached to a point.

4.2.1. Pre-processing

The raw waveforms were decomposed using the standard method, Gaussian Pulse Fitting, available in the commercial package RiAnalyze560. RiWorld 560 was used to transform the data into WGS Cartesian coordinates. The dataset was transformed to British National Grid, using Grid InQuest (Quest, 2009), before further analysis. The point density ranged from 0.5-0.8 points m⁻² for each flight line.

All the echoes were used for the analysis, which along with the overlapping swath widths of the flight lines generated above 1,000,000 points giving an average point density of

approximately 1 point m⁻². The number of echoes denotes whether the point is one of a single, two, three or more hits of a single emitted pulse. 94.32% of the points were first echoes, 5.4% were second echoes, 0.28% third echoes and 0.06% fourth echoes. 88.97% of the points were single echoes, and only one point was a fifth echo.

4.2.2. Exploratory Data Analysis

Amplitude, elevation, echo width, echo number and the number of echoes are the attributes of individual points extracted from the full-waveform data. The maximum amplitude of an echo is a measure of the strength of the return pulse. The echo width refers to the FWHM amplitude of the echo in the Gaussian decomposition. Figure 15A shows the amplitude and width of the first echo from a return with two echoes. This means that distinct echoes could be obtained from two surfaces within the footprint of the emitted laser pulse. Unless the laser beam hits the ground vertically, it is possible to represent the multiple echoes as points in GIS software for further analysis. Figure 15B shows how multiple echoes from an emitted pulse can be understood as echoes from two different surfaces. The scan angle of the emitted pulse was 13°.

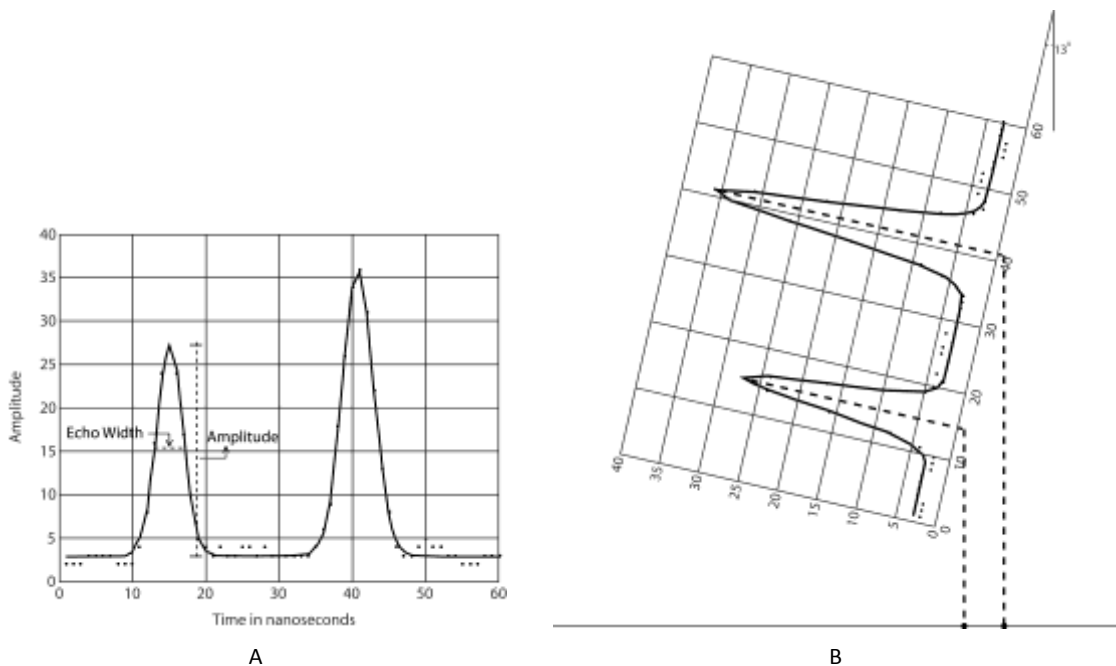


Figure 15: (A) Amplitude and width of the first echo from a return with two echoes. (B) Multiple echoes from a single pulse emitted at an angle of 13° from vertical represented as separate points on the horizontal plane, having x, y and z coordinates.

A few samples of waveforms from vegetation, buildings and roads were visually analysed. It could be seen that echoes received from trees often, though not always, consisted of complex waveforms, which could be decomposed into multiple echoes (Figure 16). The waveforms

from buildings did not follow a definite pattern. This could be due to a variety of reasons including different roofing materials, scan angles, slopes, echoes from building edges and features such as chimneys. Although the majority of the echoes from roads and grass were single, the amplitudes of the waveforms from grass were higher than those from roads were.

Elevation is useful in distinguishing buildings and trees from the terrain (Figure 17 A). However, the slope of the terrain makes it difficult to classify objects, and there does not seem to be a major difference between road and natural ground cover. The road can be clearly seen using amplitude (Figure 17 B & Figure 18 A). Since the echo width of the transmitted pulse of Riegl LMS-Q560 is 4ns, the echo width of the return waveform from a flat surface at the nadir (scan angle 90°) is also likely to be approximately 4 ns. For a single target which gives a uni-modal echo, any increase, or decrease, in the echo width would indicate a slope of the surface, a scan angle other than 90° or surface roughness (Hug et al., 2004). The echo width (Figure 17 C & Figure 18 B) and the number of echoes seem to be higher for vegetation than for other surfaces (Figure 17 D & Figure 18 C).

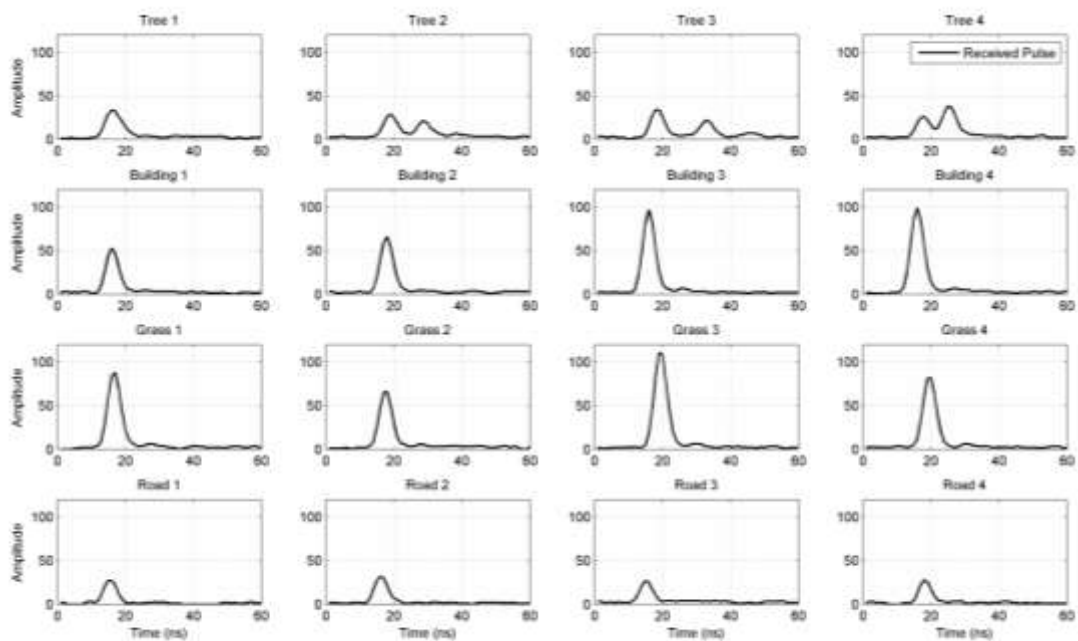
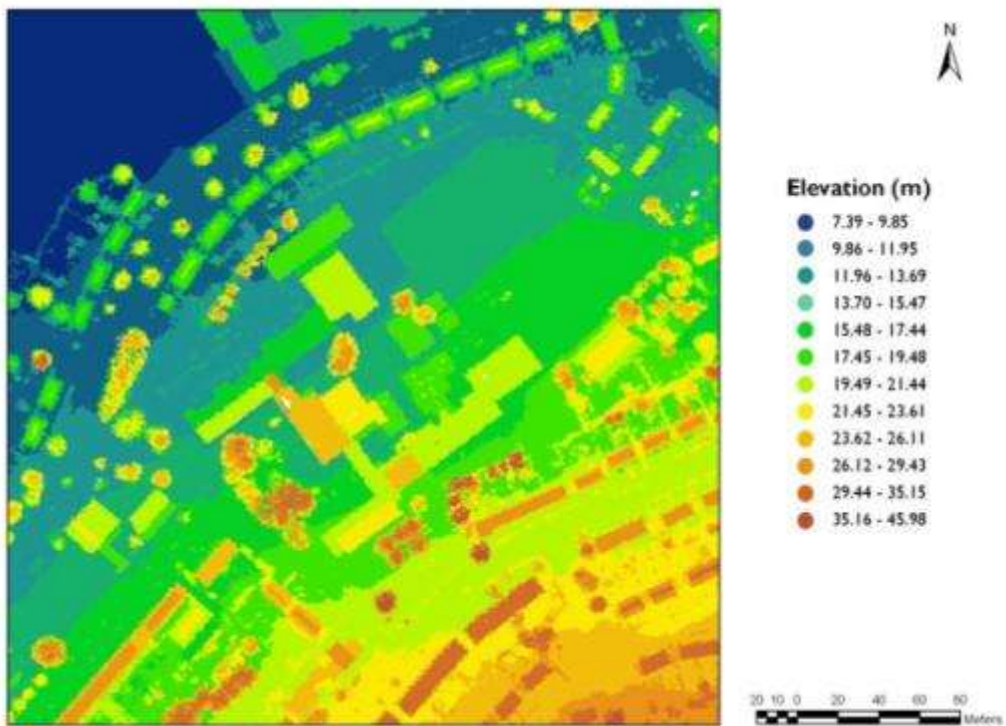
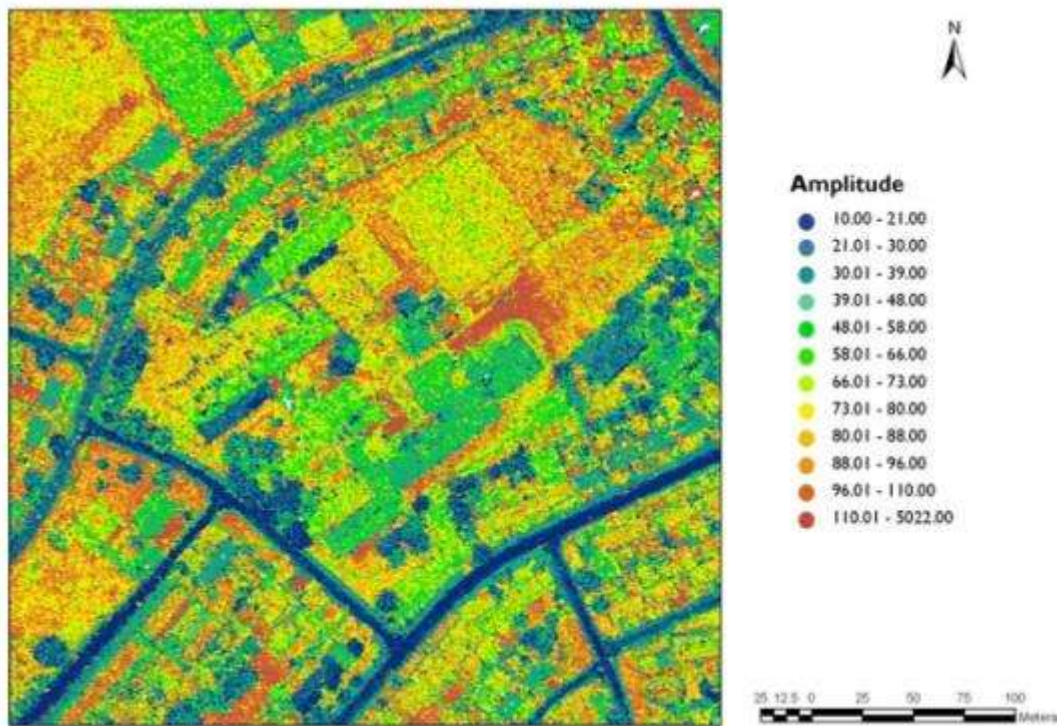


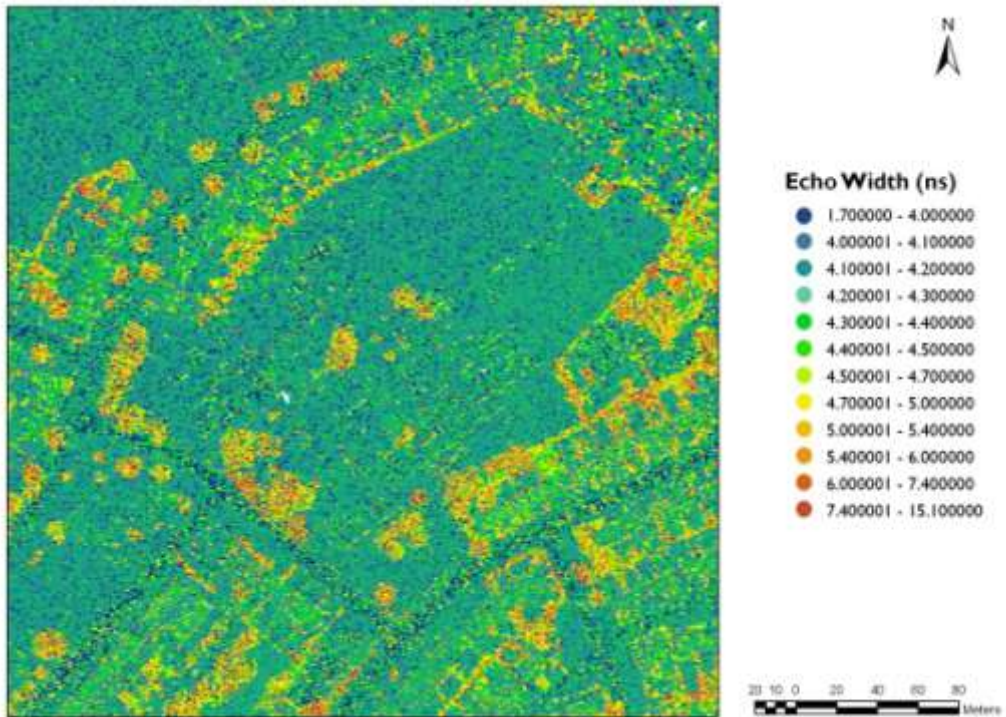
Figure 16: Samples of raw waveforms from trees, buildings, grass and roads



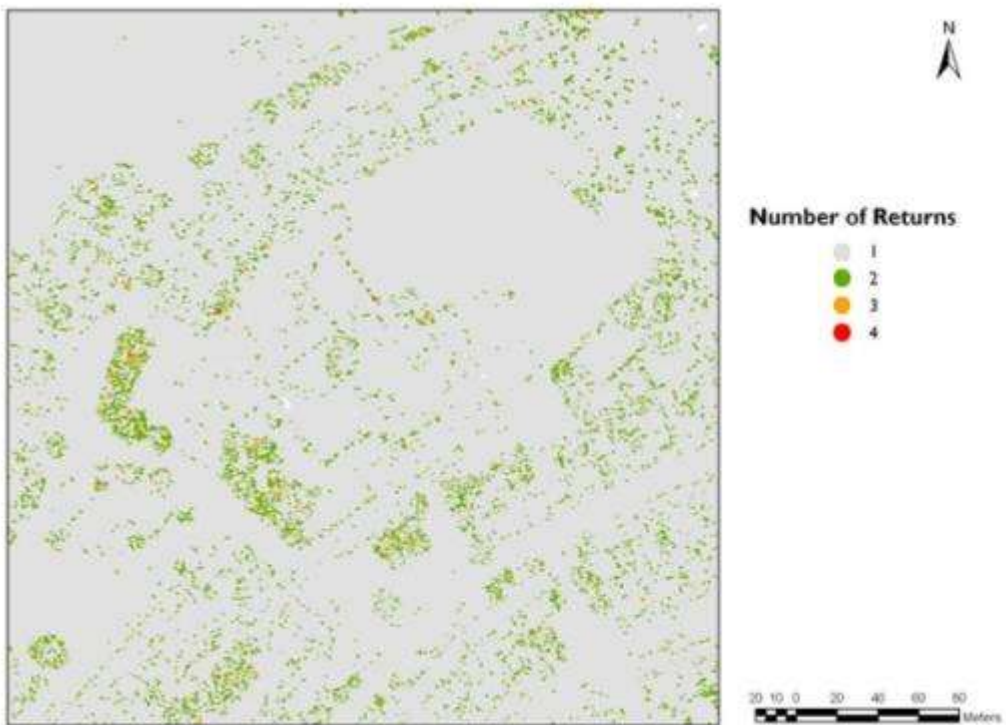
A



B

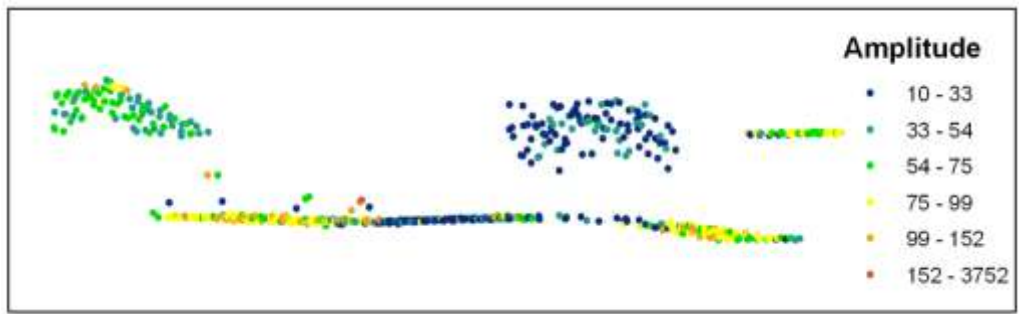


C

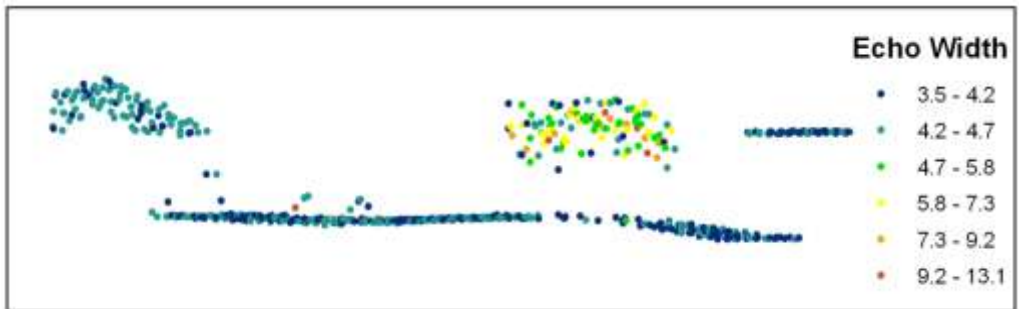


D

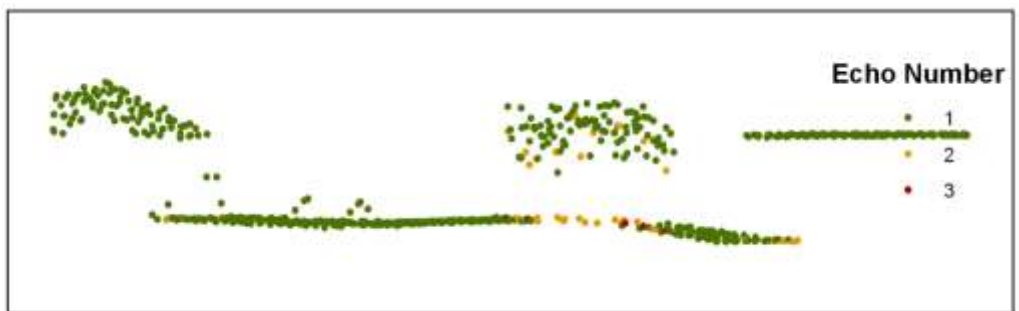
Figure 17: ALS Points displayed by (A) elevation in metres, (B) amplitude, (C) echo width in nanoseconds and (D) number of echoes for a subset of the study area (Ordnance Survey © Crown Copyright. All Rights Reserved)



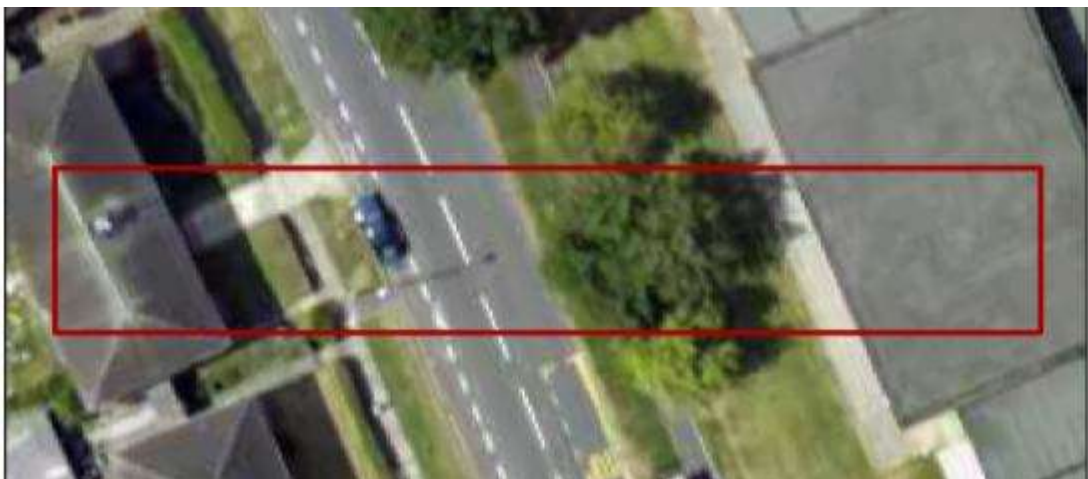
A



B



C



D

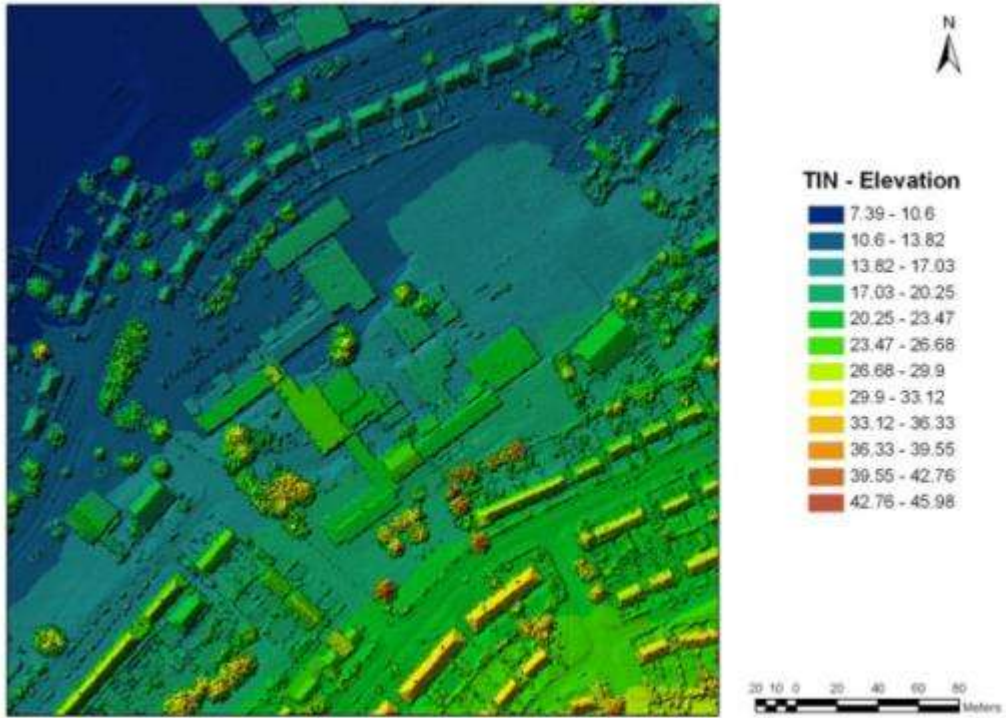
Figure 18: (A) Amplitude, (B) echo width and (C) echo number of the points within the rectangle marked in (D) (Ordnance Survey © Crown Copyright. All Rights Reserved)

4.2.3. Deriving Additional Attributes of Points from Elevation

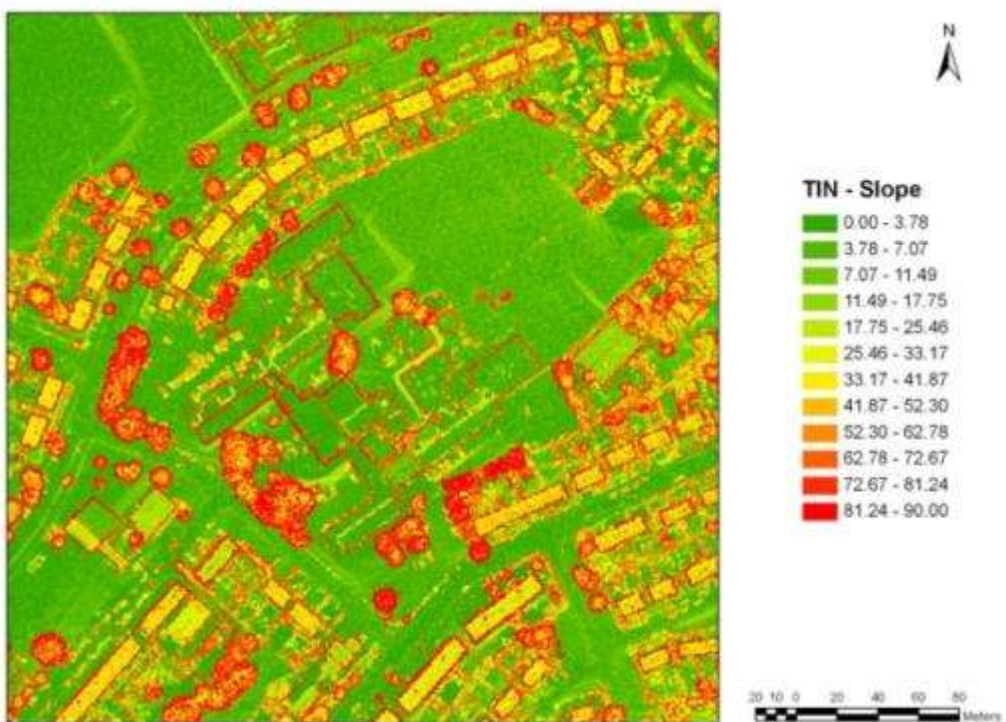
The spatial relationships between neighbouring points were based on a TIN, which was created from the elevation of all the points. The slopes of the triangular surfaces seem to be high for trees and building edges (Figure 19 A&B). The aspects are similar for each sloping surface for pitched roofs (Figure 19 C). The wave patterns in the aspect image seem to be a result of the overlaying of data from two flight lines (Figure 21). The data points from a single flight line are evenly spaced for scanners using polygon mirrors. When two flight lines are overlayed, there could be larger variations between the slopes and aspects of adjacent triangles due to the uneven spacing of points. This effect would also depend on the accuracy of elevations from the different flight lines. The TIN was converted to polygons, with slope and aspect as attributes, so that an intersection of the points and the triangular polygons could be created. This was done so that the average attributes of the connecting triangles could be assigned to the points.

Each point in this intersection file appeared in the attribute table as many times as there were TIN triangles attached to it. For example, if a point were attached to seven TIN triangles, it would appear seven times in the attribute table (Figure 20). From the attribute table of this file, a summary table was generated based on the unique identifier (id) of the TIN triangle, to calculate the minimum and maximum elevation of points constituting each triangle. This was joined to the original attribute table. The second table, based on the id of each point, calculated the average and standard deviation of slopes and the standard deviation of aspects of the TIN triangles attached to every point. It also calculated the minimum of the minimum elevation values and the maximum of the maximum elevation values in the joined table in addition to the average of all other attributes. The minimum of the minimum elevation values were now subtracted from the maximum of the maximum elevation values to obtain the height variation as an attribute of the point.

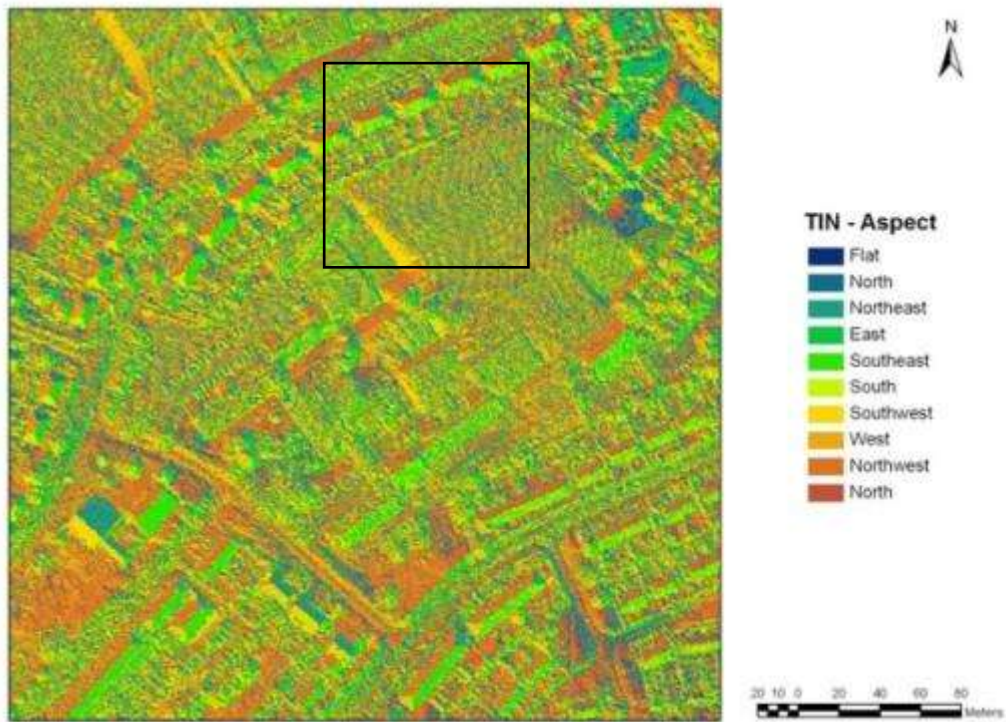
The height of points from the ground can be useful in distinguishing different surfaces. A rough DTM was therefore created from the elevation of ALS points, making use of the lowest point in a 10 m grid. A TIN was created from these points. The terrain elevation obtained from this TIN surface was subtracted from the elevation of each point to obtain an estimate of the normalised elevation.



A



B



C

Figure 19: The Triangulated Irregular Network (TIN) created from the ALS points displayed by (A) elevation, (B) slope and (C) aspect

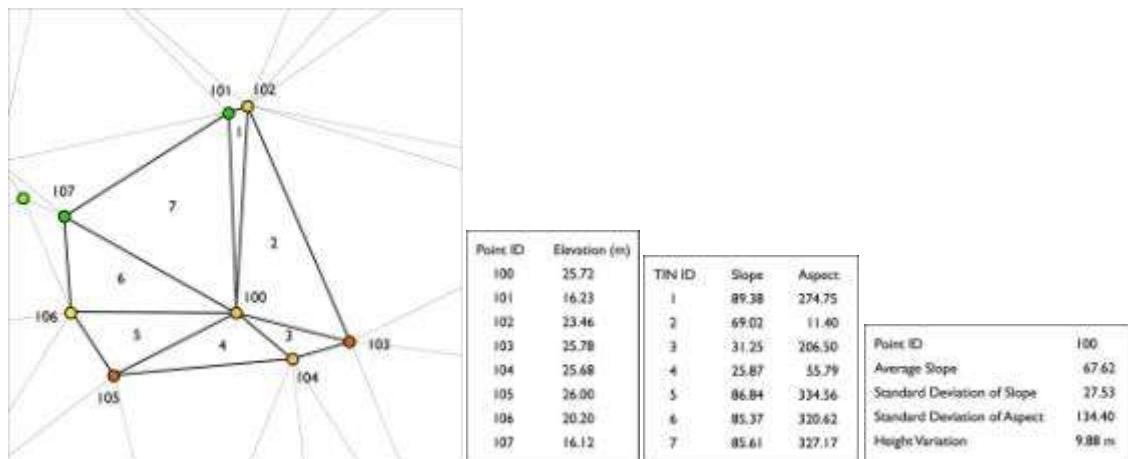


Figure 20: TIN triangles connected to the point with ID 100. The elevations of each point connected to it by the TIN triangles, the slopes and aspects of the attached TIN triangles and the derived attributes of the point are shown in the tables.

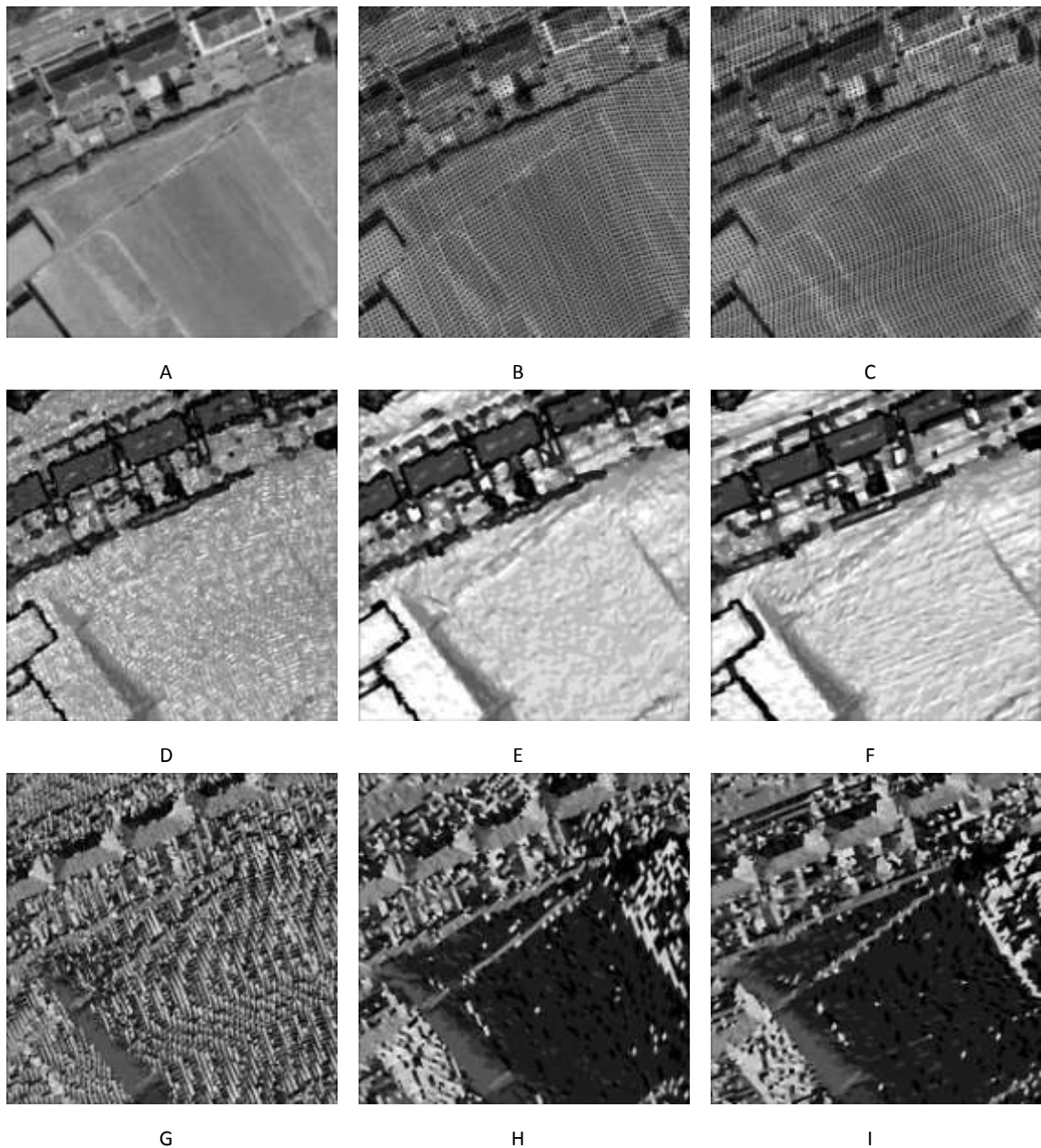


Figure 21: An aerial image of the area (A); ALS points from Flightline 1 (B) and Flightline 2 (C); Slope of TIN from the points from both the flightlines (D); Slope of TIN from the points in Flightline 1 (E) and Flightline 2 (F); Aspect of TIN from the points from both the flightlines (G); Aspect of TIN from the points in Flightline 1 (H) and Flightline 2 (I). (Aerial image and ALS data - Ordnance Survey © Crown Copyright. All Rights Reserved)

The workflow of the process for the derivation of the attributes is shown in Figure 22. The recorded and derived attributes of the points extracted from full-waveform data are used in the classification process in the following sections.

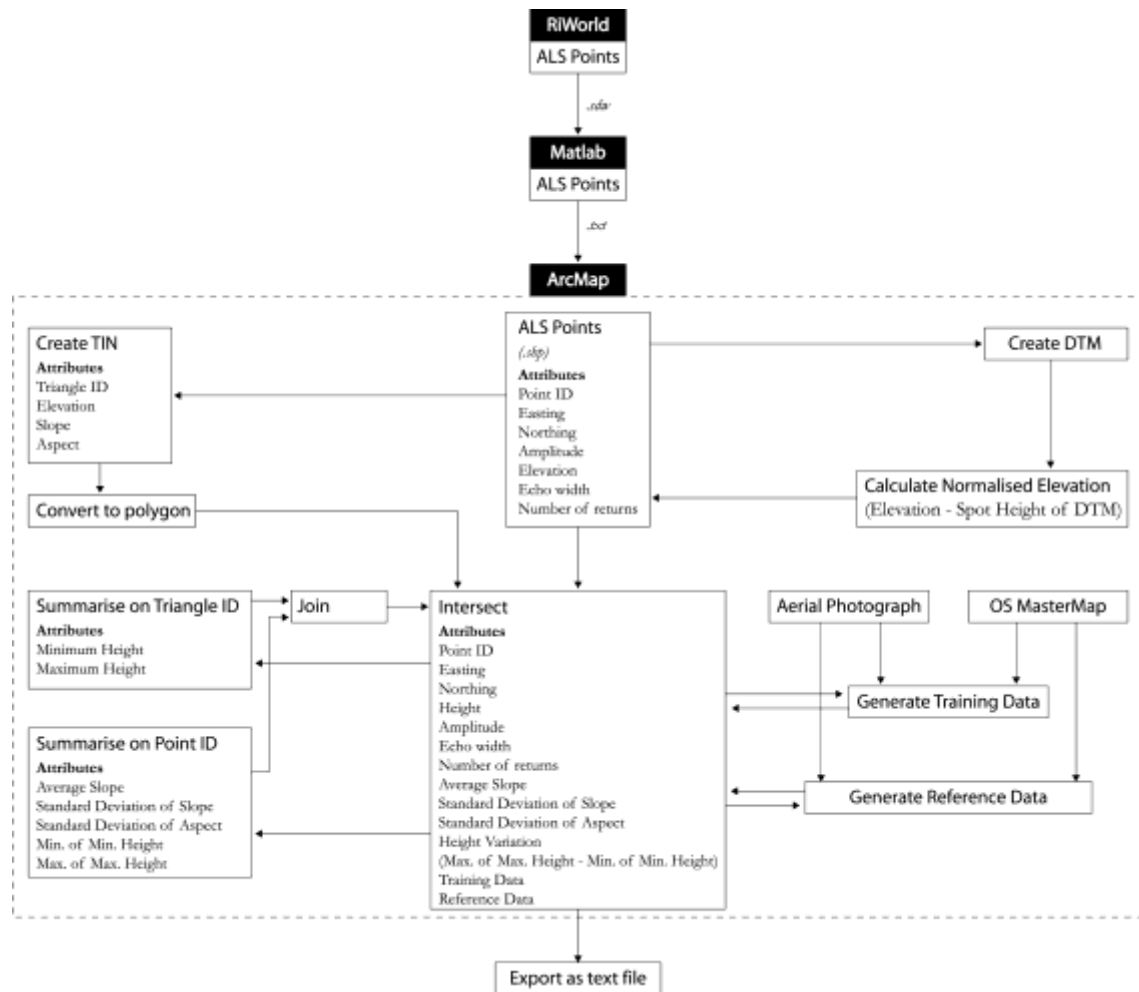


Figure 22: Workflow for the derivation of additional attributes for the full-waveform ALS data to be used in the classification process as shown in Figure 25.

4.2.4. Creation and Analysis of Training Data

The training polygons were manually delineated using the attributes of the ALS points, MasterMap and an aerial image into the six land cover classes (Figure 23). The attributes of points within the training polygons representing the different classes could now be analysed.

Box-and-whisker plots (Tukey, 1977) were used to analyse the various attributes grouped into categories. The lower and upper limits of the box, in the plot, represent the lower quartile and upper quartile values. The median is plotted within the box. The whiskers, or lines extending from each end of the box, show the extent of the rest of the data. The default extents are 1.5 times the inter-quartile range from the lower and upper quartiles. In case these values are

beyond the actual limits, the values at the minimum or maximum are taken as the extents. Outliers are data with values beyond the ends of the whiskers. The box-and-whisker plots were used for analysing the attributes within the training polygons to aid the interpretation of data. Scatter plots of the attributes, grouped by the land cover classes, were also generated to analyse the inter-relationships between the attributes.

4.2.5. Classification of Points by Clustering

Cluster analysis group objects into clusters or groups based on the similarity of their attributes. There are many algorithms for clustering and it is difficult to categorise them. Some of the major clustering methods are partitioning, hierarchical, density-based, grid-based and model-based methods. It is possible to try different algorithms or variations of algorithms to extract hidden information from data (Han and Kamber, 2006).

The k-means algorithm is a popular partitioning method, and is suitable for clustering large amounts of data. It partitions the data into k mutually exclusive clusters in a c -dimensional space where c is the number of attributes used in the classification process (Mathworks, 2008b; Miliareisis and Kokkas, 2007). The required number of clusters, k , has to be provided by the user. Before any classification, the attribute values were transformed using z-score to standardise the differing value ranges of the attributes. In z-score transformation, the mean of the attribute values is subtracted from the data value and the resulting value divided by the attribute's standard deviation. The ALS points were classified using four options with slight variations in the k-means clustering method, described in the following paragraphs.

In the first option, the number of clusters and the cluster centres in the training dataset were estimated using subtractive clustering. The range of influence of the cluster centre has to be specified for each dimension in terms of the fractions of the widths of the data spaces of the attributes. Ranges of influence between 0.2 and 0.5 are considered to be optimal, where a value of 0.5 would mean that the range of influence is half the width of the data space for the particular attribute (Mathworks, 2008a). Here, ranges of influence of 0.2, 0.3, 0.4 and 0.5 were considered, resulting in twelve, seven, four and three estimated clusters respectively. Twelve clusters were considered for further work since it would be easy to re-classify these into the six land cover classes.

The cluster centres generated by the subtractive clustering were used as initial cluster centroid positions for the k-means classifier (seed points) in order to avoid randomly chosen locations. The k-means clusters were then re-classified into the six land cover classes based on their proximity to the mean of the attribute values for the different classes in the c -dimensional

space. This was done by a k-means classification of the centroid locations, with six as the desired number of classes and the attribute value means as the seeds. In the second option, the means of the attribute values for the various classes in the training dataset were selected as the seed points.

The third option made use of principal components. There is redundancy in the information content as shown by the high correlations between some variables in the dataset (Table 7). The average slope has a high correlation, above 0.7, with the height variation and the height. Principal components analysis is a method to reduce this redundancy by generating a new set of variables. All the principal components are orthogonal to each other and each component is a linear combination of the original variables. The first four principal components of the data were seen to represent 76.1% of the total variance of the original data, and were classified using k-means clustering. As in the first option, the number of clusters was determined by subtractive clustering. Six clusters were identified, and the k-means classification was done using the mean attribute values of the transformed dataset as seed points. The six clusters were reclassified into the six land cover classes as earlier based on their proximity.

Table 7: Matrix showing correlation coefficients of the eight attributes used for classification

	Amplitude	Width	Height	Av-slope	Std-slope	Std-aspect	Ht-var	Num
Amplitude	1							
Width	-0.3	1						
Height	-0.28	0.34	1					
Av-slope	-0.43	0.38	<u>0.75</u>	1				
Std-slope	-0.19	0.29	0.45	0.44	1			
Std-aspect	-0.13	0.05	-0.09	-0.03	0.02	1		
Ht-var	-0.38	0.29	0.54	<u>0.77</u>	0.26	0.04	1	
Num	-0.4	0.07	0.28	0.57	0.12	0.07	0.42	1

In the fourth option, canonical components were used for the classification. Canonical components are considered more appropriate when there is prior information about the features of interest (Lillesand et al., 2004). The canonical variables are linear combinations of the original variables, chosen to maximise the separation between groups. In other words, it is similar to principal components, but also uses the attributes from a training dataset to determine the linear combinations. Among all possible linear combinations, the first canonical variable has the maximum separation between groups. The second canonical variable has the maximum separation subject to it being orthogonal to the first, and so on. 99% of the variances within the data are included in the first three canonical components (Table 10). The

first three canonical variables were therefore used for the k-means classification, and the means of the canonical variables were chosen as the seed points for clustering.

4.2.6. Classification of Points using a Decision Tree

A decision tree can handle high dimensional data, and is appropriate for exploratory knowledge discovery. It automatically selects the most useful attributes from a large number of attributes given as input, and is easy to understand. A decision tree has a structure similar to a flow chart, beginning at the root node, where each internal node denotes a decision node or a test on an attribute. Each branch is an outcome of the test with the terminal leaf nodes holding the class labels. Some algorithms for generating decision trees, such as the Classification and Regression Trees (CART) algorithm developed by Breiman et al. (1984), produce only binary trees where each internal node branches into exactly two other nodes. A splitting criterion is used at each decision node that separates the data into individual classes. It indicates the splitting attribute and the split-point that 'best' splits the data. It is determined so that the partitions at each branch are as 'pure' as possible, or belong to the same class as much as possible (Han and Kamber, 2006; Larose, 2004; Matikainen et al., 2007).

The decision tree that is automatically generated by the classifier can over-fit the training data. It usually contains many branches that reflect the anomalies in the training data due to noise or outliers. Tree pruning is a method to reduce the over-fitting of data by removing the least reliable lower branches using statistical methods. The two common approaches to tree pruning are pre-pruning and post-pruning. In pre-pruning, a tree is pruned by deciding not to split a tree further. In post-pruning, a fully grown tree is pruned by removing sub-trees, replacing branch nodes with leaf nodes. Pruned trees are smaller, less complex, easier to understand, and faster and better at correctly classifying test data, which were not used for training (Han and Kamber, 2006).

In this study, the decision tree was pruned using the post-pruning method. Pruning level 0 corresponds to the full tree. At each pruning level, a tree segment is taken out, or pruned, based on an optimal pruning scheme that first prunes branches giving less increase in error cost. A ten-fold cross-validation method is used to find the 'best' pruning level based on the misclassification costs. In this method, the dataset is partitioned into ten random subsamples. For each subsample, a tree is fitted to the remaining data, which is then used to predict the subsample. This is used to derive an optimum level of pruning for the decision tree (Mathworks, 2008b).

A decision tree was generated using the training dataset for classifying the ALS points into the six classes. The attributes – amplitude, echo width, height class, average slope, standard deviation of slopes, standard deviation of aspects, height variation and the number of echoes – were used as the input for generating a decision tree, with maximum deviance reduction as the splitting rule. This created a decision tree with a large number of nodes, which clearly over-fitted the training dataset.

The ‘best’ level for pruning suggested by the program appeared to change with each trial due to the random selection of the subsamples. The mode of the best pruning level out of a hundred was therefore selected. The original decision tree contained 491 nodes, which was pruned to 31 nodes with a pruning level of 23. This decision tree was used to classify the original dataset. In a decision tree, the upper decision branches use the most important attributes. The importance of the attributes was further analysed by taking out one attribute at a time and testing the accuracy of the classification, maintaining similar number of nodes for the decision tree.

Land cover maps were generated using the various classification methods. Some of the misclassifications become evident on visual analysis, and some by comparing with MasterMap polygons and aerial photographs. Thiessen polygons were generated around all the points classified using the decision tree classifier. The polygons representing each class were merged together to form larger polygons representing the six land cover classes.

4.2.7. Assessment of Classification Accuracy

Reference data were generated from a subset of the study area using the ALS data themselves, an aerial photograph, and MasterMap (Figure 24). Since the training polygons were delineated mostly from ‘pure’ data, the edges and height jumps in flat roofs and edges, ridges and features such as chimneys in pitched roofs were not included for buildings. The reference data contains parts of roofs and level differences within buildings. The road polygons in the training data included only main roads, while the reference data includes main roads and parking areas. The classes generated by the different methods for all the points within the reference polygons were compared with the manually delineated classes, to assess the accuracies of classification. The workflow of the classification process is shown in Figure 25.

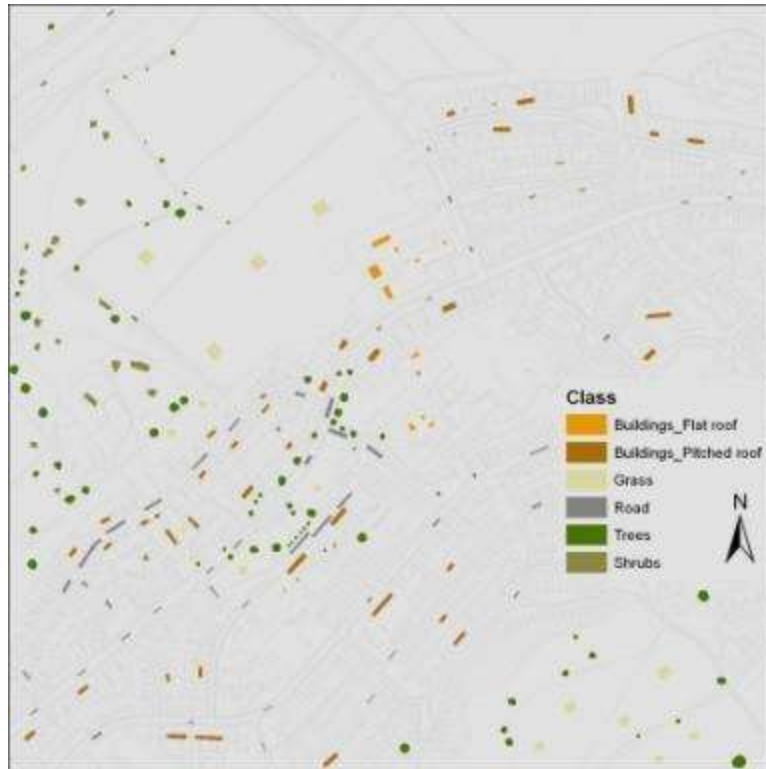


Figure 23: Polygons used for selecting the points within them to be used as the training data in Bristol (OS MasterMap - Ordnance Survey © Crown Copyright. All Rights Reserved)

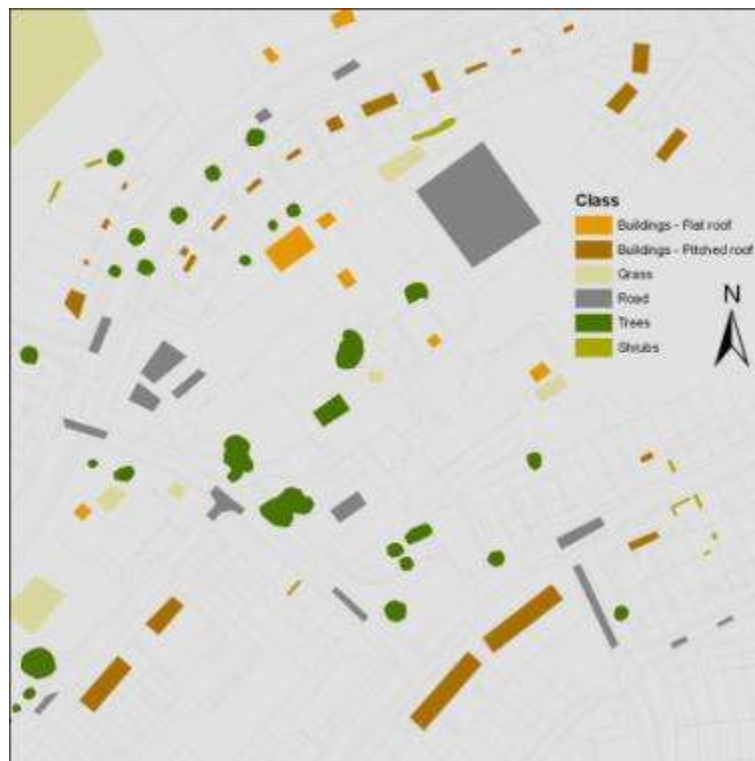


Figure 24: Polygons used for selecting the points within them to be used as the reference data in Bristol (OS MasterMap - Ordnance Survey © Crown Copyright. All Rights Reserved)

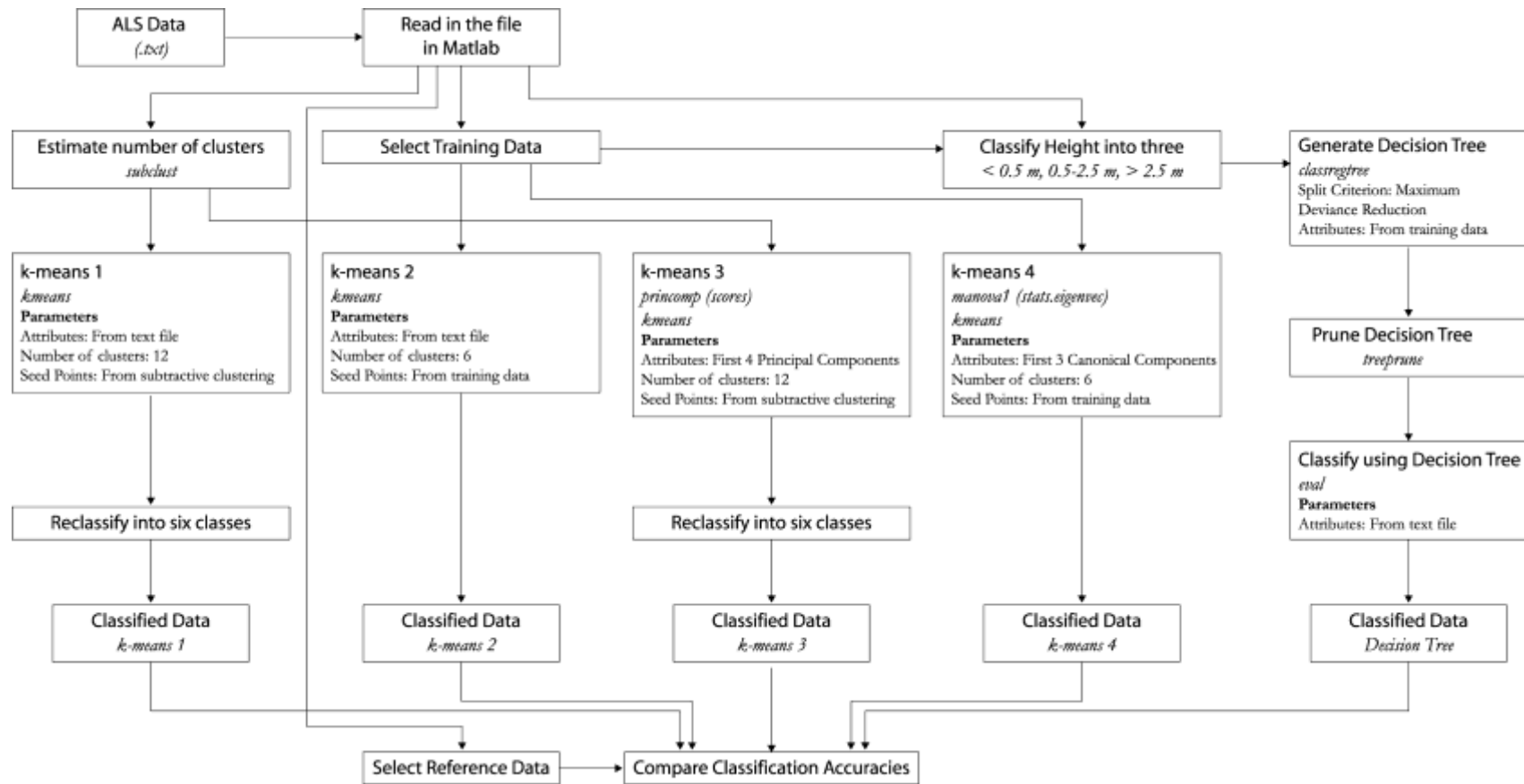


Figure 25: Workflow for the classification of full-waveform ALS data, and comparison of the k-means clustering and decision tree methods

4.3. Results

There were 16,378 full-waveform data points within the training polygons for all the categories. The number of points in each category is given in Table 20 (section 5.4.1). The box and whisker plots for the eight attributes within the training polygons show how different attributes potentially allow the classification of data (Figure 26). The amplitude values of roads and trees are lower than those of grass, shrubs and buildings. Although there are overlaps in the values, amplitude seems to be a useful attribute in separating roads from grass. The normalised elevation is useful in separating buildings from the other classes, especially road and grass. The different attributes, derived from the intersection of the points and the TIN, are shown in Figure 27.

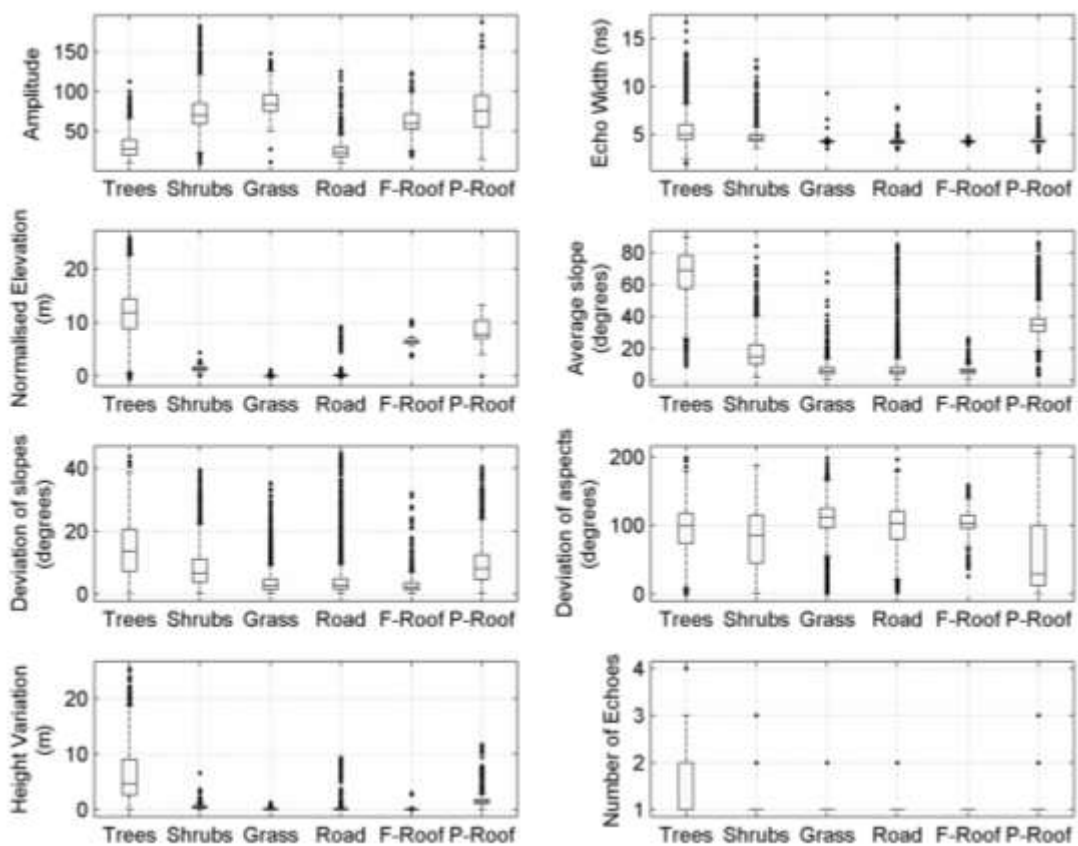
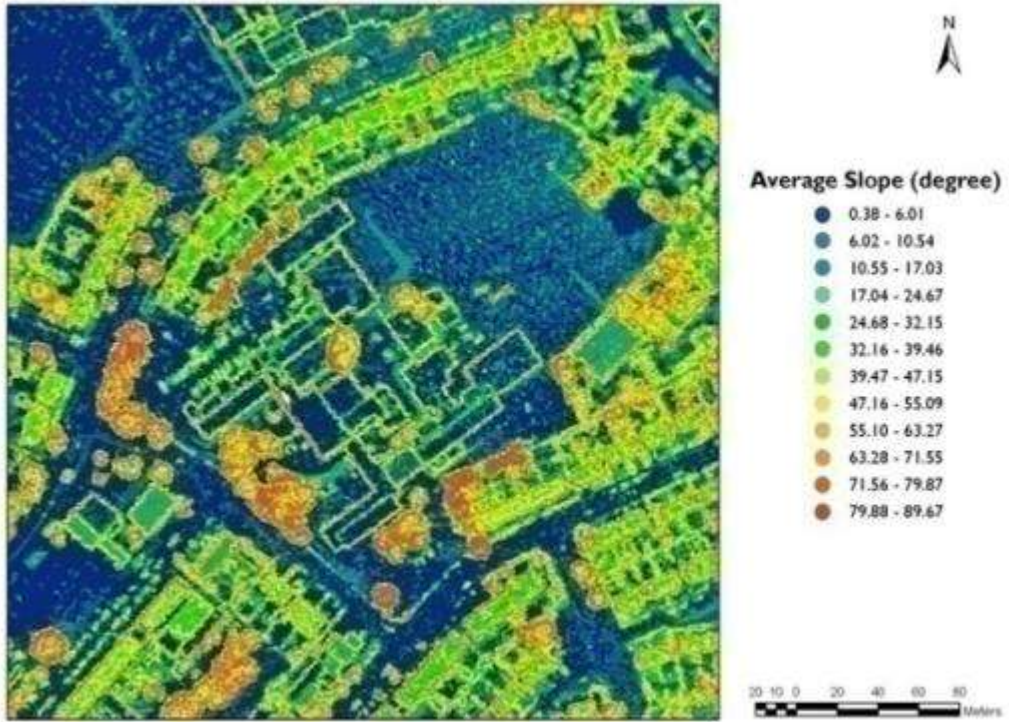
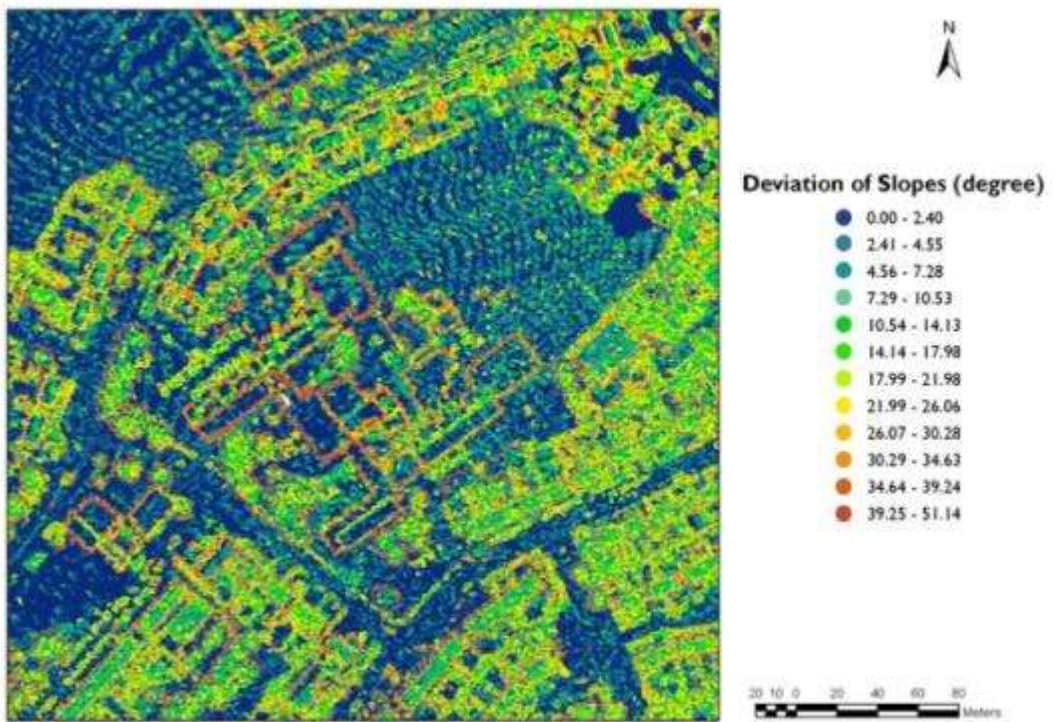


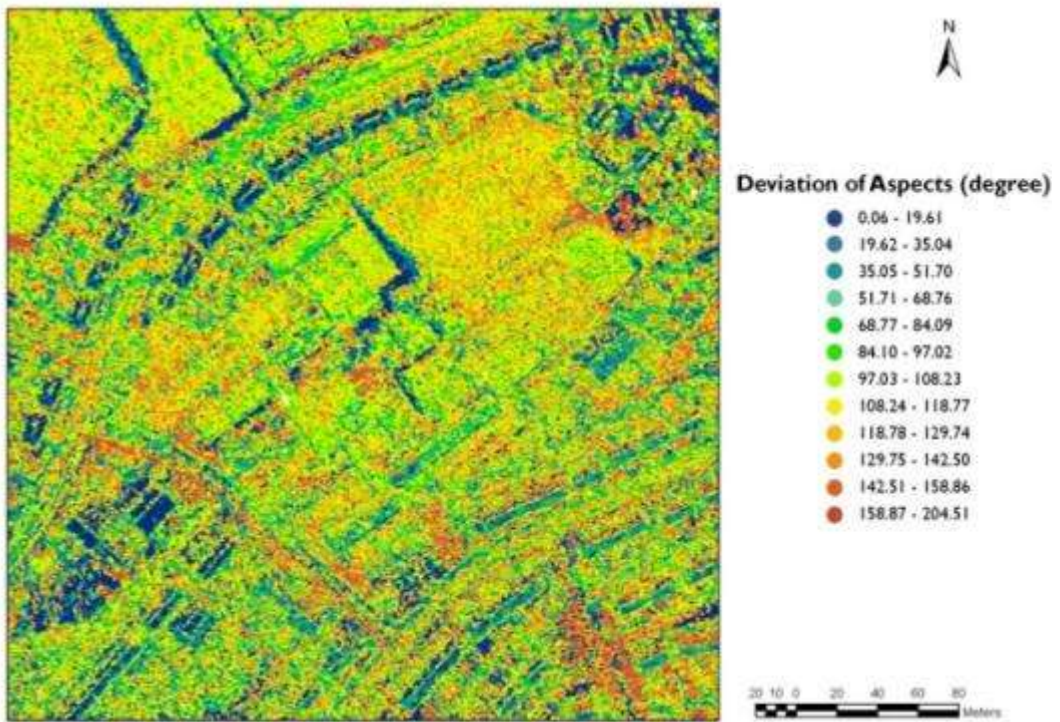
Figure 26: Box-and-whisker plots of the attributes grouped by land cover classes



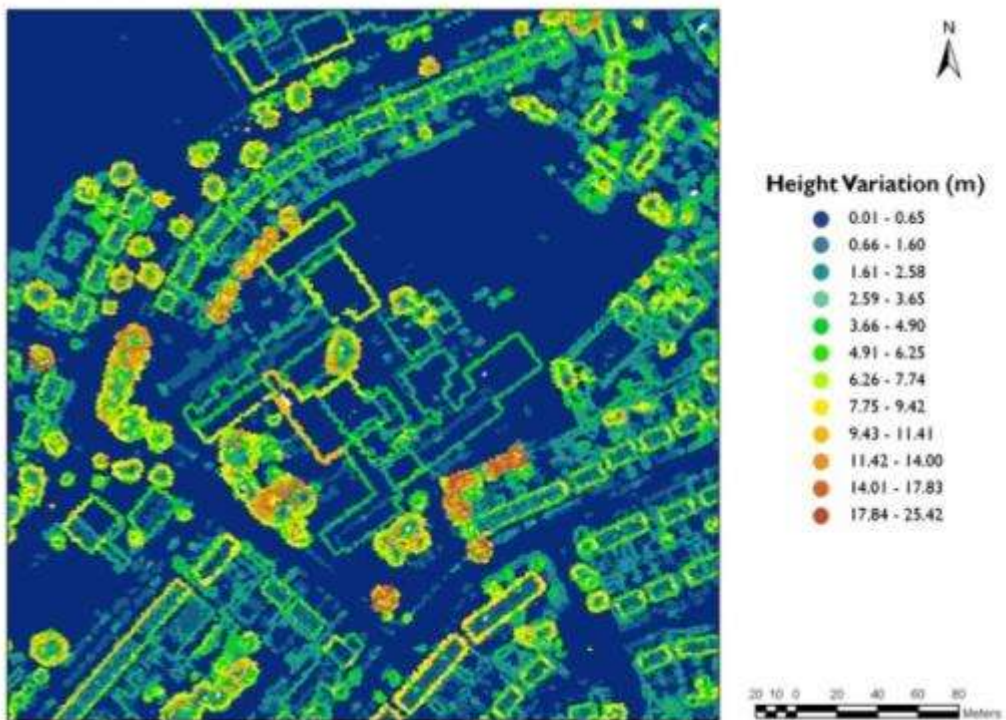
A



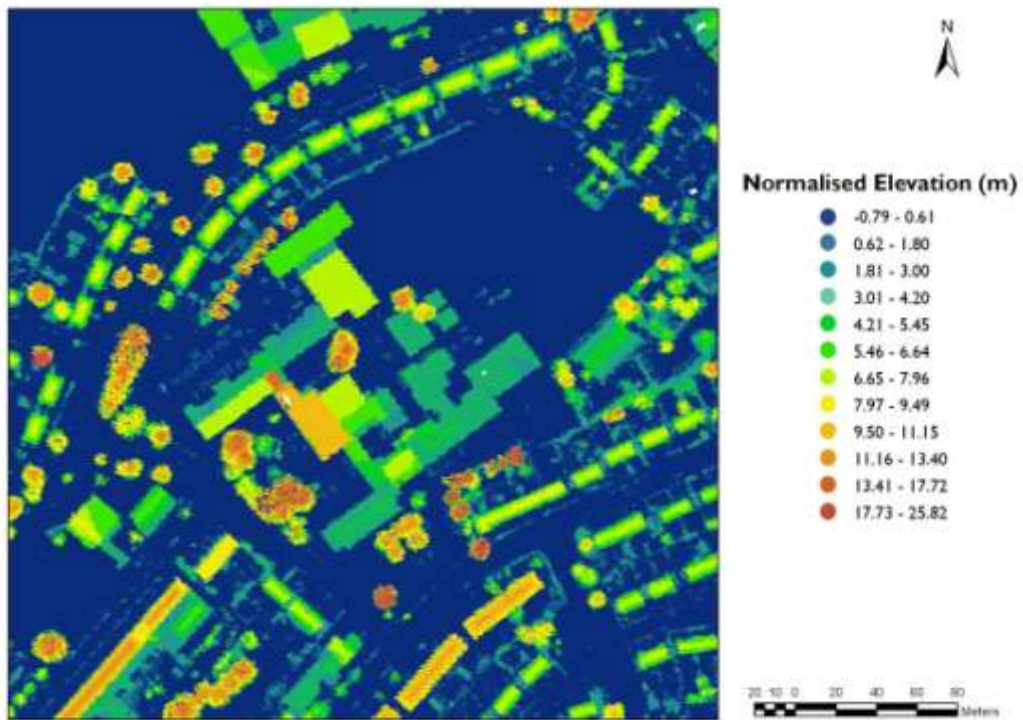
B



C



D



E

Figure 27: Derived attributes of the ALS points (A) Average Slope, mean of the slopes of attached TIN triangles; (B) Standard Deviation of slopes of attached TIN triangles; (C) Standard Deviation of aspects of attached TIN triangles; (D) Height Variation, range of the elevations of points attached to each ALS point and (E) Normalised Elevation, elevation of each point from the estimated DTM.

A comparison of the accuracies of classification using k-means clustering and the decision tree on the reference data is shown in Table 8. All the accuracies using the decision tree are higher than those using k-means clustering, for all the different options. In clustering, the option using canonical components gives higher accuracies than the others do, although in the average user's accuracy, it is comparable to the one using principal components. However, the k value for the classification using the decision tree shows a 'substantial agreement'; where as the one for k-means clustering using canonical components shows only a 'fair agreement'. The three others show 'slight agreement'.

Table 8: Kappa coefficient, overall accuracy, average producer's and user's accuracies of the classifications using k-means clustering and decision tree. k-means 1: k-means clustering; k-means 2: k-means clustering using the means of the attributes of the classes from the training data; k-means 3: k-means clustering using Principal Components; k-means 4: k-means clustering using Canonical Components

	k-means 1	k-means 2	k-means 3	k-means 4	Decision Tree
Kappa Coefficient	0.15	0.09	0.17	0.39	0.68
Overall Accuracy	34.42	27.96	32.14	51.59	74.62
Average User's Accuracy	23.13	26.03	33.78	33.58	82.86
Average Producer's Accuracy	25.83	21.39	26.06	47.16	73.63

The results of the classification using the k-means methods are shown in Figure 28A. The pruned decision tree (Figure 28B) did not make use of the two attributes, standard deviation of aspects and the number of echoes. Classified height, amplitude and average slope account for 97% of the accuracy of classification in roads, 99.8% of the accuracy in grass and 86.1% in trees for the training data. Height, average slope and height variation were able to classify 99.4% of the flat roofed buildings. Echo width was a useful attribute in distinguishing pitched roofs from trees in 88.7% of the cases. The points displayed by class from the decision tree are shown in Figure 29.

4.4. Discussion

The results are discussed in the following paragraphs. The attributes used in the classifications are discussed further in sub-section 4.4.1. The results from the classifications using clustering and decision tree are discussed in sub-sections 4.4.2 and 4.4.3 respectively.



A



B



C



D

Figure 28A: ALS points classified into flat roofs, pitched roofs, grass, shrubs, trees and road using k-means clustering for (A) option 1; (B) option 2, using the means of the attributes of the classes from the training data; (C) option 3, using Principal Components; and (D) option 4, using Canonical Components.

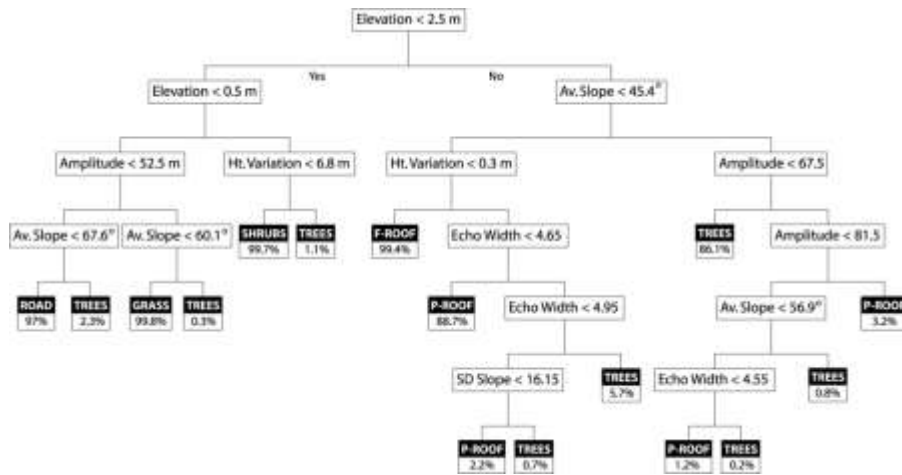


Figure 28B: The pruned decision tree used for classifying the ALS point cloud data. The boxes below the leaf nodes indicate the percentage of correctly classified points of a particular land cover class.



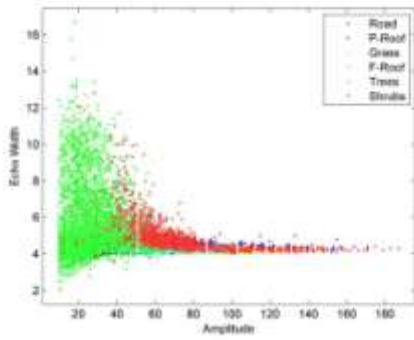
Figure 29: ALS points classified into flat roofs, pitched roofs, grass, shrubs, trees and road using the Decision Tree classifier.

4.4.1. Analysis of the Attributes

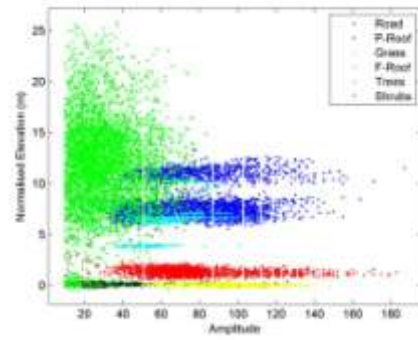
In the box and whisker plots (Figure 26), the lower outliers in vegetation for normalised elevation are probably from, or close to the ground. The echo widths are higher and of a wider range for trees than for grass, roads or buildings as seen from earlier studies (Ducic et al., 2006). The majority of the multiple echoes are from vegetation and building edges, which was also found by Chust et al. (2008). There are some multiple echoes from roads, which could be from overhanging vegetation or vehicles. The height variation is expected to be high for vegetation.

The average slope of the TIN triangles, which has the point as the common node, seems useful in identifying trees, which have larger height variations and hence, higher average slopes. The high values of the outliers in the roads could be from vehicles, or branches of trees. The standard deviation of slopes of TIN triangles attached to a point is lower and less variable for road, grass and flat roofs. This attribute is expected to aid in the correct classification of surfaces if the terrain itself is sloping. The standard deviation of aspects of attached TIN triangles is lower for pitched roofs. This could be because even for a relatively flat horizontal surface, there are minor variations in the aspects. This is less pronounced in sloping roofs. However, this is only of limited use since it is not applicable in the case of ridges and features on the pitched roof. Nevertheless, this attribute is included as the separation of vegetation and pitched roof seems to be the most difficult, and it could be useful in the classification process.

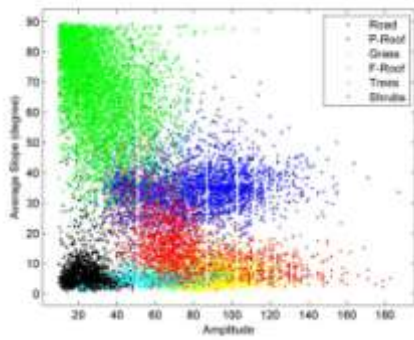
The relationships between the attributes were explored further using scatter plots. Figure 30 shows how the amplitude values relate to the other attributes. Amplitude and average slope seem to bring out the best separation between the classes from the scatter plots. The points in the plots are coloured according to the class.



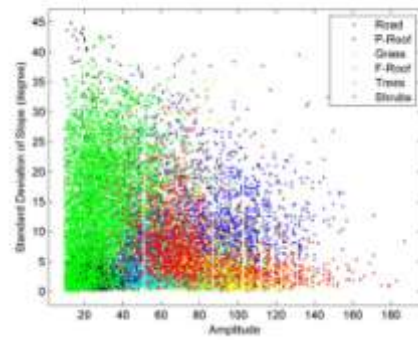
A



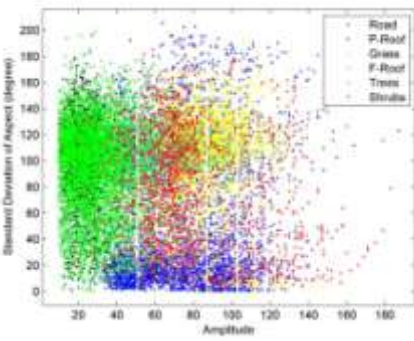
B



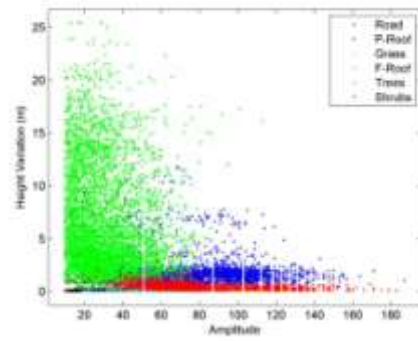
C



D



E



F

Figure 30: Amplitude values plotted against (A) echo width; (B) normalised elevation; (C) average slope; (D) standard deviation of slope; (E) standard deviation of aspect and (F) height variation grouped by class

The high correlations between height, average slope and height variation are also evident from the coefficients of principal components, also known as loadings of the attributes, in the first principal component (Table 9). These attributes of the point contribute most to the first principal component. The variances in the higher order principal components do not seem to reduce drastically. This makes it difficult to reduce the number of variables in the dataset. All the components contribute to more than 1% of the variations. Half the number of principal components was used for the analysis since they accounted for above 75% of the variations. Height, average slope and height variation contribute the most to the first canonical component (Table 10).

Table 9: Coefficients of principal components of the variables and the variance attributed to each principal component

	PC1	PC2	PC3	PC4	PC5	PC6	PC7	PC8
Amplitude	0.28	-0.05	-0.63	0.05	0.46	-0.55	-0.09	0.02
Echo Width	-0.25	0.31	0.30	0.69	-0.07	-0.50	-0.02	-0.12
Height	-0.40	0.27	0.02	-0.02	0.56	0.32	-0.58	-0.09
Average Slope	-0.53	-0.07	-0.12	-0.05	0.02	-0.12	0.16	0.81
Std. Deviation of Slope	-0.29	-0.23	-0.58	0.27	-0.54	0.16	-0.34	-0.17
Std. Deviation of Aspect	0.02	-0.82	0.25	0.39	0.32	0.11	-0.03	0.01
Height Variation	-0.48	-0.03	-0.22	-0.04	0.23	0.08	0.66	-0.47
Number of Echoes	-0.33	-0.30	0.24	-0.55	-0.13	-0.53	-0.28	-0.26
Eigen Values	3.07	1.06	1.03	0.93	0.75	0.63	0.38	0.16
Variance (percentage)	38.39	13.20	12.85	11.66	9.40	7.82	4.70	1.98
Variance (cumulative percentage)	38.39	51.59	64.44	76.10	85.50	93.32	98.02	100.00

Table 10: Coefficients of canonical components of the variables and the variance attributed to each canonical component

	CC1	CC2	CC3	CC4	CC5	CC6	CC7	CC8
Amplitude	0.03	0.91	1.49	0.24	-0.05	0.00	0.07	0.04
Echo Width	0.05	-0.18	0.38	0.51	0.81	-0.15	-0.08	-0.58
Height	3.92	1.68	-1.24	0.63	0.01	0.00	0.01	0.04
Average Slope	1.09	-1.75	1.72	-1.41	-0.83	0.29	-1.15	-0.55
Std. Deviation Slope	-0.01	-0.26	0.19	-0.13	0.58	0.02	0.04	0.99
Std. Deviation Aspect	-0.03	-0.09	-0.05	0.80	-0.42	-0.03	-0.61	0.23
Height Variation	0.18	0.12	-0.28	0.70	-0.10	-0.94	1.13	0.34
Number of Echoes	0.05	0.15	0.11	0.70	0.31	0.90	0.66	0.07
Eigen Values	22.67	2.66	0.91	0.21	0.04	0.00	0.00	0.00
Variance (percentage)	85.57	10.06	3.44	0.80	0.14	0.00	0.00	0.00
Variance (cumulative percentage)	85.57	95.63	99.07	99.86	100.00	100.00	100.00	100.00

Medians on roads, marked in white, have higher amplitudes and therefore classified as grass. Height and height variation were the only attributes used in the classification of shrubs. This is mainly because no attempt was made to classify other objects below the height of buildings and above roads and grass. Some of the vehicles are therefore classified as shrubs in the original dataset. As seen from the decision tree diagram, it is difficult to separate pitched roofs and vegetation higher than 2.5m. This was mainly for the building edges and features such as chimneys on the roof. Some points on trees, possibly with dense foliage, are classified as buildings. It can be seen from the MasterMap data that some of the smaller buildings are not detected, being classified as vegetation of medium height.

4.4.2. Classification by Clustering

Only 34.42% (overall) of the points were correctly classified using the first option (Table 11). The majority of the flat roofed buildings were misclassified, and the accuracy was very low for pitched roofs, trees and shrubs. The producer's and user's accuracies were the highest for grass (86.54% and 55.19% respectively).

Table 11: Error Matrix for k-means clustering of the attributes of full-waveform data

Reference Data	Classified Data						Producer's Accuracy
	Trees	Shrubs	Grass	Road	F-Roof	P-Roof	
Trees	329	4	0	445	268	1643	12.24
Shrubs	38	19	1	77	9	14	12.03
Grass	251	4	2296	102	0	0	86.54
Road	139	41	1860	1041	0	1	33.78
F-Roof	69	39	3	468	1	20	0.17
P-Roof	1452	2	0	493	4	223	10.26
User's Accuracy	14.44	17.43	55.19	39.64	0.35	11.73	34.42 (Overall)

The overall accuracy of the classification decreased to 27.96% in the second option (Table 12). All the points from road were incorrectly classified, but the accuracies of classification of trees increased.

Table 12: Error Matrix for k-means clustering, with the mean of the attribute values for the various classes in the training dataset as the seed points

Reference Data	Classified Data						
	Trees	Shrubs	Grass	Road	F-Roof	P-Roof	Producer's Accuracy
Trees	779	7	103	1459	7	334	28.97
Shrubs	12	10	7	81	39	9	6.33
Grass	0	290	2358	0	5	0	88.88
Road	1	185	2851	0	45	0	0.00
F-Roof	11	93	378	93	24	1	4.00
P-Roof	32	914	23	1200	1	4	0.18
User's Accuracy	93.29	0.67	41.22	0.00	19.83	1.15	27.96 (Overall)

In the classification using principal components, there was an increase in the user's accuracy for pitched roofs, when compared to the first and second options (Table 13).

Table 13: Error Matrix for k-means clustering using Principal Components

Reference Data	Classified Data						
	Trees	Shrubs	Grass	Road	F-Roof	P-Roof	Producer's Accuracy
Trees	813	1309	78	30	431	28	30.23
Shrubs	10	30	8	9	10	91	18.99
Grass	0	0	2362	287	0	4	89.03
Road	1	0	2872	174	0	35	5.65
F-Roof	11	53	314	162	0	60	0.00
P-Roof	33	846	16	1003	5	271	12.47
User's Accuracy	93.66	1.34	41.81	10.45	0.00	55.42	32.14 (Overall)

The overall accuracy from canonical variables was the highest among the options using k-means clustering at 51.59%. The producer's accuracy of classification of flat-roofed buildings increased from 0 in Table 13 to 90.17% (Table 14). The significant misclassification was that of grass as road, and in the classification of pitched roofs.

Table 14: Error Matrix for k-means clustering using Canonical Components

Reference Data	Classified Data						Producer's Accuracy
	Trees	Shrubs	Grass	Road	F-Roof	P-Roof	
Trees	2232	144	0	0	304	9	83.00
Shrubs	40	16	0	1	14	87	10.13
Grass	0	2	0	2651	0	0	0.00
Road	0	14	0	3067	0	1	99.51
F-Roof	31	11	0	0	541	17	90.17
P-Roof	394	4	0	0	1773	3	0.14
User's Accuracy	82.76	8.38	0	53.63	20.55	2.56	51.59 (Overall)

Height was grouped into three – less than 0.5, 0.5 to 2.5 and greater than 2.5 – and a classification was done using this instead of the actual height from the terrain. This increased the classification accuracy from 36% to 54% for the first, from 58% to 60% for the second and from 88% to 94% for the fourth options. However, for the third method based on principal components, the accuracy reduced from 44% to 40%.

4.4.3. Classification using Decision Tree

The overall accuracy of the classification using the decision tree on the reference dataset was 74.62% (Table 15). It was seen that the classified height and amplitude contributed the most to the accuracy of classification. Accuracies of classifications on a train-all-test-all basis were compared to estimate the contributions of each of the attributes. The average of the producer's and user's accuracies using the decision tree on the training dataset was 98.1%. Excluding height from the decision tree reduced the overall accuracy to 80%. Excluding amplitude reduced the accuracy to 88%. However, excluding echo width reduced the accuracy only slightly to 97.65%.

Table 15: Error matrix for classification using the pruned decision tree on the full-waveform data

Reference Data	Classified Data						Producer's Accuracy
	Trees	Shrubs	Grass	Road	F-Roof	P-Roof	
Trees	2505	0	1	2	104	77	93.16
Shrubs	50	87	13	2	1	5	55.06
Grass	0	0	2653	0	0	0	100.00
Road	0	1	2217	864	0	0	28.03
F-Roof	35	17	4	0	470	74	78.33
P-Roof	276	1	0	0	2	1895	87.17
User's Accuracy	87.40	82.08	54.28	99.54	81.46	92.39	74.62 (Overall)

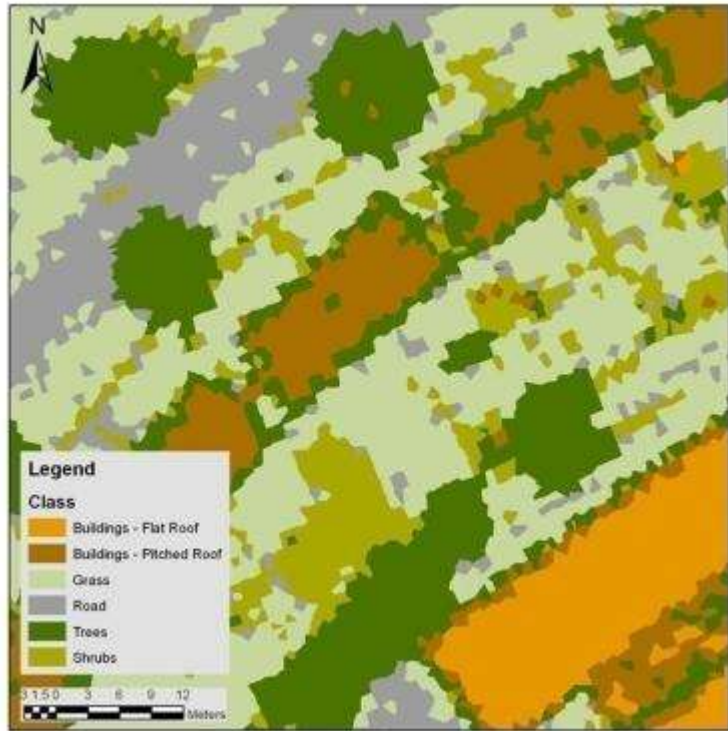
As seen from the decision tree diagram, it is difficult to separate pitched roofs and vegetation higher than 2.5 m. Apart from the root node, five decision nodes are used to separate grass, road and shrubs from trees, whereas nine nodes are required to separate buildings from trees. Out of the ten leaf nodes resulting from these nine decision nodes, only one leaf node results in flat roof. The major difficulty is therefore in separating trees and pitched roof.

In the case of pitched roofs, the roof edges and features such as chimneys on the roof were often classified as trees (Figure 31). For flat roofs, the roof edges and the edges of height variations within the buildings were classified as either pitched roofs or trees. It can be seen from the aerial photograph that some of the buildings were not detected, and were classified as shrubs. Medians on roads, marked in white, had higher amplitudes and they were classified as grass. Similarly, some of the vehicles were classified as shrubs. Some points on trees, possibly with dense foliage, were classified as buildings.

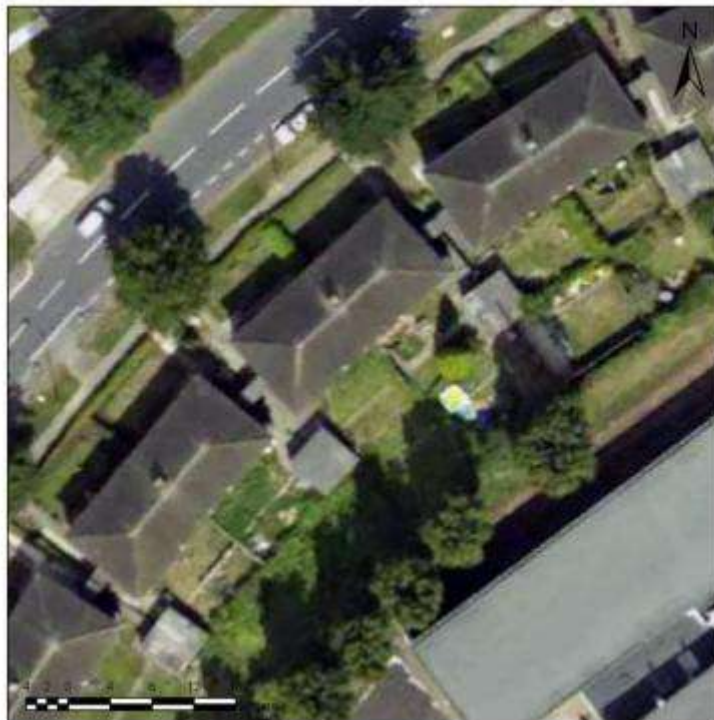
Although it was seen that the standard deviation of aspects and the number of echoes were not as useful as expected, it could be due to the selected classes. Standard deviation of aspects could be useful in segmenting the pitched roofs for roof modelling and the number of echoes could be useful in sub-classifying vegetation. The average slope and height variation are dependent on the point density and the algorithm used for generating the TIN, and the echo width depends on the method of waveform decomposition. These will have to be modified for other datasets. Amplitude is dependent on various factors including the sensor, flying altitude, incidence angle and surface reflectance. Amplitude, corrected for these factors, would be a useful attribute if the classification method were to be applied on other datasets.

A decision tree classifier performs significantly better (73.63%) than k-means clustering (47.16%) based on the producer's accuracy for the classification of data points from full-waveform data. Features such as vehicles, street furniture, barriers and any feature above 0.5 m and below 2.5 m are now likely to be classified as shrubs, and need to be merged with the adjacent feature, or identified as a separate class.

The classes in this study are user-defined rather than the result of natural clustering. This is probably the reason why the decision tree, a logical classifier performed better than k-means clustering, a statistical classifier. However, other classification techniques might yield better results for a more detailed classification, and need to be explored.



A



B

Figure 31: (A) The roof edges and features such as chimneys on the roof classified as trees; the roof edges and the edges of height variations within the with flat roofs classified as either pitched roofs or trees; a few smaller structures not detected and classified as shrubs; medians on roads, marked in white classified as grass; some points on trees, possibly with dense foliage, classified as building roofs; (B) An

aerial image of the area is shown for comparison (Ordnance Survey © Crown Copyright. All Rights Reserved)

4.5. Summary

This chapter described the classification of airborne laser scanning points into six classes – trees, shrubs, grass, road, and flat and pitched roofs. Two methods, clustering and decision trees, were used for the classification. The accuracies of the methods were assessed using manually delineated reference data. Three attributes of the individual points – amplitude, echo width and number of echoes – and five attributes derived from the elevation – normalised elevation, average slope, standard deviation of slope, standard deviation of aspect and height variation – were used as inputs for the classification methods. The decision tree classifier performed significantly better ($k = 0.68$) than the four options making use of k-means clustering ($k = 0.15, 0.09, 0.17$ and 0.39).

The next chapter describes the classification of discrete return data from the same study area, using a decision tree. The accuracy of this classification is compared with the one using full-waveform data, described in this chapter, to estimate the advantages, if any, of using full-waveform data for classification in urban areas.

5. Comparison between Full-waveform and Discrete Return Data

This chapter addresses the second objective, and compares the results of classifications from processed full-waveform (Bristol_Riegl) and discrete return (Bristol_Optech) datasets using the decision tree method described in Chapter 4. The accuracies of the results are compared to determine whether full-waveform data from Bristol_Riegl give significant improvement in the accuracy of classification. The results show that the Bristol_Optech data seem to be better at separating road and grass. Average and standard deviation of slopes seem to be highly dependent on the point spacing.

5.1. Introduction

The decision tree classifier described in Chapter 4 makes use of the six attributes – height, amplitude, echo width, average and standard deviation of slopes, and height variation. Out of this, the information about echo width is now available only in full-waveform data. In the full-waveform system used in this study, Bristol_Riegl, the wavelength of the laser pulse is 1550 nm. In the discrete return system, Bristol_Optech, the wavelength is 1064 nm. This will have an effect on the amplitude or intensity values for the two datasets (Herold et al., 2003). The amplitude or intensity values have a linear relationship with the strength of the return pulse. This would depend on the way the information is recorded in the two systems. The values are also dependent on the scanning geometry. This will be described in more detail in the next chapter. In addition to this, the number of points per emitted pulse depends on the laser scanning system. The majority of the discrete return systems, including the one used in this study, record only the first and last pulses.

Since the Bristol_Optech data has a point density of 25 points per m², the data are thinned to a point density comparable to the Bristol_Riegl data. The polygons used for training the Bristol_Riegl data are used with the Bristol_Optech data as well. The training data points are used to generate a decision tree, which is used for classifying the dataset. The accuracies are assessed using the same methods as in Chapter 4. The classifications from the two datasets are compared to estimate whether the additional attributes from full-waveform data contribute significantly to the accuracy of classification. All the points in the original discrete return dataset, the one before thinning, are then used to assess the effect of point density on the attributes used for classification.

5.2. Methodology

5.2.1. Classification of Bristol_Optech Data

There were 25,476,798 data points in this dataset, including first and last echoes, in an area of 1 sq. km. The density of the point cloud was therefore a little more than 25 points m⁻². As in the earlier analysis, a rough DTM was created from the Bristol_Optech ALS points, making use of the lowest point in a 10 m grid. A TIN was created from these points. From this, points within a distance of 1 m from buildings were removed. This was done using the buildings layer in MasterMap. The initial TIN was created from 12,453 points. The outliers were manually removed. They could be identified as nodes of the triangles with steeper slopes or with higher

elevation than the surrounding points. These were removed in two steps by creating a TIN after each selection. The final TIN was created using 12,367 points.

The Bristol_Optech points were thinned to that of the processed Bristol_Riegl data, by selecting the point closest to each point in the Bristol_Riegl data. The average distance from the Bristol_Optech point to the nearest Bristol_Riegl data point was 0.14 m, and the standard deviation was 0.09 m. There were 996,745 points in the Bristol_Optech data as against 1,027,655 points in the Bristol_Riegl data. The number of points is different in the two datasets as two points in the Bristol_Riegl data could have one corresponding point in the Bristol_Optech data that is closer to these points than all the others are.

The additional attributes based on elevation were derived using the methods described in section 4.2.3. The training polygons representing the six land cover classes, used in the earlier analysis, were used to analyse the attributes of points within them. Some of the road polygons had to be modified since they seemed to contain points from objects that looked like vehicles. There were 15,439 points in all the categories (Table 20).

Box-and-whisker plots were used to analyse the various attributes grouped into categories. A decision tree was generated using the attributes of the six classes from the training points. This decision tree was used to classify the thinned Bristol_Optech dataset. The classes generated by the decision tree classifiers for the Bristol_Optech data were compared with those from the Bristol_Riegl data, and with the manually delineated classes.

5.2.2. Influence of Point Density on the Attributes

All the points in the Bristol_Optech dataset within the training polygons were used to analyse whether the point density has an influence on the generated decision tree. A TIN was created using all points within the training polygons and within a buffer of 2 m from the polygons. This was done to decrease the time for computation. The methods described in sections 4.2.3, 4.2.4 and 4.2.6 were used to derive additional attributes from elevation, analyse the training data and generate a decision tree.

5.3. Results

5.3.1. Comparison of the accuracies of classification using Bristol_Riegl and Bristol_Optech Data

The decision tree generated using the Bristol_Optech data contained 503 nodes, which were pruned to 47 nodes with a pruning level of 20, as against 31 nodes for the full-waveform data (Figure 32). The kappa coefficient, overall, average user's and average producer's accuracies of the classifications were higher for the decision tree using Bristol_Optech data than the one using Bristol_Riegl data (Table 16).

Table 16: Kappa coefficient, overall accuracy, average producer's and user's accuracies of the classifications using the decision trees generated from Bristol_Optech and Bristol_Riegl data

	Bristol_Optech	Bristol_Riegl
Kappa Coefficient	0.92	0.68
Overall Accuracy	94.18	74.62
Average User's Accuracy	91.80	82.86
Average Producer's Accuracy	91.50	73.63

A subset of the study area consisting of 135,757 points was considered for more detailed analysis. Table 17 shows the confusion matrix comparing the classification from Bristol_Riegl and Bristol_Optech points. Since the Bristol_Optech points are not at exactly the same locations as the Bristol_Riegl points, and were collected two years earlier, there are difficulties in comparing the two. If a Bristol_Optech point was within the Thiessen polygon constructed around a Bristol_Riegl point, they were considered the same for the purposes of comparison. The major incorrect classifications, above 10% of the total in each class in the Bristol_Optech data, are underlined and will be discussed later in section 5.4.1.

Table 17: Comparison of classifications from Bristol_Riegl and Bristol_Optech data. The underlined numbers highlight the major misclassifications, above 10% of the total, in each column.

Bristol_Riegl (Full-waveform – 1550 nm)	Bristol_Optech (Discrete Return – 1064 nm)						Total
	Trees	Shrubs	Grass	Road	F-Roof	P-Roof	
Trees	15,921	1,870	929	1,309	137	<u>4,685</u>	24,851
Shrubs	2,479	5,768	732	1,138	190	748	11,055
Grass	<u>3,918</u>	<u>11,195</u>	28,591	<u>17,213</u>	26	420	61,363
Road	1,920	1,672	709	13,843	87	228	18,459
F-Roof	139	54	91	1	6,063	808	7,156
P-Roof	1,492	185	87	77	786	10,246	12,873
Total	25,869	20,744	31,139	33,581	7,289	17,135	

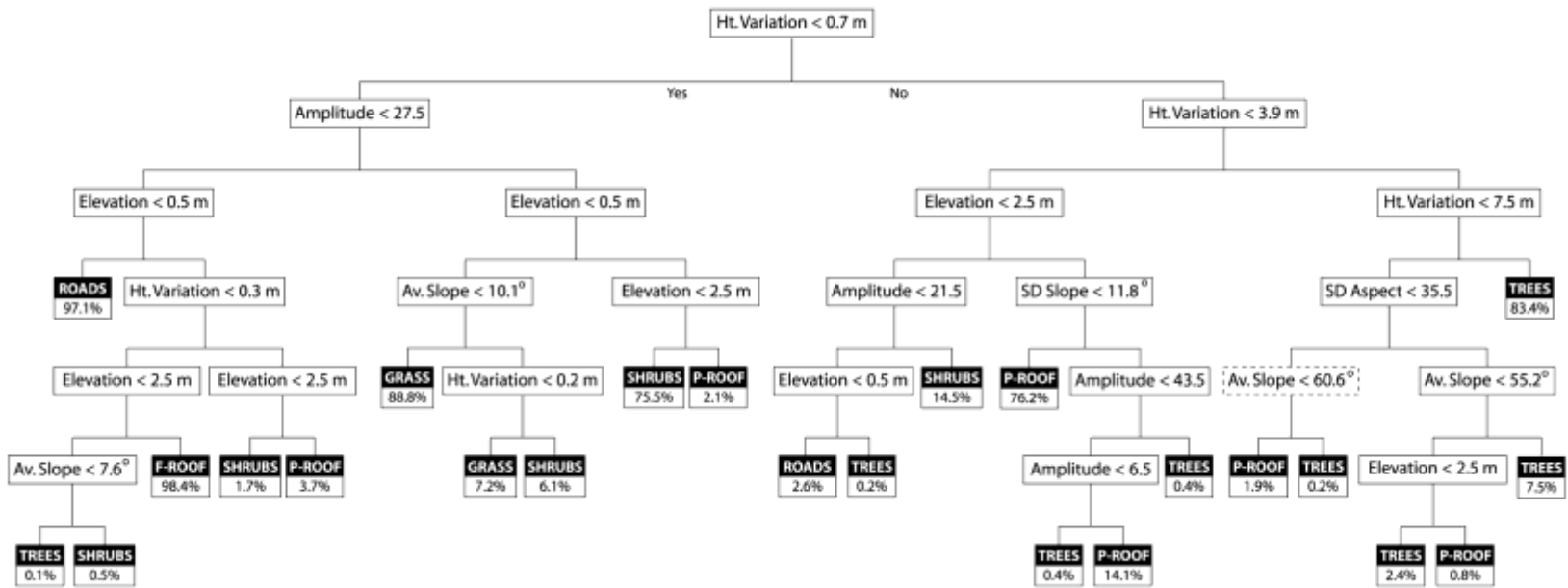


Figure 32: The pruned decision tree used for classification. The percentages of points classified at each leaf node are also shown.

15,921 (61.5%) of the points classified as trees using the Bristol_Optech data, were also classified in the Bristol_Riegl points as trees. Similarly, 5,768 (27.8%) points classified as shrubs, 28,591 (91.8%) points classified as grass, 13,843 (41.2%) of the points classified as roads, 6,063 (83.2%) points classified as buildings with flat roofs and 10,246 (59.8%) points classified as pitched roofs in Bristol_Optech data were also classified in the same category using the Bristol_Riegl data.

Considering only the correct classifications in each class, the accuracies are higher for the Bristol_Optech data than for the Bristol_Riegl data for the following classes: shrubs, roads and pitched roofs (Table 18 & Table 15). The large difference in the accuracies of classification of roads is due to the inclusion of parking areas in road polygons. The accuracy of the classification of roads increased to 98% from 28.03% if the surfaces from other paved surfaces were excluded. Bristol_Optech data seem to be better at differentiating grass from paved surfaces (Table 19).

Table 18: Error matrix for classification using the pruned decision tree on the Bristol_Optech data

	Trees	Shrubs	Grass	Road	F-Roof	P-Roof	Producer's Accuracy
Trees	2290	6	13	65	109	73	89.59
Shrubs	13	154	0	0	0	3	90.59
Grass	0	6	2558	22	0	0	98.92
Road	1	0	14	3006	0	0	99.50
F-Roof	26	2	0	0	467	90	79.83
P-Roof	194	0	0	0	6	1921	90.57
User's Accuracy	90.73	91.67	98.96	97.19	80.24	92.05	94.18 (Overall)

Table 19: Number of points from road polygons correctly classified in ALS data, separated into roads and other paved surfaces

	Number of points	Bristol_Riegl	Bristol_Optech
Main Road	852	835 98%	846 99.3%
Other	2169	15 0.69%	2160 99.58%

5.3.2. Influence of Point Density on the Attributes

When all the points within the Bristol_Optech dataset were considered, the box-and-whisker plots were similar to the thinned data for amplitude and normalised elevation (Figure 33). However, some of the attributes derived from elevation were different from the thinned dataset, which will be discussed in section 5.4.4.

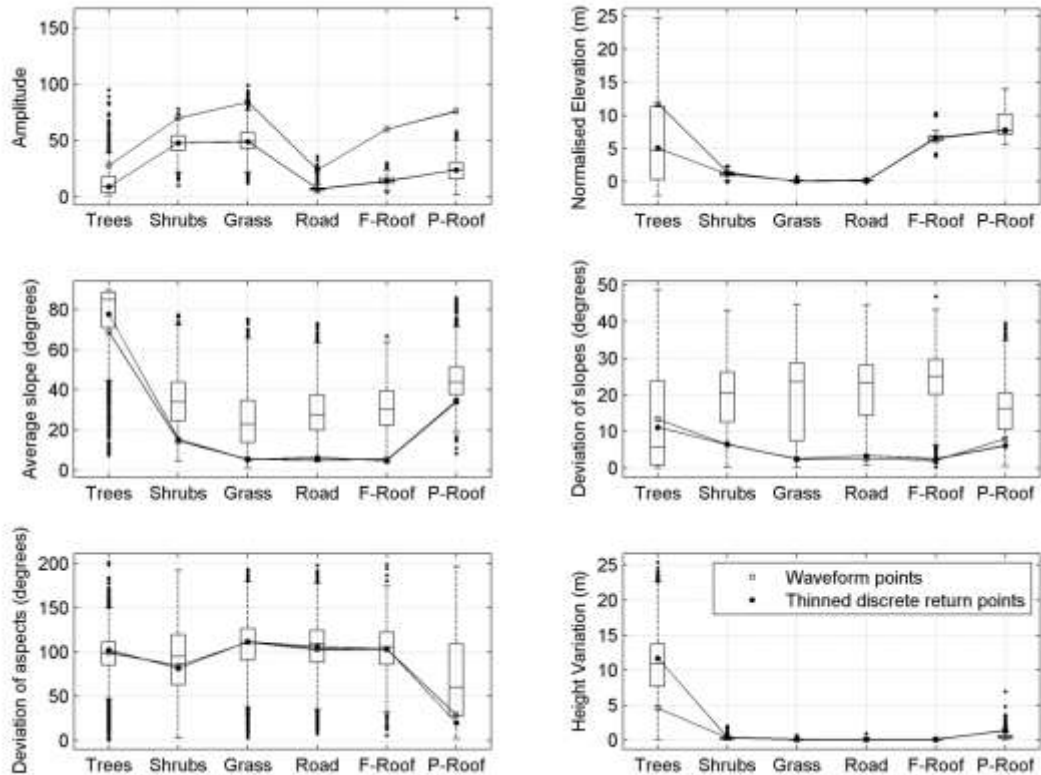


Figure 33: Box-and-whisker plots of the six attributes grouped by categories for the Bristol_Optech dataset. The median values for the processed Bristol_Riegl data and the thinned Bristol_Optech data are also shown.

5.4. Discussion

The amplitude values for the Bristol_Optech data are different from the Bristol_Riegl points due to the difference in the wavelengths of the laser pulses used in the sensors, and the method of recording the data. The intensity values of the Bristol_Optech data points seem to be more useful than the amplitude values from the Bristol_Riegl data to distinguish between the points from road and grass. The differences in the accuracies could therefore be due to the differences in the intensity values, which could be a result of the difference in wavelengths. The results are discussed in the following paragraphs. Sub-section 5.4.1 discusses the comparison of the classifications from the Bristol_Riegl and the Bristol_Optech data, sub-sections 5.4.2 and 5.4.3 deals with the decision tree generated using the Bristol_Optech data, and the effect of pruning. Sub-section 5.4.4 discusses the influence of point density on the attributes.

5.4.1. Comparison of Thinned Bristol_Optech and Bristol_Riegl Data

The points from the two datasets are not exactly at the same location. Some of the differences in the classifications could be attributed to this. For example, if a point is classified as road in one dataset, and tree in the other, it is quite possible that one point could have hit a branch of the tree, and the other, the ground seen through the tree. The number of points in each category in the training data was also slightly different (Table 20).

The full-waveform data provided up to five echoes per emitted pulse, whereas only the first and last echoes were available from the Bristol_Optech data. For a similar scanning geometry, Bristol_Riegl data would therefore provide more data points than the Bristol_Optech data. This advantage of the Bristol_Riegl data was not used since the echo number of the Bristol_Optech dataset was not directly available from the dataset, and the points nearest to the Bristol_Riegl data were used for the comparison.

Table 20: Number of points in the training data for Bristol_Riegl and Bristol_Optech data

	Trees	Shrubs	Grass	Road	F-Roof	P-Roof	Total
Bristol_Riegl	5,412	1,927	2,496	2,367	674	3,502	16,378
Thinned Bristol_Optech	5,006	1,877	2,425	2,010	679	3,442	15,439

Even if the above factors are taken into consideration, there seems to be two major differences in the classifications. The first one is between trees and pitched roofs, trees in the Bristol_Riegl data classified as pitched roof in the Bristol_Optech data. As noticed in section 6.2, the major difficulty in the decision tree classifier is in the separation of trees and pitched roofs. From Table 15 & Table 18, the Bristol_Riegl data seem to provide a better accuracy for trees and the Bristol_Optech data, for pitched roofs. The other major difference is in the classification of points as road using Bristol_Optech data and as grass using Bristol_Riegl data, which is discussed in more detail in the following paragraphs.

Of the 33,581 points classified as road in the Bristol_Optech data, 17,213 (51%) points were classified as grass in the Bristol_Riegl data. 74.5% of these points are within polygons classified as 'manmade' in OS MasterMap, which include buildings, roads, paths and car parks. From a visual analysis of the aerial image, it can be seen that the majority of the remaining points are also within paved surfaces such as car parks (Figure 34). The classification using Bristol_Optech data therefore seems to be better at distinguishing grass and paved surfaces.

The intensities of the Bristol_Optech data points classified as grass, road and other paved surfaces are compared with the amplitudes of the Bristol_Riegl data points in Figure 35. It can

be seen that the paved surfaces other than main roads have a different spectral signature to grass in the Bristol_Optech data. However, they occupy a very similar space in the Bristol_Riegl data. This was also noted by Mallet et al. (2008), who used support vector machines to classify full-waveform points from Riegl LMS-Q560 in an urban area. They noted that the rate of misclassification was high for natural and artificial ground, as the clusters are close in feature space.



Figure 34: (A) Points classified as grass in Bristol_Riegl data and road in Bristol_Optech data; (B) MasterMap polygons showing the 'man-made' features in grey; and (C) features seen to be correctly identified as paved areas in the Bristol_Optech data marked in the aerial image (Aerial image, OS MasterMap and ALS data - Ordnance Survey © Crown Copyright. All Rights Reserved)

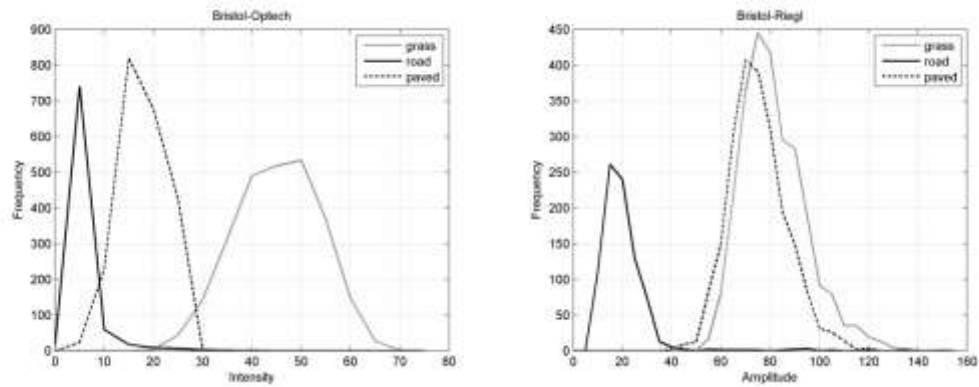


Figure 35: Comparison of the intensities and amplitudes of the Bristol_Optech and Bristol_Riegl data for points from grass, road and other paved surfaces

More information is available about the attributes of full-waveform (Bristol_Riegl) data than those of discrete return (Bristol_Optech) data. In spite of this, the intensity value from Bristol_Optech proved to be more useful than the amplitude value from Bristol_Riegl in separating natural and artificial surfaces. A possible reason could be the different wavelengths of the lasers used in the two systems. As noted earlier, the Bristol_Optech scanner uses laser at a wavelength of 1064 nm, whereas Bristol_Riegl uses a wavelength of 1550 nm.

5.4.2. Decision tree from the Bristol_Optech Data

The decision tree generated from the Bristol_Optech data does not make use of all the attributes for classifying the points, as it automatically selects the most important attributes for the classification at each node. The classification of flat roofs depends only on amplitude, normalised elevation and height variation. 76.17% of the points in the pitched roofs can be classified using normalised elevation, standard deviation of slopes and height variation. 14.09% of the points depend on the amplitude as well. From a visual analysis of all the points, displayed by nodes, nodes 38, 45 and 47 represent building edges or edges of height variation within buildings. 97.06% of the points from asphalt roads can be classified using amplitude, normalised elevation and height variation. All the points have amplitudes below 27.5. Node 34 represents points near objects such as trees, buildings or sometimes vehicles. Amplitude seems to be the main attribute for distinguishing vegetation of low height from roads, as in the full-waveform analysis.

All points with height variation above 7.5 m are classified as tall vegetation at node 15. This might not work if there are buildings with edges at an elevation greater than 7.5 m from the ground. 75.54% of the points from vegetation of medium height are classified based on amplitude, normalised elevation and height variation.

The accuracies using the Bristol_Optech points are higher than that using the Bristol_Riegl data. However, the pruned decision tree for the Bristol_Optech data needs 47 nodes as against 31 nodes for the Bristol_Riegl data. This suggests a better classification for Bristol_Riegl data, since complex trees with more branches are considered to be site-specific or data-driven, and hence less robust and transferable (Rutzinger et al., 2008).

5.4.3. Pruning level of a decision tree

The decision tree was pruned further to make the number of nodes similar to the earlier decision tree generated from the Bristol_Riegl data (Figure 36). Pruning was done one level at a time until the number of nodes was less than or equal to 31, which is the number of nodes in the decision tree from the Bristol_Riegl data. At each pruning level, the levels of misclassifications at the leaf nodes increase. For example, at the fourth level of further pruning, three branch nodes and four leaf nodes are replaced by a leaf node representing pitched roofs. The classification of 90.3% of the pitched roofs is performed at this node. However, the pruning also results in the node containing impurities or misclassifications. 0.8% of the trees would be classified as pitched roofs at this node. The misclassifications therefore increase with pruning, while the larger trees are considered to be data-driven and could be site-specific.

5.4.4. Influence of Point Density on the Attributes

Some of the attributes derived from elevation were different in the original and the thinned Bristol_Optech datasets. The major differences seem to be in average and standard deviation of slopes. Even points with minor differences in elevation can have large slopes for TIN triangles if the distance between them is small. In ArcMap, the slopes of the TIN triangle are calculated from the horizontal plane, and given values from 0 to 90°. Since there are no negative slopes, the averages of slopes tend to be higher than with the lower point density. With the higher point density, the standard deviations of slopes are also higher for most of the classes.

The median height of points from trees is approximately 5 m where as it is above 10 m for the points from the full-waveform data. This could be due to various reasons. The discrete return data using Bristol_Optech were collected in the leaf-off season in November from a lower flying height. There could therefore have been more hits from within and below the canopy. In addition to this, the Bristol_Optech system records only the first and last pulses. There could also be differences in the way the systems analyse and record the signals.

The decision tree for the Bristol_Optech dataset with the higher point density had 869 nodes, which were pruned to 209 nodes. This would make it less replicable than the one from the lower point density. The train-all-test-all accuracy using the pruned decision tree was 97.2%. The tree was further pruned to 31 nodes for a better comparison with the earlier decision trees, and to identify the attributes used (Figure 37). The accuracy reduced to 95.5%. However, this decision tree used only four attributes: normalised elevation, amplitude, height variation and average slope. Only one out of the fifteen branch nodes made use of average slope. This node separated flat and pitched roofs.

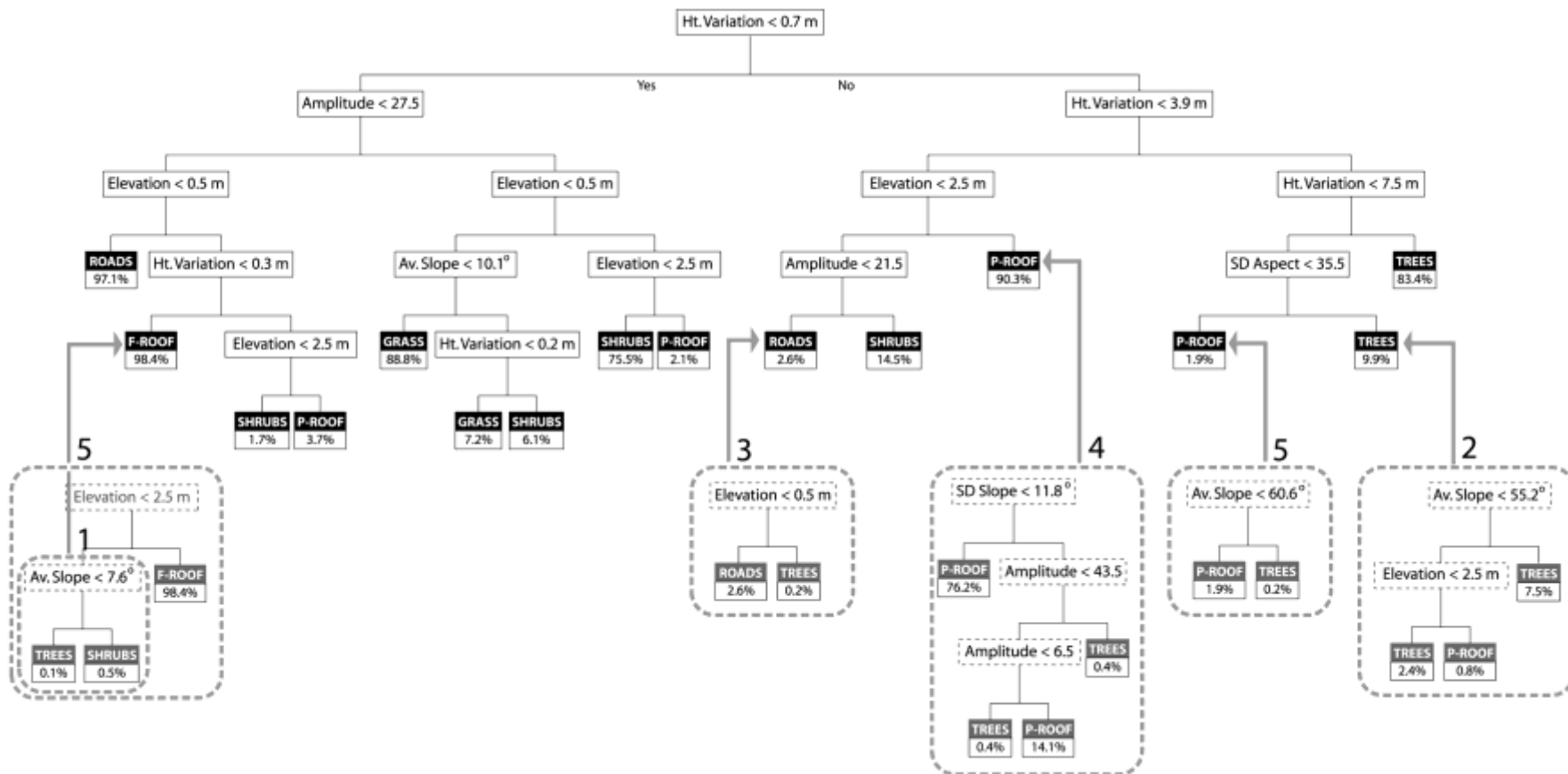


Figure 36: The decision tree using the Bristol_Optech data pruned to have similar number of nodes as that of the Bristol_Riegl data. The nodes pruned at each pruning level are also shown.

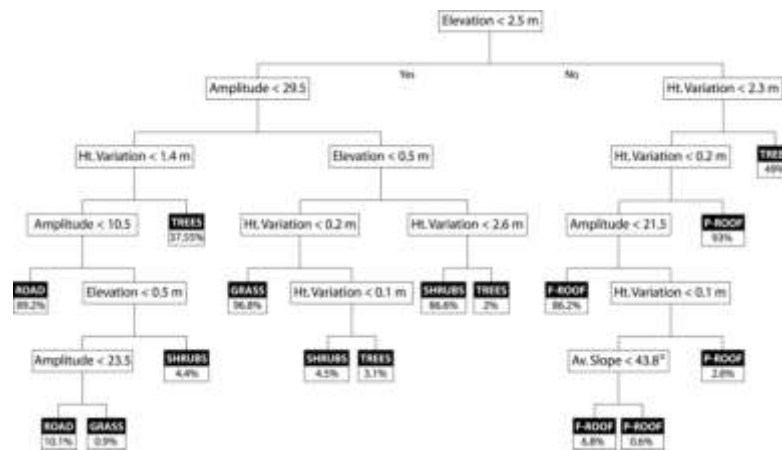


Figure 37: The decision tree for the un-thinned Bristol_Optech data pruned to 31 nodes for a better comparison with the earlier decision trees

5.5. Summary

This chapter compared the accuracies of classification using decision trees on Bristol_Riegl and Bristol_Optech point datasets to determine whether the additional attributes from full-waveform data from Bristol_Riegl give significant advantages over discrete return data from Bristol_Optech. Although echo width is an additional attribute from full-waveform data, it does not seem to be significant for urban land cover classification. An overall accuracy of 95.5% could be achieved on the training dataset using the original un-thinned Bristol_Optech data points with 31 nodes and using only four attributes: height, average slope, height variation and amplitude. The average and standard deviation of slopes seem to be highly dependent on the point density. For a decision tree classifier, using the attributes in the study, increasing point density did not result in a major increase in the accuracy of classification.

The decision tree classifier generated from the thinned Bristol_Optech data contained more nodes, but seemed to perform better than the one from Bristol_Riegl data. This was mainly due to the misclassification of road as grass using the Bristol_Riegl data. Since amplitude is the most important attribute in separating grass from roads, this could be attributed to a number of reasons including wavelength of the laser pulse, method of recording data and weather conditions. Although this attribute in both the datasets are related to the amplitude of the pulse, they may not be identical. Amplitude is dependent on various factors including the sensor, flying altitude, incidence angle and surface reflectance. Intensity, corrected for these factors, would be a useful attribute if the classification method were to be applied on other datasets. The next chapter looks at the application of the decision tree classifier on the full-

waveform dataset from Bournemouth, and ways to modify the attribute related to intensity in full-waveform data to make it applicable in different sites.

6. Backscatter Coefficient as an Attribute in the Decision Tree Classifier

The decision tree classifier generated in Chapter 4 uses an attribute - amplitude of the echo pulse - that is dependent on factors including the flying height of the aircraft and scan angle of the emitted pulse. This chapter describes the application of the decision tree classifier on a dataset from the second study area in Bournemouth. The backscatter cross section of each echo and its derivatives are analysed for replacing amplitude. The results indicate that the backscatter coefficient, the backscatter cross section per unit area, is more useful than amplitude in decision tree classifiers for the considered classes.

6.1. Introduction

The decision tree classifier described in Chapter 4 makes use of the echo amplitude as an attribute. However, the echo amplitude is dependent on various factors including the wavelength and the flying altitude of the sensor, the incidence angle of the emitted beam, and reflectance of the surface. Full-waveform ALS data are considered to be suitable for calibration so that observed laser intensities can be converted to values proportional to surface reflectance (Höfle and Pfeifer, 2007; Kaasalainen et al., 2005; Wagner et al., 2006). The backscatter cross section, which can be derived from the range, amplitude and width of an echo, makes it possible to compare data from different places, sensors and times. An advantage of the calibration procedure is that the amplitude units need not be known as long as they are linearly related to the received power.

The calibration constant is a single value that sums up the parameters that are constant for a particular flight taking into consideration the system and atmospheric parameters. The calibration constant can be estimated using reference targets with a known backscatter cross section, or a known surface reflectance at the wavelength of the sensor (Briese et al., 2008). Asphalt roads have been used for deriving the calibration constant based on an assumed or field-measured reflectance value. In this study, the intensity values in the study area in Bristol were calibrated to obtain the backscatter cross section of each point in the training data. These values, or values derived from them, were used to construct decision trees for classifying the ALS points. The backscatter cross sections of points in the study area in Bournemouth were also calculated. The decision trees generated using the data from Bristol_Riegl were now used to classify data points from Bournemouth_Riegl.

The calibration constant can be calculated based on assumptions about the reflectance of asphalt at the wavelength of the sensor. Wagner et al. (2006) derived the value of the calibration constant based on the assumption that an asphalt road has a reflectance of 0.2 at a wavelength of 1550 nm. Briese et al. (2008) made use of a reflectometer developed by Riegl, to measure the reflectance of three surfaces of interest: two sections of asphalt road and one building roof. The Riegl reflectometer made use of a laser diode operating at 1550 nm, producing a spot of approximately 15 cm diameter at a distance of 1-1.5 m. The reflectance of two Spectralon® reference targets, of reflectance 99% and 60%, were measured using the reflectometer and used to calculate the reflectance of the areas of interest. In this case, the reflectance of asphalt at the said wavelength was found to be 0.25. A reflectance of 0.25 is therefore used in this study.

6.2. Methodology

Initially, the calibration constants for the two study areas are calculated. The backscatter cross sections are calculated based on this value. The backscatter cross sections for the two study areas would have been comparable if the flying height and footprint diameters were the same. Since this is not the case, the backscatter coefficients are calculated by normalising the backscatter cross sections with the area of the footprint. The decision tree classifier is modified by replacing amplitude by the backscatter cross section and the backscatter coefficient derived from the training points in Bristol_Riegl. These decision tree classifiers are now applied on the data from Bournemouth_Riegl. The classifications are then compared to determine whether the calibrated intensity values give advantages over amplitude, in terms of accuracy. The workflow is as shown in Figure 38 (page 110).

6.2.1. Calculation of the Calibration Constant

The theoretical backscatter cross section at nadir is (Briese et al., 2008; Höfle and Pfeifer, 2007; Jelalian, 1991; Wagner et al., 2006):

$$\sigma = \pi \rho R^2 \beta^2 \quad [18]$$

where σ is the backscatter cross section in m^2 , ρ is the reflectance of the target surface, R is the range (the distance from the sensor to the target) in m and β is the laser beam divergence angle in radians.

From the radar equation, Wagner et al. (2006) derived the following equation for the 'apparent' cross section of each surface within the laser footprint:

$$\sigma = C_{cal} R^4 PW \quad [19]$$

where C_{cal} is the calibration constant, P is the amplitude of the echo, W is the echo width

Assuming a reflectance of 0.25 for asphalt, the calibration constant can be calculated from the equations, [18] and [19] as:

$$C_{cal} = \frac{0.25\pi\beta^2}{R^2PW} \quad [20]$$

where P is the amplitude and W is the echo width of each point on the selected sections of asphalt road. The laser beam divergence angle (β), is 0.5 mrad for Riegl LMS-Q560. As seen earlier in section 3.2.2, the width of the echo from the Riegl software corresponds to the

FWHM of amplitude of the Gaussian pulse. This was converted to the echo width in seconds using equation [15] (page 41).

Nine sections of asphalt road were selected from the study area in Bristol. From these sections, the points with scan angle from 89.5 to 90.5, amplitude less than 40 and standard deviation of elevations less than 0.2 m, were selected. The scan angle being almost 90°, almost horizontal sections were chosen to avoid the influence of incidence angle on the echo. Points with amplitude greater than 40 were removed so that points from white road markings were not included. There were 566 points from the nine road sections. The mean of the calculated calibration constants, $4.45 \cdot 10^{-6}$, was used for the calculation of backscatter cross section and backscatter coefficients.

6.2.2. Derivation of Attribute Values Based on Backscatter Cross section

The backscatter cross section (Chilton et al.) increases with the area of the laser beam footprint on the target. For a particular beam width, the area of the footprint changes with the flying height at nadir. The cross section per unit area, denoted as γ , is considered to be a better attribute for comparing the scattering characteristics of area-extensive targets which produce single echoes from different sensors and flight parameters (Ulaby et al., 1982; Wagner et al., 2008b). However, the illuminated area changes with the incidence angle of the beam on a given surface. Even then, the scattering strength is often related to the cross section of the incoming beam for convenience (Schanda, 1986; Wagner et al., 2008b).

Cross sectional area of the incoming beam (Wagner et al., 2008b) is:

$$A_c = \frac{\pi \cdot R^2 \cdot \beta^2}{4} \quad [21]$$

where R is the distance from the sensor to the target in m and β is the laser-beam divergence angle in radians.

The back scatter cross section per unit area of the incoming beam can be calculated as (Wagner et al., 2008b):

$$\gamma_{ci} = \frac{\sigma}{A_c} \quad [22]$$

A problem with using this equation on multiple targets, as pointed out by Wagner et al. (2008b), is that the cross section of individual targets are normalised with the area of the incoming beam, rather than the area of the footprint on the individual target. The scattering properties of small targets, such as the multiple echoes from vegetation, would therefore

become less comparable. However, as noted by Wagner et al. (2008a), the total backscatter cross section per emitted pulse is the sum of the individual cross sections. Therefore, this could probably be corrected to a certain extent by calculating the total backscatter cross section from a single emitted pulse before normalising with the area as:

$$\gamma_{cs} = \frac{\sigma_1 + \sigma_2 + \dots + \sigma_n}{A_c} \quad [23]$$

where σ_1, σ_2 etc. are the backscatter cross sections of the different targets within the laser footprint.

The cross section per unit illuminated area (σ^0) is the most widely used parameter in radar remote sensing. However, this requires the incidence angle of each echo, and significant processing and modelling are necessary to estimate the local incidence angle on an inclined surface. The use of σ^0 is therefore not recommended in ALS (Wagner et al., 2008b).

The off-nadir laser footprint is elliptical in shape, with the area increasing with the scan angle. On a horizontal flat surface, the area of the footprint is about 5% larger at a scan angle of 10°, 21% at 20° and 54% at 30° than the area at nadir (Yongwei, 2008). The increase in the area of the footprint with increasing scan angle may therefore have to be taken into consideration depending on the maximum scan angle of a dataset.

The area of the laser footprint on a horizontal surface can be calculated as (Yongwei, 2008):

$$A_e = \pi \cdot R^2 \cdot \frac{1 - \cos \beta}{\cos \theta \cdot (\cos 2\theta + \cos \beta)} \quad [24]$$

where θ is the instantaneous scan angle and β is the divergence angle of the laser-beam.

The equations [22] and [23] can be adapted for the area of the footprint corrected for scan angle as:

$$\gamma_{ei} = \frac{\sigma}{A_e} \quad [25]$$

$$\gamma_{es} = \frac{\sigma_1 + \sigma_2 + \dots + \sigma_n}{A_e} \quad [26]$$

To summarise, γ_{ci} is the backscatter cross section of each target (σ) divided by the cross sectional area of the incoming beam (A_c). γ_{cs} is the sum of the backscatter cross sections of multiple targets of a single emitted beam ($\sum_{i=1}^n \sigma_i$) divided by the cross sectional area of the incoming beam (A_c). γ_{ei} is the backscatter cross section of each target (σ) divided by the corrected area of the footprint (A_e). γ_{es} is the sum of the backscatter cross sections of multiple targets of a single emitted beam ($\sum_{i=1}^n \sigma_i$) divided by the corrected area of the

footprint (A_e). These derived attributes were used to replace amplitude, and generate decision trees to classify the full-waveform dataset.

6.2.3. Generation of Additional Decision Trees for Classification

The backscatter cross section of each point (σ) in the training data from Bristol_Riegl was calculated. Decision trees were generated, replacing the amplitude by the backscatter cross section as an attribute. This was repeated using the backscatter coefficients: γ_{ci} , γ_{cs} , γ_{ei} and γ_{es} . The six decision trees were then used to classify the data from Bournemouth_Riegl. The attributes used in the decision trees were selected, or calculated for the thinned Bournemouth_Riegl dataset as described in the following sections.

6.2.4. Pre-processing of the ALS Data from Bournemouth

The full-waveform data, Bournemouth_Riegl, in LAS format, included information about the time at which the pulse was emitted (also referred to as the time stamp), the location, height, amplitude and echo number of each echo and the number of echoes detected in the full-waveform. The echo number corresponds to whether the point is a first, second or higher order echo from multiple echoes. In the case of a single echo, the echo number as well as the number of echoes is one.

Another output from the proprietary RiAnalyze software, described in section 3.2.2, provided the time stamp of the emitted pulse, and the range, scan angle and width of each received echo. Since these two files had the time stamp as a common attribute, the two files could be joined. The joined file had attributes from both the files.

6.2.5. Classification of Points using Decision Trees

The dataset contained 12,914,815 points from seven flight lines (Figure 13 B, page 48), providing a point density of above 50 points m^{-2} . The points had to be thinned to make a better comparison with the data from Bristol_Riegl, which was approximately 1 point m^{-2} . A point shapefile was created with points at 1m spacing in a grid within the study area. Data points that were nearest to the grid points were selected (Figure 39, page 110). In the case of multiple echoes, all echoes with the same time stamp were also added to the selection. After thinning, there were 337,198 points in an area of 250,000 sq. m in the dataset.

This thinned data from Bournemouth_Riegl had the following attributes for each received echo: unique identifier, time stamp, easting, northing, elevation, amplitude, echo number, number of echoes, range, scan angle and echo width. A TIN was created from the points, using

elevation as the attribute. This was converted to TIN triangles and intersected with the points. The attribute values were calculated as explained earlier, in section 6.2.2.

Ten sections of asphalt road were selected from the un-thinned Bournemouth_Riegl data. The points selected were from road sections with scan angle from 89.5° to 90.5° and the range of heights less than 0.2 m. There were 1,898 points from the ten road sections. The mean of the calculated calibration constants, 1.74×10^{-5} , was used for the calculation of backscatter cross section and backscatter coefficients for each point in the dataset.

The six decision trees generated using the training data from Bristol_Riegl, mentioned in section 6.2.3 were now used to classify the points. The attributes 'class' and 'node' were added to the existing attributes of each point. The points could now be displayed according to their class for visual analysis. The classification results using the six decision trees were compared, as discussed in the following section.

6.2.6. Assessment of Accuracies

Reference polygons belonging to the different classes were manually delineated using the attributes of the ALS points, and visual analysis of the aerial photograph and MasterMap (Figure 40, page 113). Most of the incorrect classifications of buildings as trees occur at the building edges, as discussed in Chapter 4. Care was therefore taken to include the building edges as well in the reference polygons. The points within these reference polygons were selected for assessing the accuracies of classification. There were 3,520 points in all, consisting of 1,076 points from trees, 109 points from shrubs, 708 points from grass, 702 points from road, 399 points from flat roofs and 526 points from pitched roofs. The class of the manually referenced point was added as an attribute of a point before classification. The classification of points using the six decision trees were compared with the class of the reference data to get an estimate of the accuracies of the different methods.

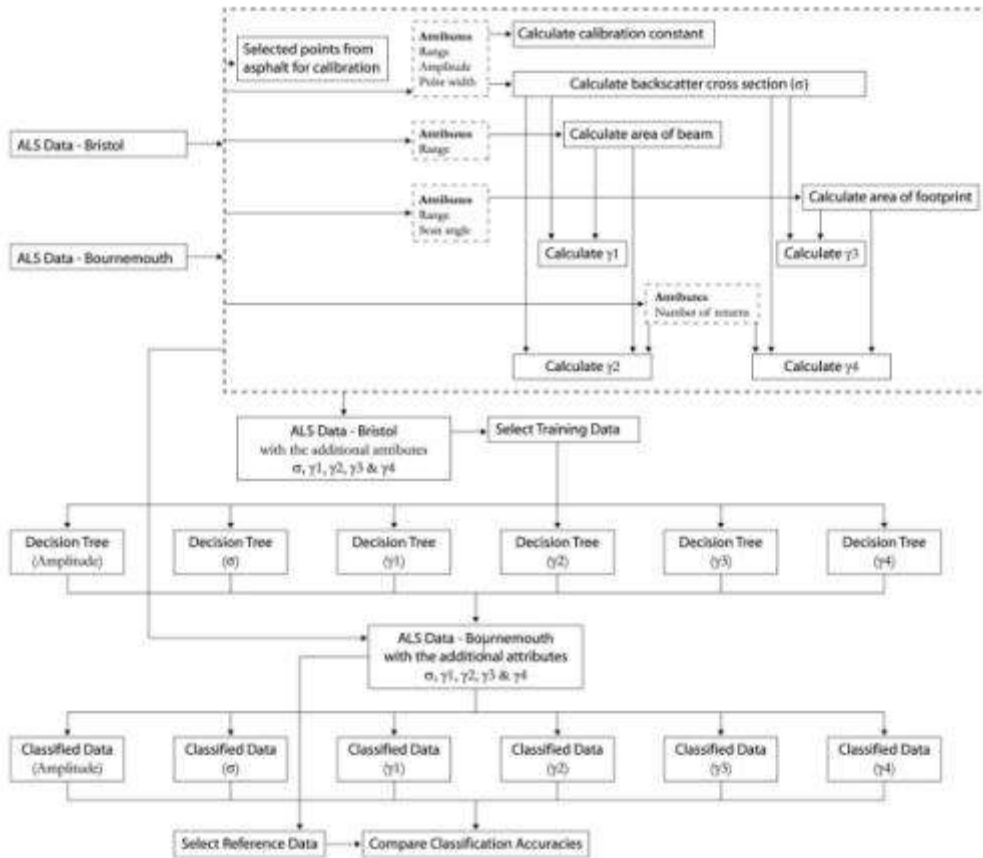


Figure 38: Workflow for the classification of full-waveform ALS data using additional attributes derived from intensity in decision tree classifiers

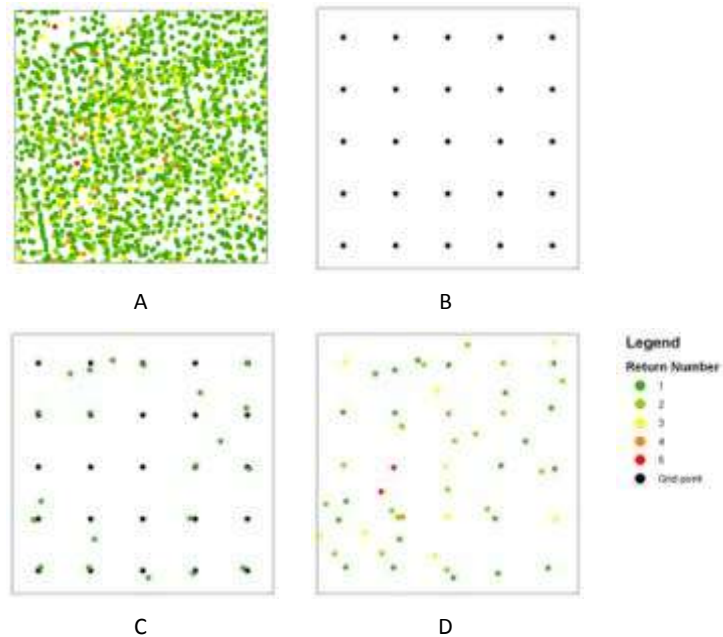


Figure 39: The workflow for thinning the data; (A) A subset of the original un-thinned ALS point cloud; (B) Grid points at 1 m spacing; (C) First echo points closest to the grid points; (D) The thinned dataset

obtained by including the second, third, fourth and fifth echo points if the selected points in (C) are the first from multiple echoes (ALS data - Ordnance Survey © Crown Copyright. All Rights Reserved)

6.3. Results

The classification from the decision tree using amplitude is shown in Figure 41 (page 113). A major misclassification is the classification of a road at a higher elevation than the land below as a building (Figure 42, page 114). On visual analysis of the data, displayed by the assigned node number, the other major misclassifications are in the nodes using amplitude (Figure 43, page 114). The resulting leaf nodes are grass, road, trees and pitched roofs.

The calibration constants in Bristol and Bournemouth were calculated as 4.45×10^{-6} and 17.4×10^{-6} respectively. These were used to calibrate the datasets from the two study areas, and estimate the backscatter cross sections and backscatter coefficients. The kappa coefficients, overall accuracies, average user's accuracies and average producer's accuracies of the six decision trees are shown in Table 21. All the accuracies are the highest for the third classification using γ_{ci} as an attribute. The accuracies of the classifications using backscatter coefficients are higher than the ones using amplitude and backscatter cross section.

Table 21: Kappa coefficients, overall accuracies, average user's accuracies and average producer's accuracies of the classifications for the six decision trees using amplitude, σ , γ_{ci} , γ_{cs} , γ_{ei} and γ_{es} as attributes

	Amplitude	σ	γ_{ci}	γ_{cs}	γ_{ei}	γ_{es}
Kappa coefficient	0.67	0.68	<u>0.89</u>	0.83	<u>0.89</u>	0.87
Overall Accuracy	73.44	74.52	<u>91.53</u>	86.76	91.11	89.91
Average User's Accuracy	82.23	68.24	<u>90.36</u>	87.63	90.14	89.74
Average Producer's Accuracy	78.93	76.70	<u>91.11</u>	84.29	90.90	87.89

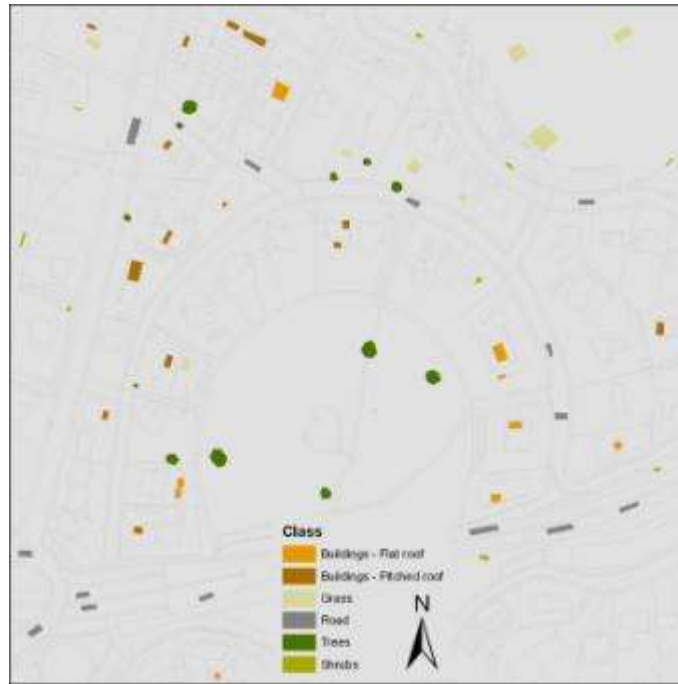


Figure 40: Polygons used for selecting the points within them to be used as the reference data in Bournemouth (OS MasterMap - Ordnance Survey © Crown Copyright. All Rights Reserved)

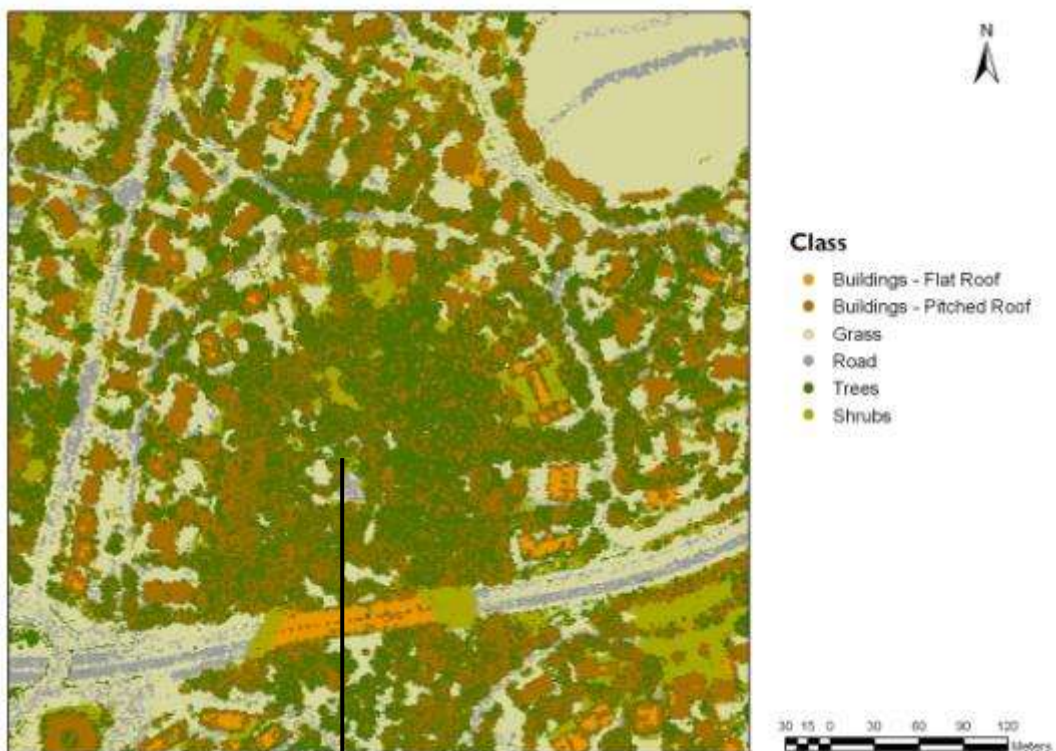


Figure 41: Points classified using the decision tree with amplitude as an attribute, converted to polygons by merging Thiessen polygons based on class. The section line through the misclassified road is shown in black.

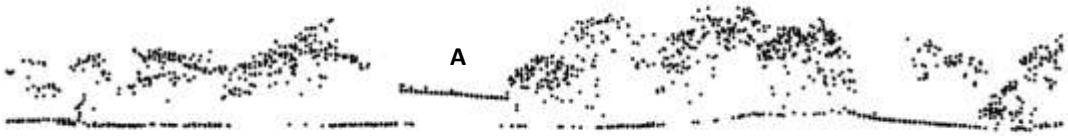


Figure 42: Section through the misclassified road (A). The section line is shown in Figure 41. (ALS data - Ordnance Survey © Crown Copyright. All Rights Reserved)

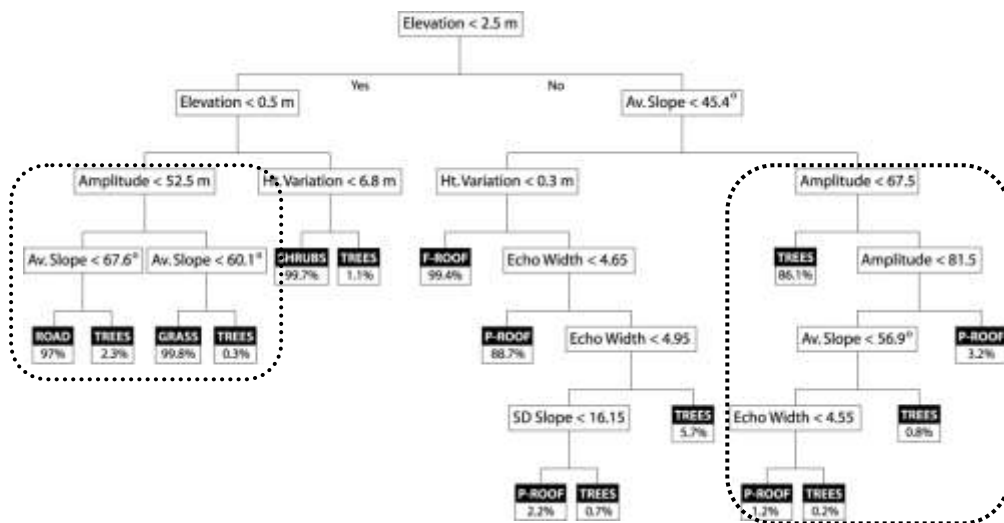


Figure 43: Nodes of the decision tree dependent on amplitude values for classification (within the rectangles)

After pruning, the decision tree using γ_{ci} as an attribute had 31 nodes including 16 leaf nodes. Grass, road and flat roofs required only one leaf node each. As in the decision tree using amplitude as an attribute, the greatest difficulty was in the separation of pitched roofs and trees (Figure 44). The classified points for the decision tree using γ_{ci} are shown in Figure 45.

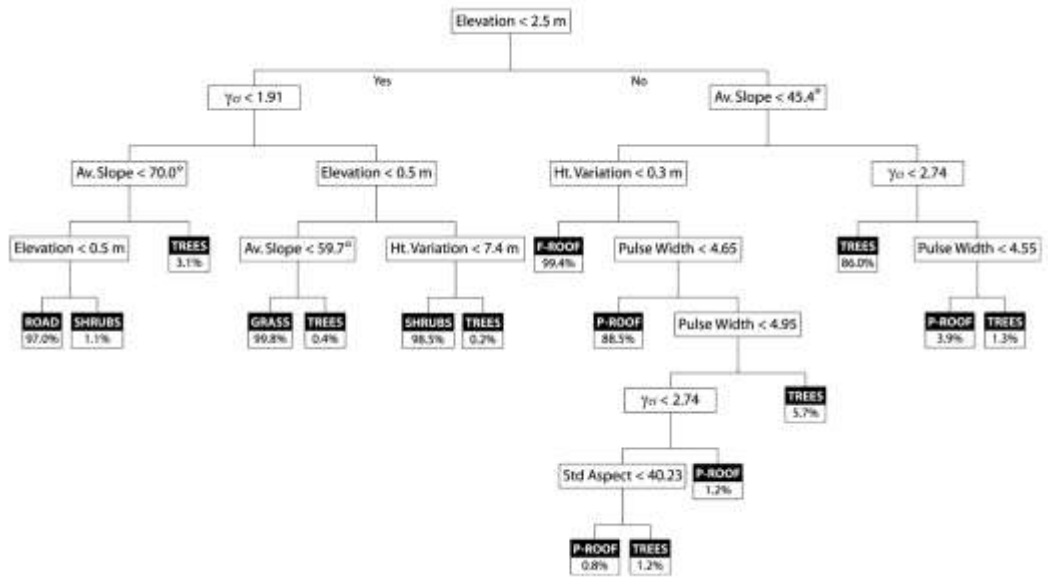


Figure 44: Decision tree with γ_{ci} as an attribute.

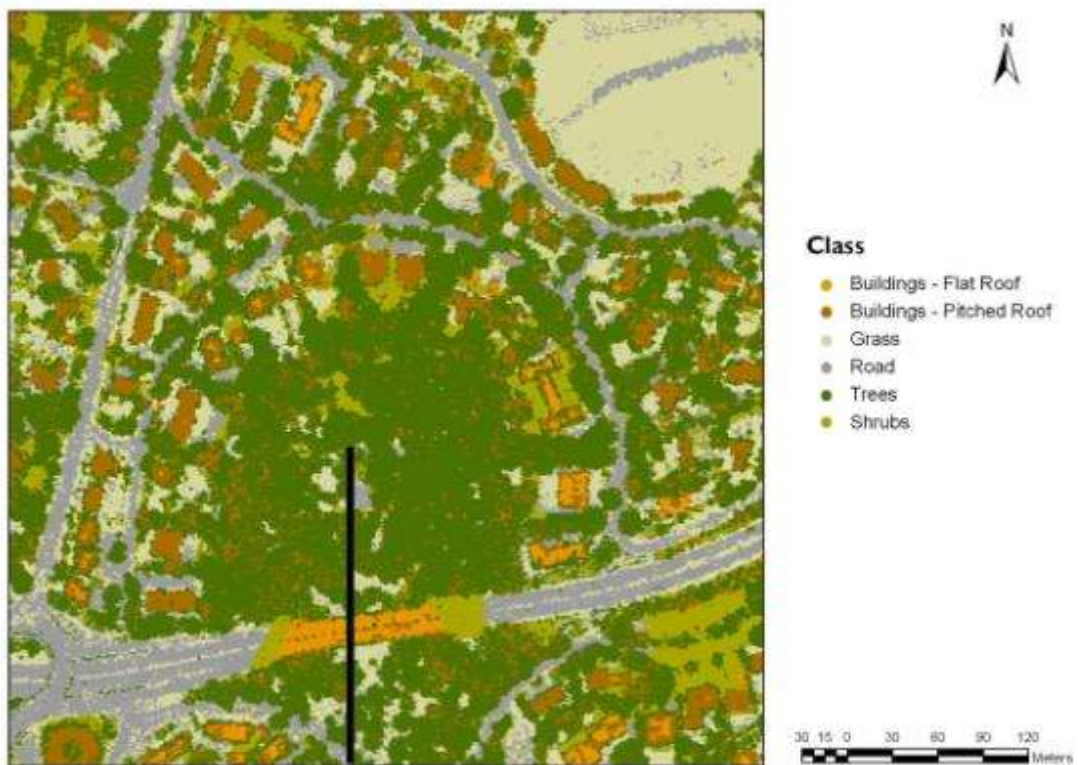


Figure 45: Points classified using the decision tree with the backscatter coefficient (γ_{ci}) as an attribute, converted to polygons by merging Thiessen polygons based on class.

6.4. Discussion

6.4.1. Comparison of the Calibration Constants

The calibration constant in Bournemouth is nearly four times the calibration constant in Bristol. As noted in chapter 3, the average flying heights, in Bristol and Bournemouth, were 950 m and 300 m. This accounts for much of the difference in the values of the calibration constants in the two study areas, as shown in equation [27]. From equation [20] (page 105), the calibration constant is derived from the divergence angle of the laser beam, range, amplitude, and echo width of each point on the selected sections of asphalt road. The divergence angle of the laser beam is the same for the two study areas as the same sensor is used in both the cases. The ratio of the mean range of the selected points in Bournemouth to the mean range in Bristol is approximately 2.85. Similarly, the ratios of the mean amplitude and echo width are approximately 0.48 and 0.98 respectively. Therefore, the ratio of the calibration constants in Bristol, C_{cal1} , and Bournemouth, C_{cal2} , is:

$$C_{cal1} = \frac{0.25 \pi \beta^2}{R_1^2 \cdot P_1 \cdot W_1}; \quad C_{cal2} = \frac{0.25 \pi \beta^2}{R_2^2 \cdot P_2 \cdot W_2}$$
$$\frac{C_{cal2}}{C_{cal1}} = \frac{R_1^2 \cdot P_1 \cdot W_1}{R_2^2 \cdot P_2 \cdot W_2} = \left(\frac{R_1}{R_2}\right)^2 \cdot \frac{P_1}{P_2} \cdot \frac{W_1}{W_2} = 2.85^2 \cdot 0.48 \cdot 0.98 = 3.82 \quad [27]$$

where β is the laser beam divergence angle, and P_1 and P_2 are the average amplitudes and W_1 and W_2 are the average echo widths of points on the selected sections of asphalt road in Bristol and Bournemouth.

The road sections were selected to have scan angles close to 90° to reduce the effects of scan angles on the amplitude and echo width. Even then, there were slight differences in the calculated calibration constants within each study area (Figure 46A & Figure 47A). The means of the calibration constants for all the points in the selected sections of road in both the study areas were used for the analysis (Figure 46B & Figure 47B). The mean of the calculated calibration constants in Bristol was found to be 4.45×10^{-6} , when the average of all the points was calculated. When the means of the sections were calculated, and the calibration constant was taken as the mean of these means, a value of 4.84×10^{-6} was obtained. The mean of the calculated calibration constants in Bournemouth was found to be 17.38×10^{-6} , when the mean of all the points was calculated. When the means of the sections were calculated, and the calibration constant was taken as the mean of these means, a value of 16.86×10^{-6} was obtained. The slight differences in the values could be due to the differences in the age and

material used for surfacing the roads, leading to differences in reflectance values. This could have an impact on the calibration constant, and thereby on the classification.

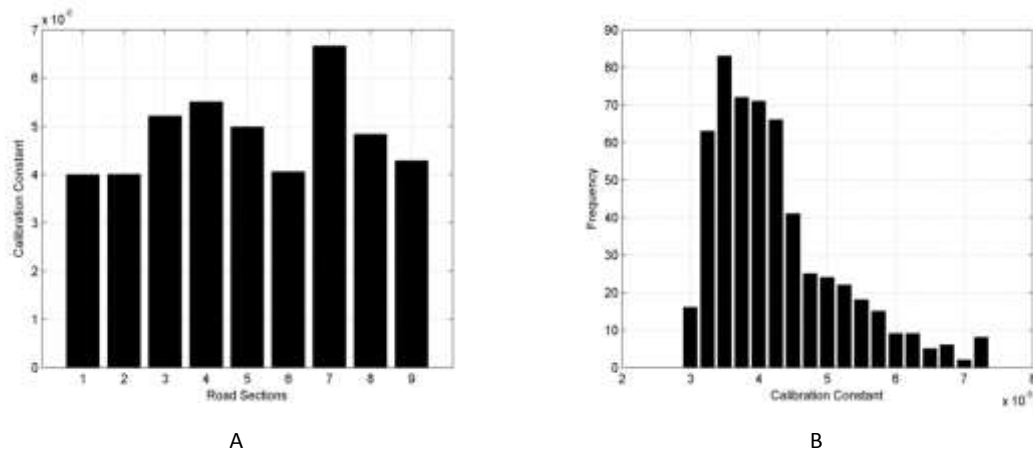


Figure 46: (A) Mean of the calibration constants for the nine road sections and (B) the frequencies for all the points in Bristol

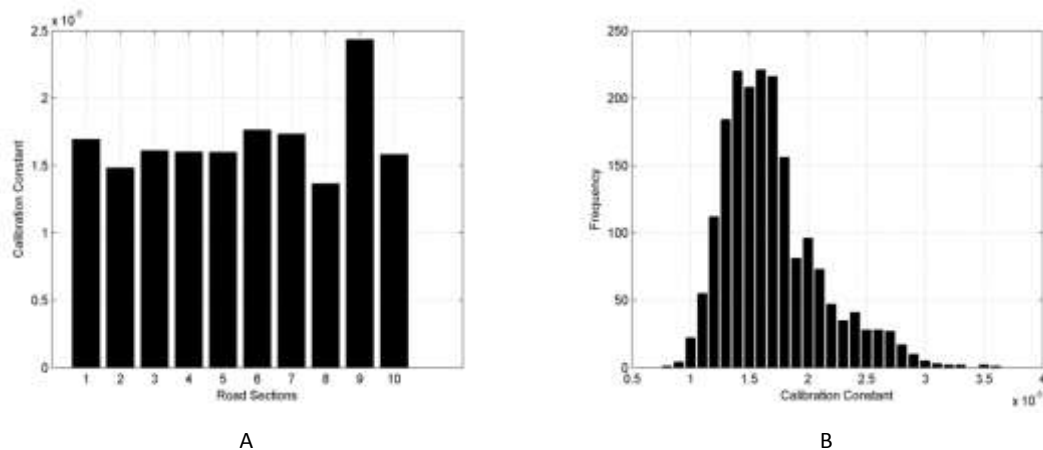


Figure 47: (A) Mean of the calibration constants for the ten road sections and (B) the frequencies for all the points in Bournemouth

The reflectance of asphalt chosen for calculating the calibration constant could also have an influence on the results of the classifications. The calibration constants for both the datasets were calculated assuming the reflectance of asphalt to be 0.25 from Briese et al. (2008). However, the fact sheet for the scanning system gives this value as 0.20. From equation [27] (page 116), it does not make a difference to the ratio of the calibration constants, if the chosen values were different, as long as they were the same for the two sites. A more accurate way would be to measure the reflectance values using a spectrometer during the field campaign, and use those instead of 0.25.

6.4.2. Accuracies of Classification

The six decision trees based on amplitude, backscatter cross section and the four backscatter coefficients had different numbers of nodes after pruning. Since the decision tree using amplitude as an attribute contained 31 nodes, the five other decision trees were pruned further to have a maximum of 31 nodes for a better comparison (Table 22). The pruning level 1 refers to the initial pruning, and pruning level 2 denotes the pruning level selected to have no more than 31. The numbers of nodes from the initial and modified pruning levels are also shown.

Table 22: (Column 1) The six decision trees are based on amplitude, backscatter cross section (Chilton et al.) and the four backscatter coefficients (γ_{ci} , γ_{cs} , γ_{ei} and γ_{es}); (Column 2) The number of nodes in the unpruned decision tree generated using the six attributes; (Column 3) The initial pruning level; (Column 4) The number of nodes resulting from pruning level 1; (Column 5) The pruning level selected to have no more than 31 nodes, the number of nodes in the pruned decision tree using amplitude as an attribute in pruning level 1; (Column 6) The final number of nodes using pruning level 2.

	Number of nodes - Initial	Pruning level 1	Number of nodes - Pruned 1	Pruning level 2	Number of nodes - Pruned 2
Amplitude	485	25	31	25	31
σ	465	18	41	20	31
γ_{ci}	487	18	45	20	31
γ_{cs}	467	21	43	25	29
γ_{ei}	533	27	41	29	31
γ_{es}	519	22	41	24	31

The classification using σ gave the highest number of correctly classified trees. It would also seem from Table 21 that the accuracies are comparable to the one using amplitude. However, it can be seen from Table 23 that all the points from grass are incorrectly classified using σ . The majority of them seem to be classified as road.

The average user's and producer's accuracies are the highest for the classification using γ_{ci} , the backscatter coefficient using the circular area of the beam and the backscatter cross section of the individual points [22], although they are only slightly better than the one using γ_{ei} (Table 24). Although the producer's accuracies for the classification using σ are the highest for trees, shrubs and road, the accuracies for grass are 0%. It would therefore be better not to use this attribute for classification when all the classes are considered. Points from no other class are classified as flat roof using any of the attributes. Their user's accuracies are therefore 100%. The user's and producer's accuracies for all the classes using the backscatter coefficients, except for two instances in the classification using γ_{cs} , are higher than 70%.

Table 23: Error matrix showing points in each class in the reference data and from the decision tree classifications using amplitude, backscatter cross section (Chilton et al.) and backscatter coefficients (γ_{ci} , γ_{cs} , γ_{ei} and γ_{es}).

	Reference Points	Classified Points					
		Trees	Shrubs	Grass	Road	F-Roof	P-Roof
Amplitude	Trees	<u>625</u>	0	0	1	0	450
	Shrubs	4	<u>105</u>	0	0	0	0
	Grass	1	1	<u>705</u>	1	0	0
	Road	0	0	361	<u>341</u>	0	0
	F-Roof	7	23	27	3	<u>284</u>	55
	P-Roof	1	0	0	0	0	<u>525</u>
σ	Trees	<u>1029</u>	3	0	2	0	42
	Shrubs	2	<u>107</u>	0	0	0	0
	Grass	0	1	<u>0</u>	707	0	0
	Road	0	0	0	<u>702</u>	0	0
	F-Roof	13	23	0	30	<u>284</u>	49
	P-Roof	25	0	0	0	0	<u>501</u>
γ_{ci}	Trees	<u>973</u>	1	0	3	0	99
	Shrubs	4	<u>105</u>	0	0	0	0
	Grass	1	1	<u>669</u>	37	0	0
	Road	0	0	27	<u>675</u>	0	0
	F-Roof	11	23	23	7	<u>284</u>	51
	P-Roof	10	0	0	0	0	<u>516</u>
γ_{cs}	Trees	<u>862</u>	0	0	1	0	213
	Shrubs	3	<u>76</u>	0	29	0	1
	Grass	1	1	<u>674</u>	32	0	0
	Road	0	0	59	<u>643</u>	0	0
	F-Roof	11	13	23	17	<u>284</u>	51
	P-Roof	11	0	0	0	0	<u>515</u>
γ_{ei}	Trees	<u>956</u>	1	0	3	0	116
	Shrubs	4	<u>105</u>	0	0	0	0
	Grass	1	1	<u>693</u>	13	0	0
	Road	0	0	50	<u>652</u>	0	0
	F-Roof	11	23	23	7	<u>284</u>	51
	P-Roof	9	0	0	0	0	<u>517</u>
γ_{es}	Trees	<u>963</u>	0	0	2	0	111
	Shrubs	4	<u>90</u>	0	15	0	0
	Grass	1	1	<u>697</u>	9	0	0
	Road	0	0	86	<u>616</u>	0	0
	F-Roof	9	15	23	15	<u>284</u>	53
	P-Roof	11	0	0	0	0	<u>515</u>

Table 24: User's and producer's accuracies of classifications for the six decision trees – using amplitude, backscatter cross section (Chilton et al.) and backscatter coefficients (γ_{ci} , γ_{cs} , γ_{ei} and γ_{es}).

User's Accuracies						
	Amplitude	σ	γ_{ci}	γ_{cs}	γ_{ei}	γ_{es}
Trees	<u>97.96</u>	96.26	97.40	97.07	97.45	97.47
Shrubs	81.40	79.85	80.77	84.44	80.77	<u>84.91</u>
Grass	64.50	0.00	<u>93.05</u>	89.15	90.47	86.48
Road	<u>98.55</u>	48.72	93.49	89.06	96.59	93.76
F-Roof	100.00	100.00	100.00	100.00	100.00	100.00
P-Roof	50.97	<u>84.63</u>	77.48	66.03	75.58	75.85
Average	82.23	68.24	<u>90.36</u>	87.63	90.14	89.74
Producer's Accuracies						
	Amplitude	σ	γ_{ci}	γ_{cs}	γ_{ei}	γ_{es}
Trees	58.09	<u>95.63</u>	90.43	80.11	88.85	89.50
Shrubs	96.33	<u>98.17</u>	96.33	69.72	96.33	82.57
Grass	<u>99.58</u>	0.00	94.49	95.20	97.88	98.45
Road	48.58	<u>100.00</u>	96.15	91.60	92.88	87.75
F-Roof	71.18	71.18	71.18	71.18	71.18	71.18
P-Roof	<u>99.81</u>	95.25	98.10	97.91	98.29	97.91
Average	78.93	76.70	<u>91.11</u>	84.29	90.90	87.89

When kappa coefficients were used to estimate the agreement between the six classifications, there was 'almost perfect agreement' between the classifications using γ_{ci} and γ_{ei} (Table 25). The backscatter coefficients using the elliptical area of the footprint therefore do not seem to have an advantage over those using the circular footprint, when the overall accuracies are considered. There is at least 'substantial agreement', kappa coefficient higher than 0.6, between all the classifications using backscatter cross section, and four out of the six relations can be considered to be 'almost perfect agreement'. The classification using γ_{ci} has the highest accuracy and is the least complex in terms of computation. It is therefore used for the comparisons with amplitude and σ in the following paragraphs.

Table 25: Kappa coefficients of the agreements between the classifications from the six decision trees using amplitude, σ , γ_{ci} , γ_{cs} , γ_{ei} and γ_{es} as attributes

	Amplitude	σ	γ_{ci}	γ_{cs}	γ_{ei}	γ_{es}
Amplitude	1	0.40	0.64	0.62	0.67	0.65
σ	-	1	0.70	0.51	0.67	0.59
γ_{ci}	-	-	1	0.78	<u>0.94</u>	<u>0.82</u>
γ_{cs}	-	-	-	1	0.76	<u>0.82</u>
γ_{ei}	-	-	-	-	1	<u>0.85</u>
γ_{es}	-	-	-	-	-	1

The classification using amplitude is compared with the one using γ_{ci} (Table 26). The values representing the incorrectly classified points, which are more than 10% of the total number, are underlined in the table. There are 50,251 points that are classified as pitched roofs using amplitude and trees using γ_{ci} , of which only 3848 (7.6%) points seem to be within the building polygons from MasterMap (Figure 48A). The majority can therefore be considered to be correctly classified using γ_{ci} .

26,135 points are classified as grass using amplitude and road, using γ_{ci} , of which 15,215 (58.2%) points are within the polygons classified as road or track, roadside or path. Again, the majority of them seem to be correctly classified using γ_{ci} (Figure 48B). There are 3,098 points that are classified as shrubs using amplitude and trees using γ_{ci} . These misclassifications could be less important, as they are classified as vegetation in both the classifications.

Table 26: Comparison of classifications using decision trees with amplitude and γ_{ci} as attributes

Amplitude	γ_{ci}						Total
	Trees	Shrubs	Grass	Road	F-Roof	P-Roof	
Trees	140,818	1,676	0	1,792	0	270	144,556
Shrubs	<u>3,098</u>	19,367	0	0	0	0	22,465
Grass	77	0	49,099	<u>26,135</u>	0	0	75,311
Road	1	0	3	15,848	0	0	15,852
F-Roof	0	0	0	0	4,162	0	4,162
P-Roof	<u>50,251</u>	0	0	0	0	24,601	74,852
Total	194,245	21,043	49,102	43,775	4,162	24,871	337,198

Some of the points classified as shrubs using γ_{ci} seem to be within the polygons classified as roads in MasterMap (Figure 49A). These were probably classified incorrectly due to their estimated elevations from the ground. Some of the other points incorrectly classified as shrubs seem to be from vehicles, which would also have a normalised elevation greater than 0.5 m. Water has low reflectance in the infrared wavelengths. This is probably the reason for the inland water body to be classified as road (Figure 49B).

The decision tree using γ_{ci} gave the best results out of the six. It made use of five additional attributes – classified normalised elevation, height variation, average slope of TIN triangles attached to each point, echo width and standard deviation of aspects of TIN triangles to provide an overall accuracy of 91.5% and a Kappa coefficient of 0.89. Ten of the nodes in the decision tree using γ_{ci} required only three attributes for classification (Table 27). Five nodes required four attributes, and one node required all six attributes.

Flat roofs were classified based only on height, average slope and height variation. Grass and road were classified based on height and γ_{ci} . Average slope was used only to filter out points from trees in both grass and road. Node 9 is most likely to represent points on the road under trees, and node 19 could be points on grass under trees. Backscatter coefficient and echo width are used to separate trees and pitched roofs. The value for echo width seems to be generally larger for trees than pitched roofs.

Table 27: Attributes for classifying each leaf node in the decision tree using γ_{ci} as an attribute, and the percentage of correctly classified points in each class in the training data

Class	No de	Height	Average Slope	Height Variation	γ_{ci}	Echo Width	Deviation of Aspects	% of points
Trees	9	< 2.5	> 70.0°	-	< 1.91	-	-	3.1%
	14	> 2.5	> 45.4°	-	< 2.74	-	-	86.0%
	19	< 0.5	> 59.7°	-	> 1.91	-	-	0.4%
	21	< 0.5	-	> 7.41	> 1.91	-	-	0.2%
	25	> 2.5	> 45.4°	-	> 2.74	> 4.55	-	1.3%
	27	> 2.5	< 45.4°	> 0.27	-	> 4.95	-	5.7%
	31	> 2.5	< 45.4°	> 0.27	< 2.74	4.65-4.95	> 40.2	1.2%
Shrubs	17	0.5- 2.5	< 70.0°	-	< 1.91	-	-	1.1%
	20	0.5- 2.5	-	< 7.41	> 1.91	-	-	98.5%
Grass	18	< 0.5	< 59.7°	-	> 1.91	-	-	99.8%
Road	16	< 0.5	< 70.0°	-	< 1.91	-	-	97.0%
F-Roof	12	> 2.5	< 45.4°	< 0.27	-	-	-	99.4%
P-Roof	22	> 2.5	< 45.4°	> 0.27	-	< 4.65	-	88.5%
	24	> 2.5	< 45.4°	-	> 2.74	< 4.55	-	3.9%
	29	> 2.5	< 45.4°	-	> 2.74	-	-	1.2%
	30	> 2.5	< 45.4°	-	< 2.74	-	> 40.2	0.8%

The backscatter coefficient γ_{ei} , taking into consideration the increase in the area of the footprint with increasing scan angle, was thought to be better than the one using the area of the incoming beam, at the beginning of the study. This does not seem to have an influence on the accuracy of the classification. The addition of individual backscatter coefficients for multiple pulses within a footprint before calculating the backscatter coefficients γ_{cs} and γ_{es} does not have a positive influence on the classification. The attributes are analysed in more detail in the following section.



A

B

Figure 48: (A) Points classified as pitched roofs using amplitude, and trees using γ_{ci} . Polygons classified as buildings in MasterMap are shown for comparison; (B) Points classified as grass using amplitude, and road using γ_{ci} . Polygons classified as road or track, roadside or path in MasterMap are also shown for comparison. (OS MasterMap and ALS data - Ordnance Survey © Crown Copyright. All Rights Reserved)



A

B

Figure 49: (A) The three sections of road were incorrectly classified as shrubs due to their estimated elevations from the ground; (B) Water having low reflectance in the infrared wavelength, an inland water body was incorrectly classified as road. These classifications are from the decision tree using γ_{ci} as an attribute. (OS MasterMap and ALS data - Ordnance Survey © Crown Copyright. All Rights Reserved)

6.4.3. Analysis of the Attributes

The training data in Bristol, and the manually classified points in Bournemouth, were used for further analysis of the attributes related to intensity. The training data contains ‘purer’ data than the manually classified points. For example, the points from a building would not include points from the edges for training data. In the manually classified points, they are included to get a better idea about the classification accuracy. This has to be taken into consideration when the attributes are analysed.

As noted earlier, grass, road, pitched roof and trees require intensity for their classification. The values of the echo amplitude for grass and road are more clearly separated in the Bristol_Riegl data than in Bournemouth_Riegl (Figure 50). There is considerable overlap between the amplitudes of pitched roofs and trees in Bournemouth.

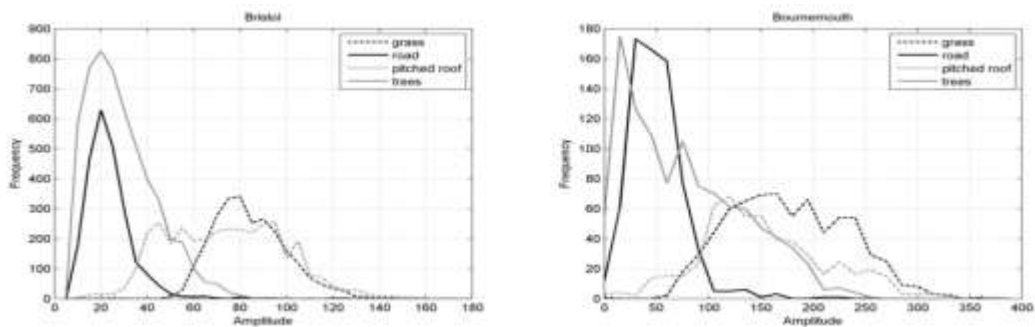


Figure 50: Frequency distribution of the amplitudes of echoes from grass, road, trees and pitched roofs in Bristol_Riegl and Bournemouth_Riegl

The footprint diameter at nadir of Bristol_Riegl is approximately 0.475 m whereas that of Bournemouth_Riegl is approximately 0.15 m. The effects of the different resolutions are more pronounced in trees than the other features, as trees reflect echoes from different surfaces within the footprint. At a higher spatial resolution, as in Bournemouth_Riegl, the variation in amplitudes of the individual elements within the smaller footprint would be higher than that at a lower resolution. This could have resulted in the different signatures of trees in Bristol and Bournemouth. Bournemouth_Riegl was collected at a lower flying height than Bristol_Riegl, 300m and 950 m respectively. The maximum scanning angle was higher for Bournemouth_Riegl at 30° than for Bristol_Riegl at 22.5°. This could also have contributed to the different shapes of the histograms.

The values for amplitude and backscatter cross section seem to be very different for the two study areas (Figure 51). The amplitude values for grass and road are higher in Bournemouth than in Bristol. This could be because of the differences in the altitudes from which the data were captured. The average flying height in Bristol was 950 m whereas it was approximately

300 m in Bournemouth. The energy of the return signal is usually higher at a lower altitude, due to the reduction in the distance between the sensor and the target.

The values for backscatter cross section are higher in Bristol than in Bournemouth, in contrast to the amplitudes. This could also be due to similar reasons as above. A higher flying height would mean a decrease in the energy of the return signal, and would require a larger area, or backscatter cross section, to represent the idealised scatterer, as described in section 2.3.2.

The value of the backscatter cross section used to separate grass and road in the decision tree classifier is also shown in Figure 51. Since it was derived from the training dataset in Bristol, it seems to separate grass and road in Bristol quite well. However, all the values for grass are less than this value. This accounts for the null accuracies for grass using backscatter cross section in Table 23 & Table 24.

The backscatter coefficients are more comparable between the two sites (Figure 51). The majority of the points from grass and road are single echoes, and the values would be the similar for γ_{CS} and γ_{ES} when compared to γ_{Ci} and γ_{Ei} .

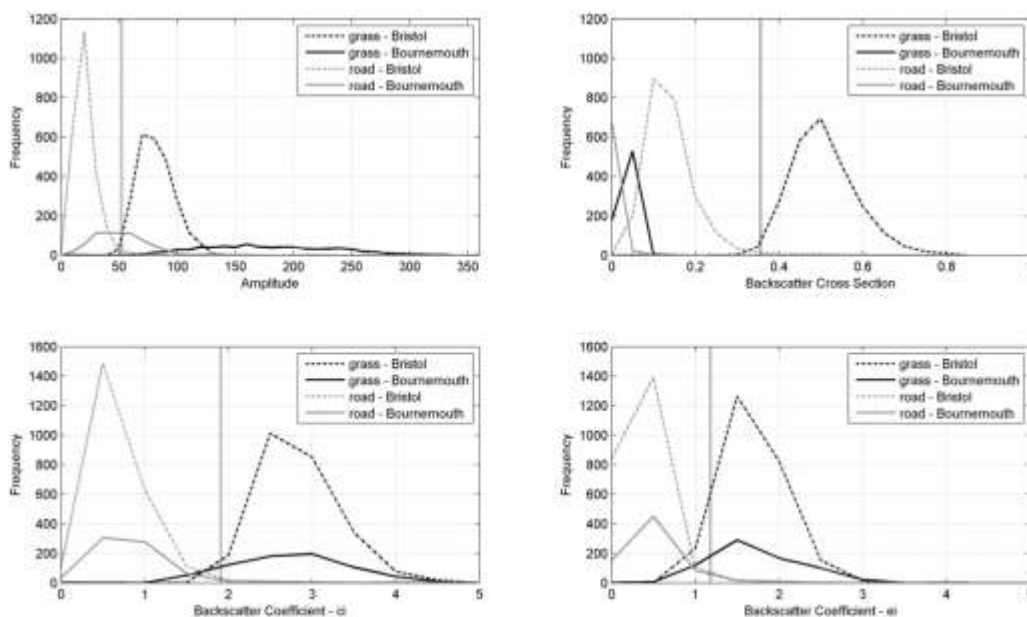


Figure 51: Frequency distribution of the amplitudes, backscatter cross sections and backscatter coefficients of echoes from grass and road in Bristol_Riegl and Bournemouth_Riegl. The values of the attributes used for separating grass and road in the decision tree classifiers are also shown.

The amplitude values for trees and pitched roofs are higher in Bournemouth_Riegl than in Bristol_Riegl (Figure 52). As seen in the case of grass and road, the backscatter cross sections are higher in Bristol_Riegl than in Bournemouth_Riegl. The values for γ_{CS} and γ_{ES} seem to be similar for pitched roofs and trees (Figure 53). The classes can be differentiated better in γ_{Ci}

and γ_{ei} . In the case of multiple echoes, the values for γ_{ci} and γ_{ei} are derived by dividing the backscatter cross section of each point with the area of the circular and elliptical footprints, and not with the area of each individual target. Although this is not correct, the coefficients derived from the total return energy from trees, γ_{cs} and γ_{es} , seem to be similar to those from pitched roofs. Even for the decision trees using γ_{ci} and γ_{ei} , this might mean that multiple echoes from trees are separated better from pitched roofs, than single echoes.

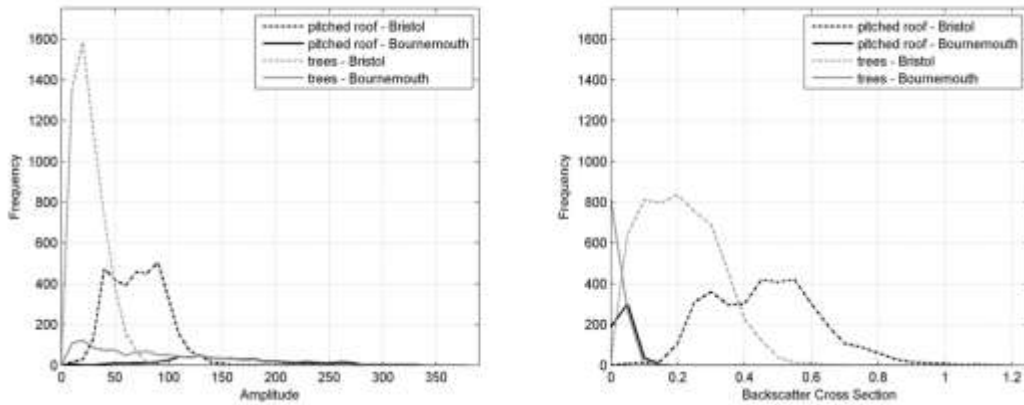


Figure 52: Frequency distribution of the amplitudes and backscatter cross sections of echoes from pitched roofs and trees in Bristol_Riegl and Bournemouth_Riegl

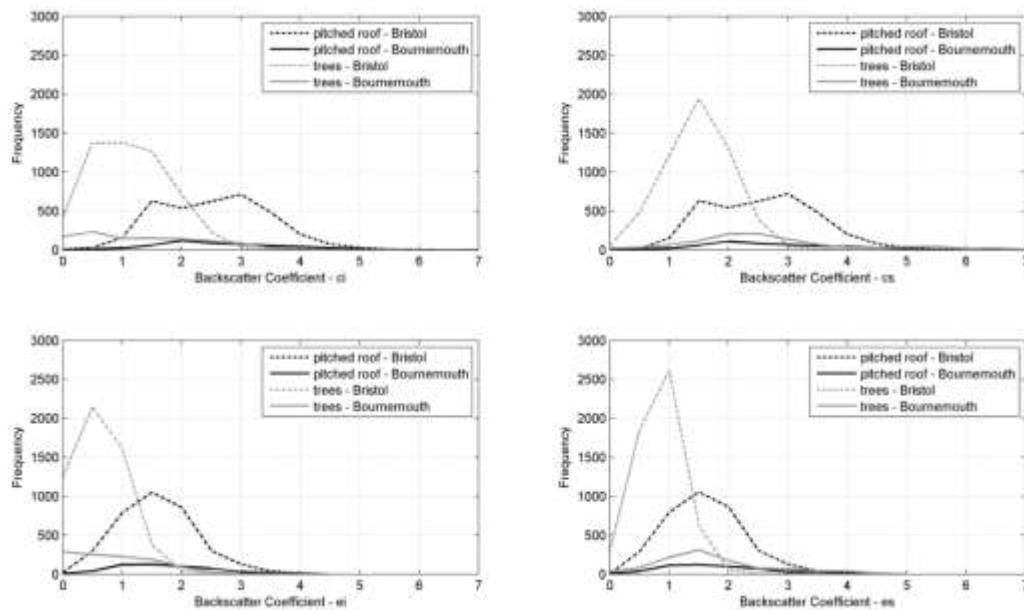


Figure 53: Frequency distribution of the backscatter coefficients of echoes from pitched roofs and trees in Bristol_Riegl and Bournemouth_Riegl

This was analysed further by separating the single echoes and the multiple echoes from trees in Bournemouth. In γ_{cs} and γ_{es} , the values from pitched roofs are similar to those from trees, for both single and multiple echoes. In γ_{ci} and γ_{ei} , the multiple echoes from trees can be

differentiated more easily than single echoes when compared with pitched roofs. This probably accounts for the incorrect classifications of trees as building roofs. This can also be seen from the values of the backscatter coefficients used in the decision trees (Figure 54 & Appendix 2).

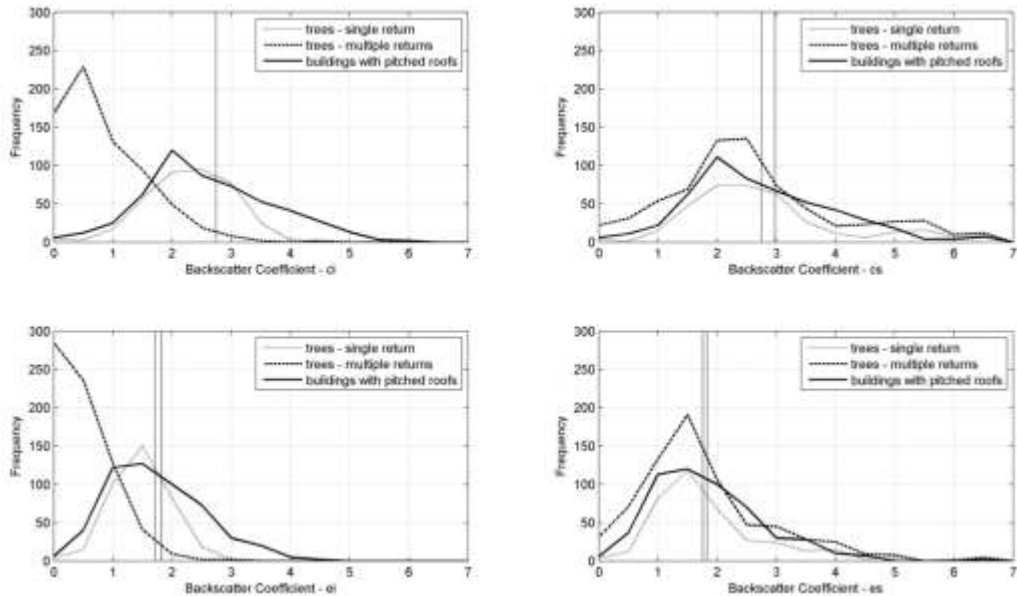


Figure 54: Backscatter coefficients of pitched roofs and trees in Bournemouth. The single and multiple echoes from trees are shown separately. The values of the attributes used for separating trees and pitched roofs in the decision tree classifiers are also shown.

6.5. Summary

Backscatter coefficient, derived from echo amplitude, width and range, proved very useful in a decision tree classifier, when it has to be used on different datasets of differing flying heights and maximum scan angles. The intensity was calibrated assuming a value of 0.25 for asphalt. The classification can probably be improved by on-site calibration before or after data capture. The calculation of normalised elevation is dependent on the accuracy of the DTM. While a rough DTM may be sufficient for an area with flat terrain, in complicated areas with bridges and flyovers, as in the study area in Bournemouth, a more accurate DTM might produce a better classification. The next chapter looks at how the classified points, especially those from vegetation and their attributes can be included in a digital topographic database.

7. Attributes of Vegetation for a Digital Topographic Database

This chapter addresses the fourth objective – to identify the three-dimensional attributes of vegetation for inclusion within a digital topographic database. The classified points cannot be directly used in a topographic map, and have to be converted to polygons.

Thiessen polygons, representing the vegetation points, are aggregated at three different scales – landscape, plot and isolated single tree. The tree crowns are delineated initially to aid the aggregation of data points. The accuracy of the single tree attributes are estimated by comparing with reference data.

7.1. Introduction

With increasing urbanisation, the relative importance of the urban vegetated environment is also increasing, due to its importance for micro-climate and recreation. Urban vegetation includes vegetation in public and private spaces – trees, groups of trees, parks and areas of shrubs and grass. Urban environments also contain a variety of other elements in complex spatial patterns (Iovan et al., 2008). In detailed topographic databases, such as MasterMap, the different surfaces are represented as polygons in vector format. They have associated attributes that could include class and height. The classified polygons could be used for urban planning, and the information about height could help in 3D visualisations.

Zhou and Troy (2008) used a hierarchical object-oriented approach for analysing and characterising urban landscape at the land parcel scale. They used colour-infrared digital aerial imagery and lidar data in eCognition software to classify the study area into five landscape elements – buildings, pavement, coarse-textured vegetation, fine-textured vegetation and bare soil. These were used to classify parcels based on the proportional composition of the five elements. They note that land parcels can be classified based on any one of the elements, or a combination of them. This approach was modified and used in this study for classifying MasterMap polygons based on the proportion of vegetation, and attributes based on elevation.

Digital topographic databases cannot directly use classified points resulting from the methods described in the previous chapters. The points need to be converted to polygons used in the digital topographic maps. Converting the points to regular raster grid would introduce errors when not all points within a cell belong to the same class. TINs have been used for creating surfaces from ALS data (Akel et al., 2005). Similarly, Thiessen polygons can also be used to convert an irregularly spaced set of points to polygons (Figure 5E; section 2.4.1).

7.2. Methodology

The Thiessen polygons, generated around ALS points, can be aggregated to larger polygons at suitable scales to derive attributes based on the points that are within each polygon. Three scales were considered for the aggregation of attributes of ALS points. At the coarser landscape scale, the Thiessen polygons are merged based on the broad classification – roads, buildings, trees and other vegetation. At the intermediate plot scale, the classified Thiessen polygons are aggregated based on the polygon features from a topographic database. At the

finer scale, the possible attributes that can be derived from ALS data within the tree polygons are explored. The trees are delineated initially to aid the aggregation of data.

7.2.1. Delineation of Tree Crowns

A subset of the study area in Bristol, from Easting 354500 to 355000 (longitude 2°39'24" W to 2°38'59" W) and Northing 178000 to 178500 (latitude 51°29'56" N to 51°30'13" N), was used for further classification and analysis. The method for delineating trees developed in this study makes use of the watershed algorithm, which has been successfully implemented for grids, on the ALS point cloud. In many of the earlier studies, the elevation from the terrain was used to find the local maximum of the elevations. Since the terrain elevation is estimated, the elevation, and not the normalised elevation, of points were used in this study. The vegetation points were selected from the points classified using the decision tree. The first echoes were selected from the data points, as these are most likely to be from the tree canopies. The spot height of each point from the DTM was used as the stopping criteria for region growing.

Delaunay triangles were created with the Easting and Northing values of the selected points (Figure 55), based on the Quickhull algorithm (Barber et al., 1996). Three different scales were used to identify the seed points. If the elevation of a point was higher than that of all the points directly connected to it by the Delaunay triangles (first-order neighbours), and normalised elevation was more than 5 m, it was flagged as a first-scale seed point. At the second scale, all the points connected to the first set of points (second-order neighbours) were also included, and if the point was higher than all the points connected to it, it was also flagged as a second-scale seed point. At the third scale, all third-order neighbours were also considered, and if the point was higher than all the selected neighbours were, it was also considered a third-scale seed point. Each set of seed points were considered the local maxima at that scale, or the estimated treetops. These were used for growing regions, or tree crowns around the seed points.

The region growing consisted of the following steps. For each seed point, at the three different scales:

1. All the points (t_1) attached to seed point, p , by Delaunay triangles, which had elevation lower than p , were identified. The algorithm searches for all points in the triangles and would include p .
2. The seed point, p , was removed from this selection.

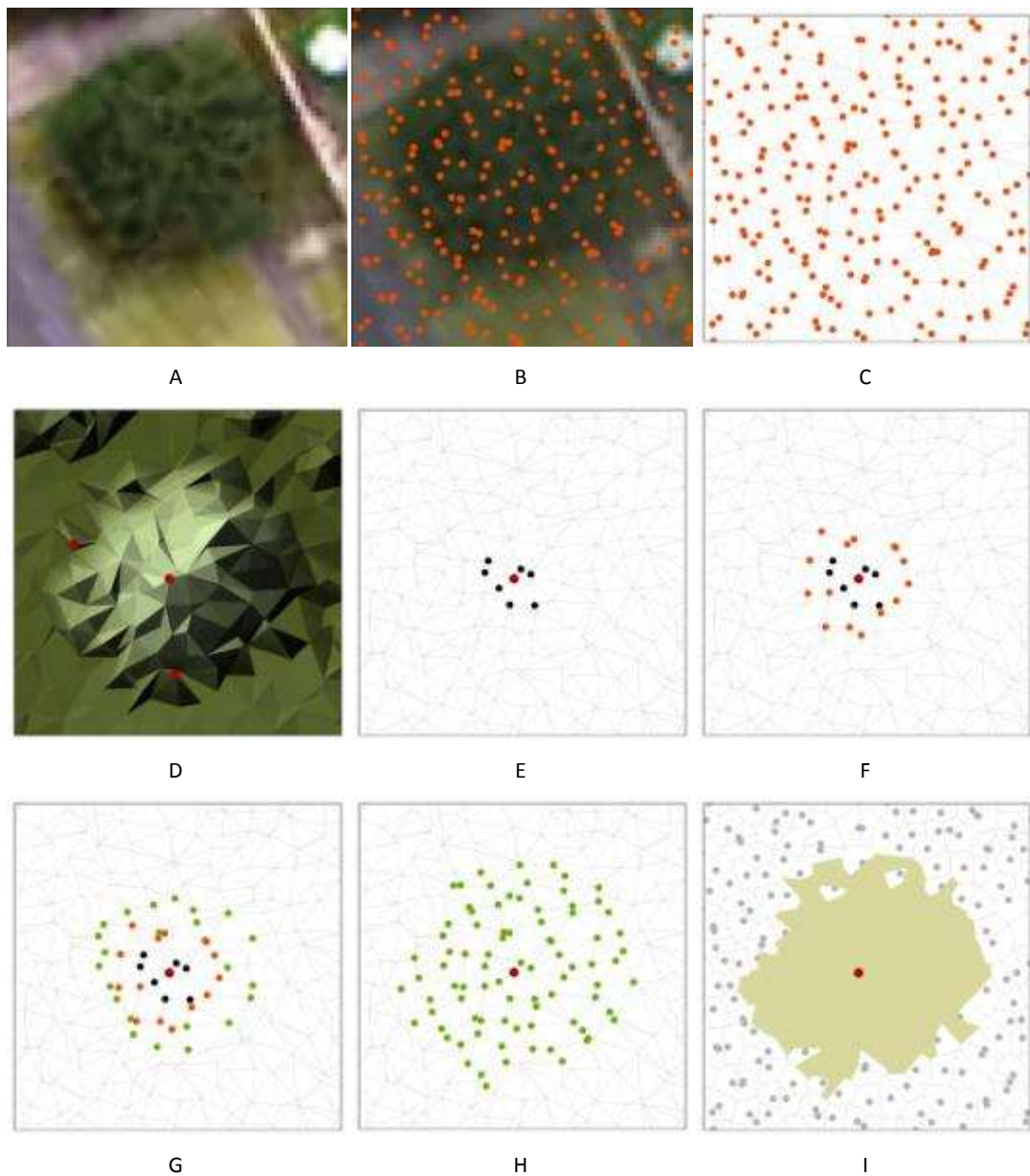


Figure 55: (A) Aerial image of a tree (Ordnance Survey © Crown Copyright. All Rights Reserved); (B) ALS point cloud; (C) Triangulated Irregular Network (TIN) generated from the points by Delaunay triangulation; (D) TIN displayed by elevation showing the estimated treetops at scale 1; (E) Seed point at scale 1 higher than one tier of points joined by TIN edges; (F) Seed point at scale 2 higher than two tiers of points; (G) Seed point at scale 3 higher than three tiers of points; (H) Points belonging to the tree at scale 3; (I) Voronoi diagram or Thiessen polygons generated from the points belonging to the tree dissolved to form the tree polygon.

3. For each point in $t1$, all the lower points attached to it, which had heights above 1 m from the ground were identified.
4. The earlier tier of points (p & $t1$) was removed from this selection.
5. The steps 3 & 4 were repeated for the third order neighbours.
6. All the selected points (p , $t1$, ...) were assigned the point ID of p , or the estimated treetop.
7. If the majority (mode) of the points assigned to a tree belonged to the 'building' class, they were reclassified as building points.

The last step was required since there were a few chimneys classified as treetops. The same methodology for delineating tree crowns was also applied in the study area in Bournemouth.

7.2.2. Aggregation at the landscape scale

Attributes can be derived for polygons representing roads, buildings, trees and other vegetation, based on elevation and the number of echoes, at the landscape scale. The flat and pitched roofs were reclassified as buildings, as the height variations within flat roofs, incorrectly classified as pitched roof, would otherwise be considered as a different building. Grass and shrubs were reclassified as other vegetation, to account for the estimated DTM. Thiessen polygons were generated around all the first return points. The Thiessen polygons representing each class were merged together to form larger polygons representing the four classes.

The reclassification step, in the process of delineation of tree crowns, corrected some of the incorrect classification of building edges. However, it also created a few incorrect reclassifications. For example, some of the building points were classified as tree points. To correct this, all the reclassified points within the polygons that were initially classified as buildings, and with an area greater than 10 m^2 , were again classified as buildings. This was based on the assumption that the minimum area of a habitable room is 10 m^2 . If a vegetation point was flagged as a tree point at any of the three scales in the tree crown delineation process, it was reclassified as tree. The Thiessen polygons were reclassified and merged based on the new classification. All building polygons, with area less than 10 m^2 , were merged with the neighbouring polygon with the largest shared border, taking into consideration the minimum area of a habitable room. This was done to correct the misclassification of points on dense tree crowns as building points.

The points within each polygon were analysed to derive attributes at the landscape scale. Since the maximum elevation of a point within the polygon would not be representative, the 95th percentile of the elevations of points within each polygon was taken as the top height (Figure 56). The average height variation, an attribute used in the decision tree, of points within a polygon was calculated as a measure of the roughness of the surface. The other attributes considered were the proportion of single echoes, and the proportion of first echoes in the case of multiple echoes (Holmgren and Persson, 2004). The proportion of single echoes would be higher for an impervious surface. In the case of vegetation, for an open canopy, the proportion of first echoes would be low.

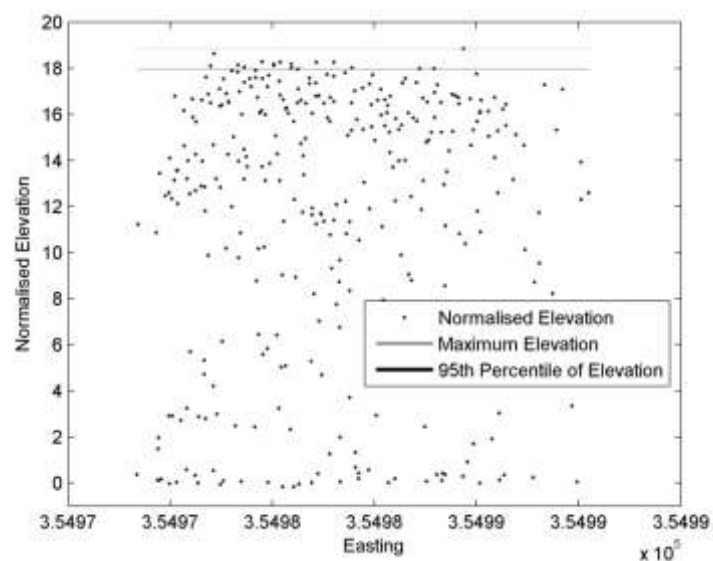


Figure 56: 95th percentile of elevation gives a more representative canopy height than maximum elevation by avoiding the outliers

7.2.3. Aggregation at the Land Parcel Scale

The classified Thiessen polygons can be aggregated at land parcel scale if digital cadastral maps are available for an area. As an example, MasterMap was used to obtain the plot divisions in the study area. However, it should be noted that building polygons are also present in MasterMap. In MasterMap, each polygon is assigned a unique topographic identifier, or ToID. An intersection of the classified polygons and MasterMap was done to assign the ToID to each polygon or sub-polygon generated by splitting of polygons by the plot divisions. The attributes at the plot scale could then be calculated.

The percentage of the area within each land parcel covered by vegetation including trees was calculated. The percentage of area covered only by trees was also calculated. The other

attributes considered, were the 95th percentile of the elevation of points within each tree polygon, polygons classified as 'other vegetation' and the polygons classified as 'tree' or 'other vegetation'. The average height variation was also calculated as a measure of the roughness of the land parcel.

7.2.4. Aggregation at the Single Tree Scale

The attributes of points can also be aggregated within the delineated tree polygons. Although there are exceptions, the points identified as third-scale seed points are the most likely to belong to treetops. They are also assumed to be the largest trees. At lower scales, the tree regions are more fragmented due to over-segmentation. The tree polygons at the landscape scale, which were assigned only one seed point in the process of tree crown delineation at scale 3, were classified as isolated single trees. In the study area in Bristol, a few of these polygons were selected by visual analysis based on circularity for further analysis. Island polygons within the single trees were merged with the tree polygon before further analysis.

The radii of the tree polygons were calculated from the areas of the polygons, which were considered circular. The ratio of height to crown radius could then be estimated. As in the landscape scale, the 95th percentile of heights and the proportions of single and first echoes were calculated. The relative 95th percentile was calculated by normalising the 95th percentile by the top height (Holmgren and Persson, 2004). The crown base height was calculated by grouping the elevations into 50 cm bins and estimating the height from the ground at which at least 1% of the total echoes are found (Holmgren and Persson, 2004; Reitberger et al., 2006). The proportion of vegetation echoes was found by estimating the echoes from above the crown base height out of the total number of echoes. The mean and standard deviation of the amplitudes were also calculated.

COMPARISON OF ATTRIBUTES WITH STREETMAPPER DATA

The data from the StreetMapper was very dense and consisted of 35,644,091 points, even though data could be collected only along the roads and paths. Thiessen polygons were generated around the points from the full-waveform data. All Thiessen polygons classified as trees were merged together to form a single polygon. This was 'exploded' in ArcMap to generate multiple polygons from spatially separate polygons. If a tree polygon contained only one third-scale seed point, it was considered to have more chances of being an isolated single tree. The data points from StreetMapper within these tree polygons were selected for comparison with the points from full-waveform data points.

The attributes considered for comparison were location, crown base height and top height. The StreetMapper data points within each tree were displayed in the Easting-Elevation and Northing-Elevation axes. The means of the Easting and the Northing values of each tree trunk were determined. If the tree trunk was not visible in both axes, it was taken to be the means of the values from the top of the tree. The crown base height and top height were taken to be the means of the manually estimated values from both the axes.

7.2.5. Applications of the Additional Attributes

In this section, a few examples to show how the information about vegetation could potentially be used in topographic maps are described. The points classified as belonging to trees in the landscape scale can be incorporated into a three-dimensional (3DLM) view of the study area. In this example, the base height was taken from the Land-form PROFILE[®] Plus, which is a DTM with a grid size of 2m. The building polygons in MasterMap were extruded to the average elevation from the terrain. The points classified as trees were converted to 3D points. The building polygons, terrain and the tree points were displayed in ArcScene[™].

The Topography Layer in MasterMap has been used to assist environmental planners in identifying and calculating hard surface areas, to identify areas at risk of flooding (Ordnance Survey, 2008). This assessment can possibly be improved if the areas covered by trees are also taken into consideration. Surface water run-off is taken as an example. It is a major contributor to flooding in urban areas, and is related to the proportion of impermeable surfaces. The surface run-off under a tree canopy is much less than that over grass. In Joffre and Rambal (1993), it was observed that surface run-off under a tree canopy was 58.97%, 48.8% and 38.89% of that on grassland outside the canopy for annual rainfalls of 797, 895 and 939 mm respectively.

A subset of the study area, 250 m x 250 m, was used to estimate the percentage of the area under natural permeable surface (Figure 64 in page 145). In MasterMap, the 'make' of a polygon is classified into manmade, multiple and natural. In this example, the areas were considered a natural permeable surface if the 'theme' was classified as 'land' and 'make' was classified as 'natural'. Some values were assumed in this example. Since the 'multiple' surface is a combination of manmade and natural surfaces, half of this area was also used in the estimation. In the classified map, the area covered by trees was assumed to be three times the ground area of other natural surface. This was to account for the additional surface area provided by the leaves, although this would depend on the leaf area index (LAI). In Scurlock et

al. (2001), the LAI of grassland, shrub and the mean LAI of temperate forests are estimated at 1.71, 2.08 and 5.41 respectively.

Isolated single trees can be considered to be point data with location, height and crown radius as attributes. Buffers can be created around each estimated treetop, with the calculated radius, to represent the trees. Some of the attributes, such as height, crown radius and crown base height, could be used for modelling trees. The identified trees were compared visually with the aerial photograph to assess the accuracy of detecting single trees.

7.3. Results

7.3.1. Delineation of Tree Crowns

The number of estimated treetops in the study area in Bristol was 3,923 at the first scale in the 500 m x 500 m area shown in the figure. The seed points reduced to 1,180 at the second scale. At the third scale, 683 treetops were detected. Figure 57 shows the estimated treetops overlaid on the aerial image at the three scales. Of the 226,301 first echo points, 53,470 were assigned to tree crowns at the first scale. At the second and third scales, 41,216 and 33,309 points were classified as belonging to tree crowns.

The detected treetops and the tree crowns at the three scales in the study area in Bournemouth are shown in Figure 58. At the first scale, the number of estimated treetops was 11,818. At the second scale, 3,161 treetops were detected. There were 1,646 estimated treetops at the third scale. There were 10,025, 2,560 and 1,318 points at the first, second and third scales, when the 'building' regions were removed. At the first scale, 118,814 points were assigned to tree crowns. This reduced to 96,930 and 85,764 points at the second and third scales.



A



B



C



D

Figure 57: (A) An aerial photograph of a subset of the study area with the seed points, or estimated tree tops displayed at (B) scale 1 (C), scale 2 and (D) scale 3 (Aerial image - Ordnance Survey © Crown Copyright. All Rights Reserved)



A



B



C



D

Figure 58: (A) An aerial photograph of a subset of the study area in Bournemouth (Ordnance Survey © Crown Copyright. All Rights Reserved) with the seed points, or estimated treetops displayed at (B) scale 1 (C), scale 2 and (D) scale 3

7.3.2. Aggregation at Different Scales

Figure 59 shows the classified polygons aggregated at the landscape scale displayed by the average height variation. The attribute table shows the values for the various attributes at this scale. The MasterMap already has some attributes assigned to each polygon. The existing attributes are shown in grey colour in the attribute table (Figure 60). The figure shows the land parcels coloured using the average height variation. The attributes of the polygons at the single tree scale are shown in Figure 61.

7.3.3. Representation of Vegetation in Topographic Maps

The single trees can be represented in MasterMap as shown in Figure 62. Only 30 (28.3%) of the 106 isolated single trees were correctly classified when compared visually with an aerial photograph of the area. There were another 41 trees (38.7%) which were single trees extending to adjacent trees or shrubs. In four cases, the single trees extended to nearby buildings. There were 24 trees (22.6%) with estimated treetops located within building roofs.

Figure 63 shows a three-dimensional view of the study area. The subset of the study area, for estimating the natural permeable surface, was 62,500 m² in area (Figure 64). From the MasterMap, the area classified as natural came to 15,567.88 m² (24.9 %). 20,570.99 m² was classified as 'multiple', and half of this was added to the area. The total percentage of permeable surfaces therefore came to 41.36%. In the newly classified map, 34,421 m² (55.07 %) was classified as vegetation and 6,876 m² as trees. The area covered by trees was tripled so that the total came to 88.08% of the study area.



Attribute	Value
ID	801
95 th percentile of heights	16.79 m
50 th percentile of heights	8.50 m
Average Height Variation	5.82 m
Proportion of single echoes	0.54
Proportion of first echoes	0.47
Total number of echoes	33919

Figure 59: Attributes of ALS points aggregated at the landscape scale



Attribute	Value
ToID	279208377
Theme	Land
DescGroup	Natural Environment
DescTerm	Non-coniferous trees; scrub
make	Natural
Vegetation Area	98.91%
Tree Area	58.74%
95 th percentile of heights (total vegetation)	12.17 m
95 th percentile of heights (trees)	13.73 m
95 th percentile of heights (other vegetation)	3.82 m
50 th percentile of heights (total vegetation)	2.46 m
Average Height Variation	3.78 m

Figure 60: Attributes of ALS points aggregated at the land parcel scale (OS MasterMap - Ordnance Survey © Crown Copyright. All Rights Reserved)



Attribute	Value
TreelD	4886
Maximum Height	25.82 m
95 th percentile of heights	24.54 m
Relative 95 th percentile	0.95
Crown base height	6.55 m
Crown radius	5.76 m
Proportion of single echoes	0.69
Proportion of first echoes	0.53
Proportion of echoes above the crown base	0.85
Mean amplitude	25.18
Mean backscatter cross section	0.2
Ratio of height to radius	4.25

Figure 61: Attributes of ALS points aggregated at the single tree scale (OS MasterMap - Ordnance Survey © Crown Copyright. All Rights Reserved)



Figure 62: Single trees represented in OS MasterMap (OS MasterMap - Ordnance Survey © Crown Copyright. All Rights Reserved)



Figure 63: A three-dimensional view of the study area with trees represented as points (OS MasterMap and ALS Data - Ordnance Survey © Crown Copyright. All Rights Reserved)

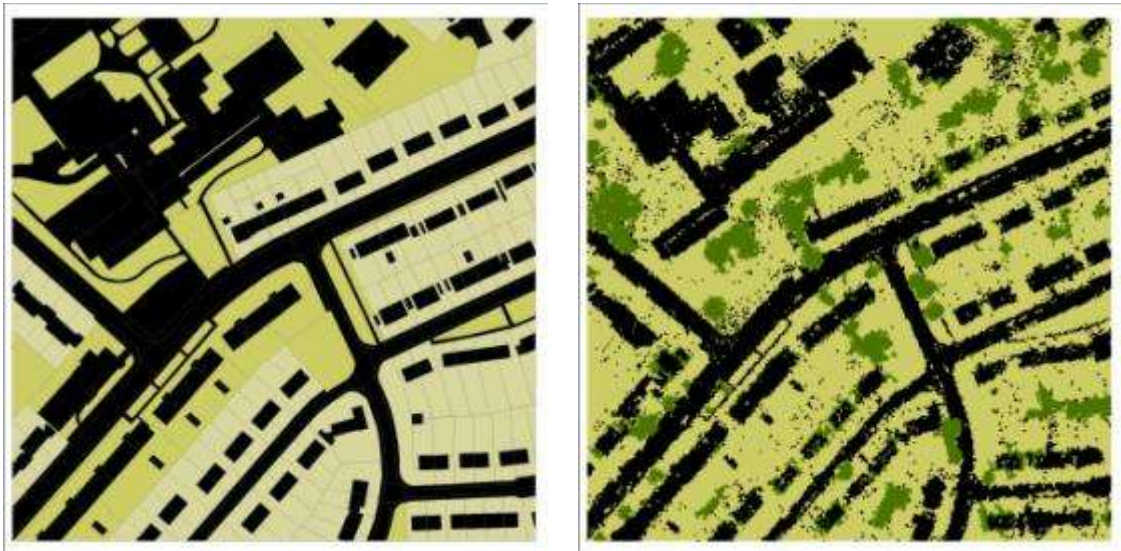


Figure 64: (A) Natural permeable surface from MasterMap and (B) from the classification (OS MasterMap - Ordnance Survey © Crown Copyright. All Rights Reserved)

21 polygons were selected as isolated single trees, for comparing with the StreetMapper data. When the points within these polygons were displayed, it was seen that four of the polygons could not be used. The points within three polygons were not clear enough to be measured, or even distinguished as a tree, and one was a lamppost. Only the points within 17 polygons could therefore be analysed. The RMS error of location was 1.65 m, and that of the height was 0.81 m. The error in the elevation of the base of the crown from the ground was 1.65 m (Table 28).

Table 28: The deviations of location, height and crown base height of trees from the reference data. The tree with ID 7 is difficult to locate, ID 10 looks like part of a building, ID 13 is a lamppost and the tree with ID 17 is not clear enough to estimate the values.

Tree ID	Deviation in Location (m)	Deviation in Height (m)	Deviation in Crown Base Height	Remarks
0	0.49	0.77	-	Coniferous; Crown base is not clearly seen
1	3.54	0.97	2.09	Bent trunk
2	1.87	-0.45	0.96	Bent trunk; Tree and lamp post
3	0.20	-1.09	0.46	Single tree
4	1.08	-0.03	-0.31	Fence below
5	1.85	0.58	-0.57	Approximate crown base height
6	1.66	-1.48	-	Location from top points; Difficult to see the base
8	1.89	-0.80	-0.79	Trees and hedge
9	1.54	-0.63	-	Group of trees
11	0.23	0.64	-	Group of trees
12	3.53	-0.06	2.64	Hedge below trees
14	0.88	-0.85	-	Base cannot be seen
15	0.65	0.05	-	Not sure whether it is a tree
16	1.43	-0.78	-1.18	Two trees
18	0.57	-1.61	-	Base is not clear
19	0.58	-0.46	-2.58	Hedge below
20	0.67	-0.23	-2.40	Shrubs below
RMSE	1.65	0.81	1.65	

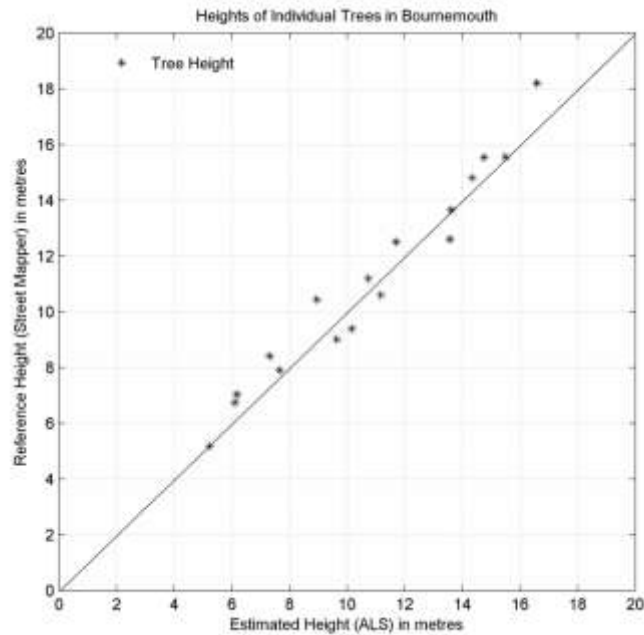


Figure 65: Estimated heights of trees plotted against the reference heights from Street Mapper.

7.4. Discussion

The average point density in the study area with the overlapping flight lines is approximately 1 point m^{-2} . The search radii for identifying the seed points in the process of tree crown delineation would therefore be 1, 2 and 3 m for scales 1, 2 and 3 respectively. Most of the tree points are identified in the region growing at the first scale (Figure 66B). However, they are highly fragmented. It is often difficult to determine whether an estimated treetop, a seed point used for region growing, is part of a larger tree, or from a small tree near a larger one. At the higher scales (Figure 66C & D), the points belonging to smaller regions are often not detected, as shown in detail in Figure 67. However, the estimation of seed points seems to be better at the third scale by visual comparison with the aerial photograph. The isolated single trees were identified using the tree segments from the first scale and third-scale seed points. Delineation of isolated trees with compact tree crowns (Figure 68) seems to be better than that of larger trees with complex structure, or groups of trees.

Some of the chimneys on pitched roofs were classified as trees using the decision tree, and later flagged as seed points in the process for tree crown delineation. In the reclassification steps in sections 7.2.1, some of these were corrected. However, it was not very effective in the cases where a large number of points on the roof were originally classified as trees. As shown

in Figure 69, many of the points within the trees classified as buildings were corrected with these steps.

The number of points is adequate to describe the tree structure in some cases as shown in Figure 70A. In others (Figure 70B), the structure is not very clear. Some of the trees, in the crown delineation process, have grown to the adjacent shrubs (Figure 70C). The ground under the trees can be clearly distinguished when the canopy is not very dense (Figure 70D). When there is under storey vegetation (Figure 70E), it is not easy to determine the altitude of the terrain, or the crown base height. It can be seen from the histograms that two modes apart from the initial one representing the ground suggests the presence of under storey vegetation (Amable et al., 2004). However, it is not always easy to distinguish between points from the ground, under storey vegetation and crown (Figure 70F). Table 29 gives the different attribute values for the trees shown below.



A



B



C



D

Figure 66: Thiessen polygons generated from the tree crown points at scales (B) 1, (C) 2 and (D) 3 (A) overlaid on the aerial photograph (Aerial image - Ordnance Survey © Crown Copyright. All Rights Reserved)

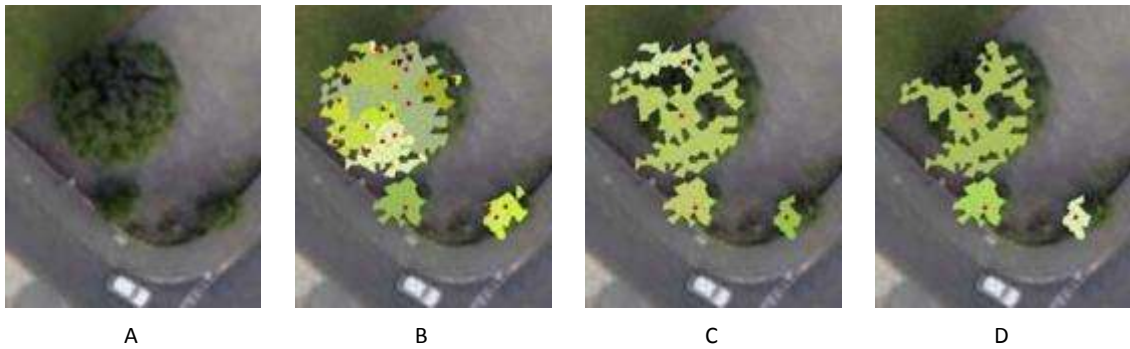


Figure 67: All the tree segments at (B) scale 1 are not detected at scales (C) 2 and (D) 3; (A) The aerial photograph is shown for reference. (Aerial image - Ordnance Survey © Crown Copyright. All Rights Reserved)



Figure 68: Compact tree crowns are not over-segmented at (B) scale 1 and they are also detected at the scales (C) 2 and (D) 3; (A) The aerial photograph is shown for reference. (Aerial image - Ordnance Survey © Crown Copyright. All Rights Reserved)

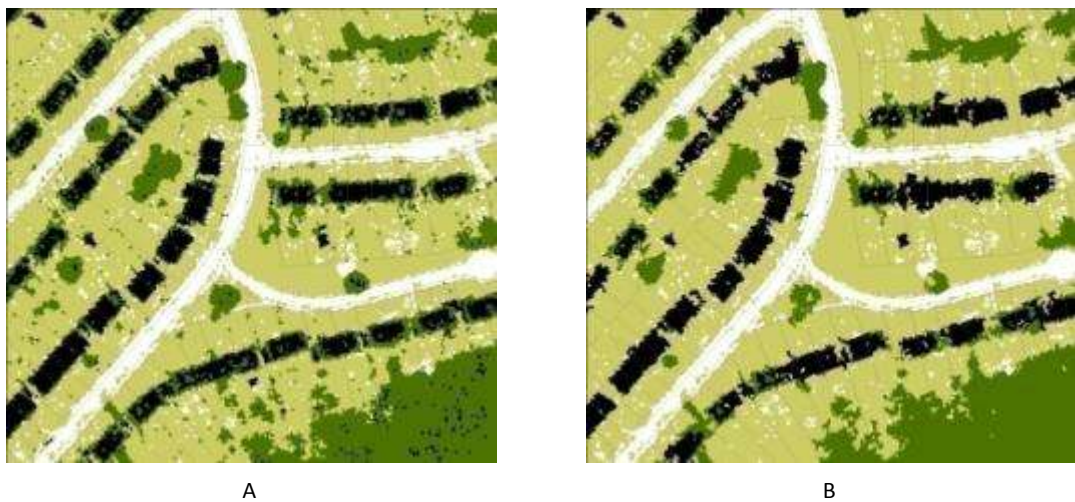


Figure 69: Classified polygons (A) before and (B) after the reclassification

Table 29: Attributes of the six trees shown in Figure 70

Attribute	a	b	c	d	e	f
TreeID	4886	4687	4979	4719	4906	4603
Maximum Height (m)	25.82 m	7.1	6.64	7.3	10.79	8.15
95 th percentile of heights (m)	24.54 m	6.26	6.15	6.97	10.16	7.46
Relative 95 th percentile	0.95	0.88	0.92	0.95	0.94	0.91
Crown base height (m)	6.55 m	4.76	4.59	1.14	1.55	1.53
Crown radius (m)	5.76 m	3.57	3.25	3.14	5.1	4.61
Proportion of single echoes	0.69	0.18	0.18	0.3	0.7	0.65
Proportion of first echoes	0.53	0.41	0.55	0.56	0.51	0.5
Proportion of echoes above the crown base	0.85	0.24	0.23	0.73	0.93	0.89
Mean amplitude	25.18	35.64	37.23	28.68	40.98	59
Mean backscatter cross section	0.2	0.28	0.32	0.2	0.34	0.36
Ratio of height to radius	4.25	1.75	1.89	2.22	1.99	1.62

The locations of single trees were taken as the Easting and Northing values of the estimated treetops. In the case of correctly classified single trees, this is often close to the centroid of the tree polygon. When groups of trees are incorrectly classified as a single tree, they can often be identified visually as the estimated treetop is not close to the centroid. Not all the single trees in the study area were included in the accuracy assessment. The omission errors are therefore not included in the assessment.

In the study area in Bournemouth, 77 isolated single trees were detected using the delineation method outlined above. However, only 61 of these tree polygons contained validation data from StreetMapper. When these were visually analysed using MasterMap and the aerial image, it was seen that 23 points were from near or within buildings. 9 points were from lampposts that could be seen in the aerial image, 4 were from trees, but extended on to buildings, one was from a built structure, one could not be clearly identified and two were from single points.

In the remaining 21 trees, it was difficult to measure the crown base height from the StreetMapper data in the case of seven trees. In some cases, the branches start almost from the base, and in some cases, the undergrowth makes it difficult to determine the base of the crown (Figure 71). The trees identified as isolated single trees often have other trees growing close to it (Figure 72). It is therefore difficult to locate the trunks of the trees, which are selected wherever possible, as the location of the trees in the reference data.

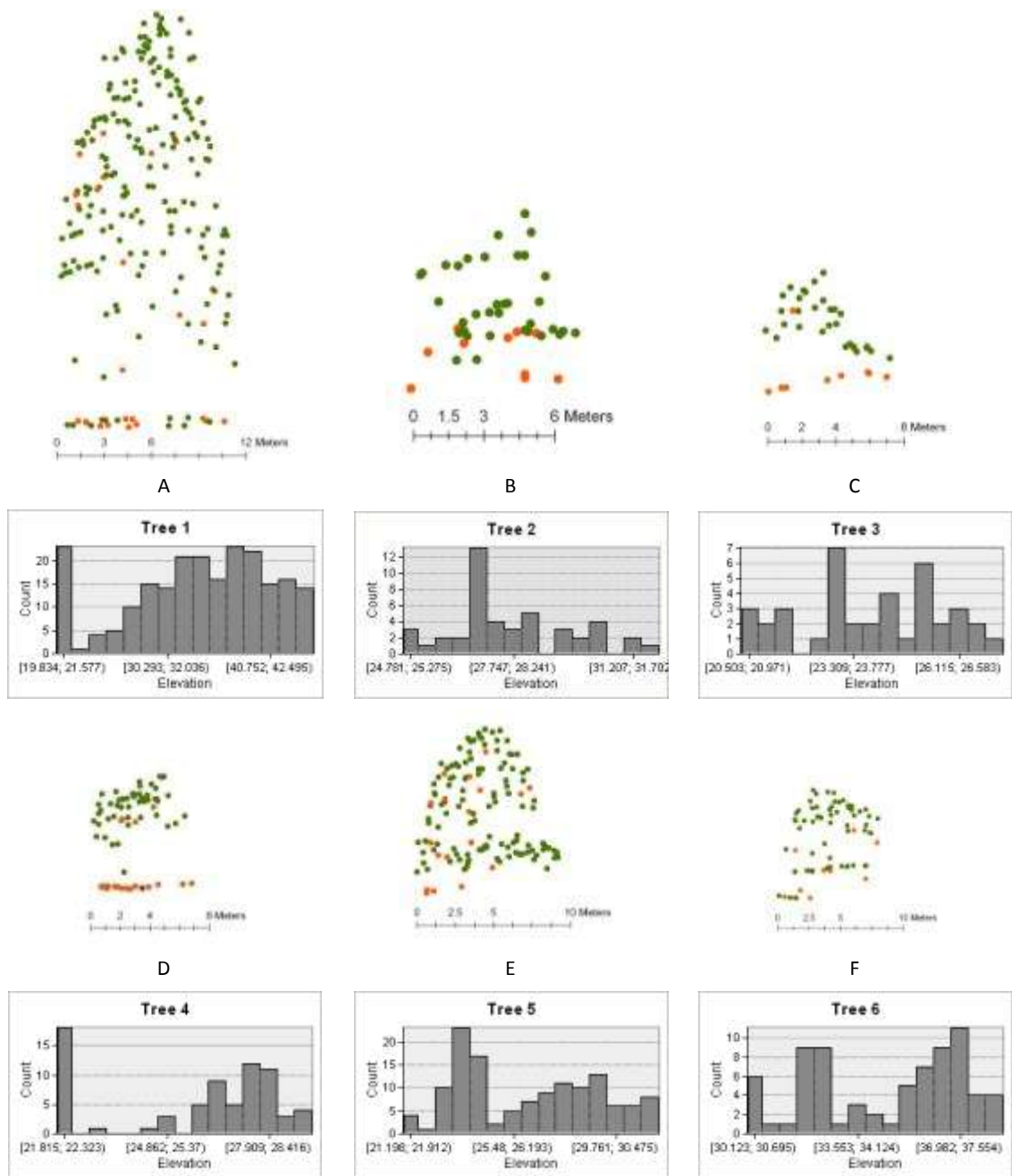


Figure 70: Examples of isolated single trees (A-F) in the study area showing the first echoes (Congalton and Green), second echoes (orange) and third echoes (black). The histograms of elevations are also shown for each tree.

The location of a tree is estimated as the location of the treetop, or the estimated seed point at the third scale. This is true in the majority of the cases. However, if the tree trunks are bent, the location error increases, as in the tree whose ID is 1 (Figure 73A). As seen earlier, it is not easy to locate trees that grow very close together, or which have hedges or shrubs near them (Figure 73B, C & D)

The developed method for delineating single tree crowns avoids a few problems of grid-based methods, especially over-estimation of tree crowns, and errors introduced by interpolation. However, some of the problems such as the choice of scales for identifying the estimated treetops remain. Further work is required to determine how far the method is applicable on data with other point densities. More trees could probably be identified making use of proximity of tree segments to the location of seed points and average attribute values within the tree segments. One solution could be to make use of the backscatter cross section and echo width to determine whether they belong to different trees (Höfle et al., 2008). However, this requires more information about the characteristics of different trees and the solution would not work if the trees belong to the same species.

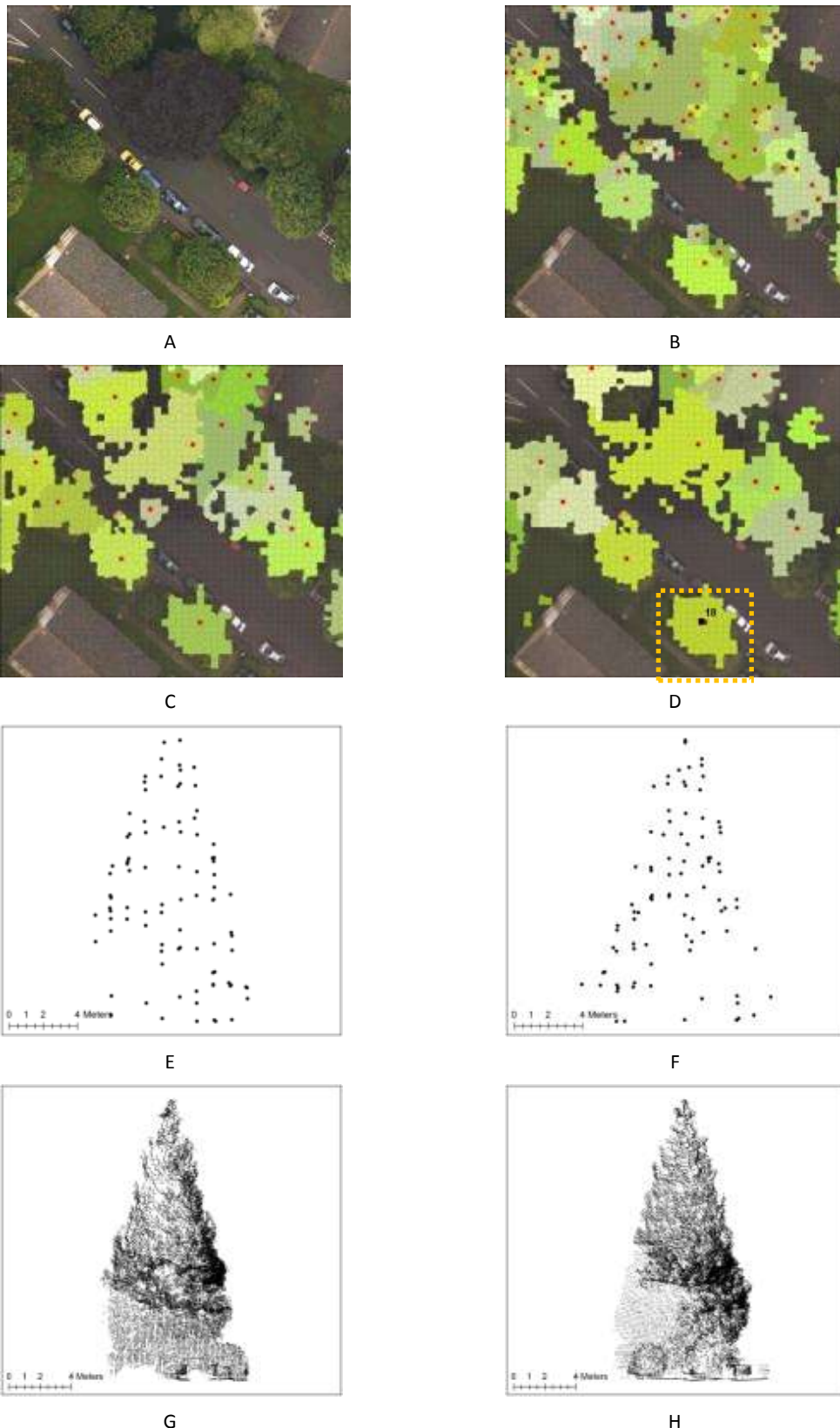


Figure 71: (A) Aerial image of a subset of the study area in Bournemouth containing the tree with ID 18; (B) the Thiessen polygons classified as tree crowns at the first scale, (C) second scale and (D) third scale; (E) points from the full-waveform data displayed in the x-z axis as viewed from the South and (F) in the y-z axis as viewed from the East (G) the reference data from StreetMapper displayed in the x-z axis and

(H) in the y-z axis. (Aerial image and StreetMapper data - Ordnance Survey © Crown Copyright. All Rights Reserved)

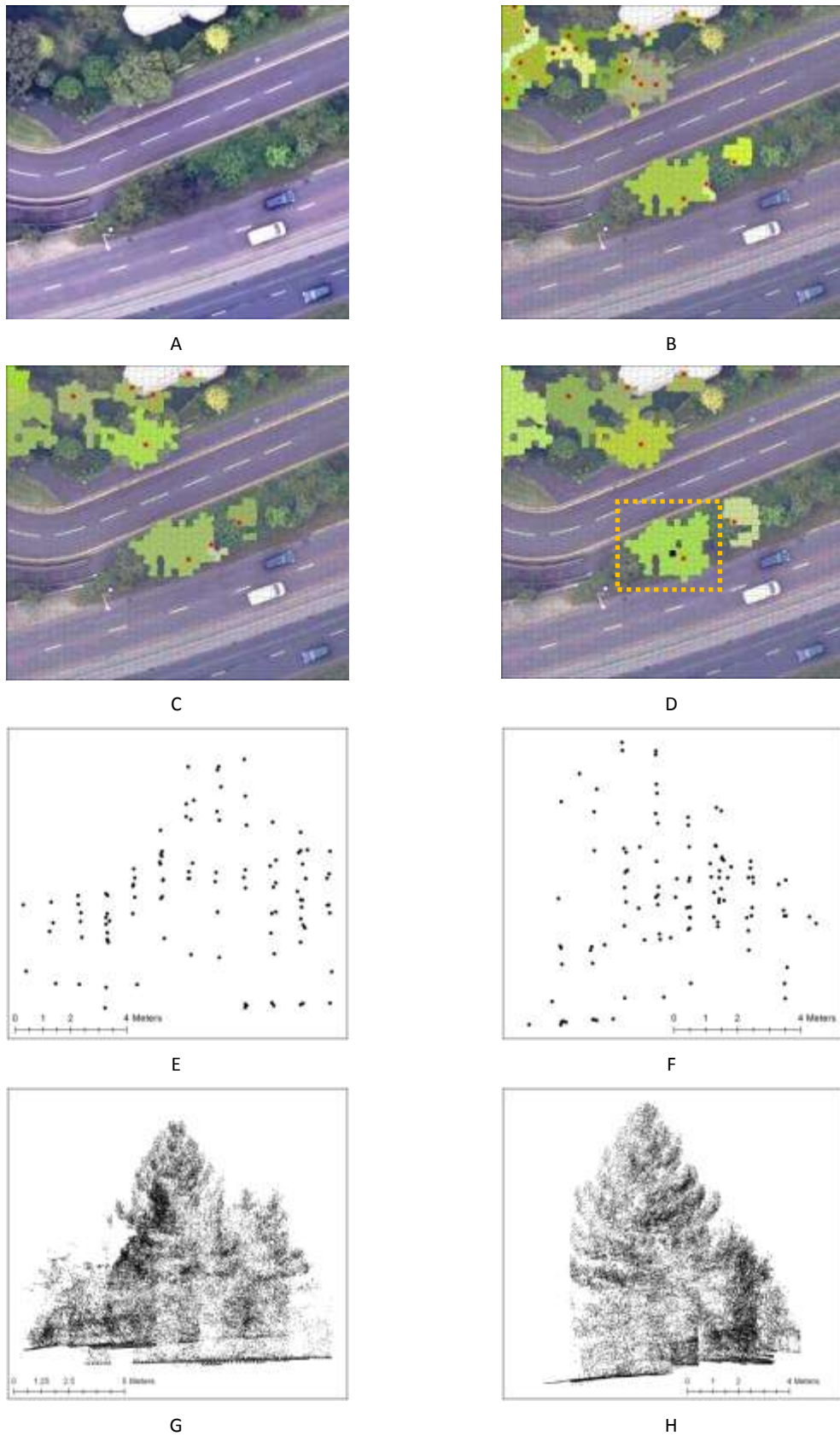
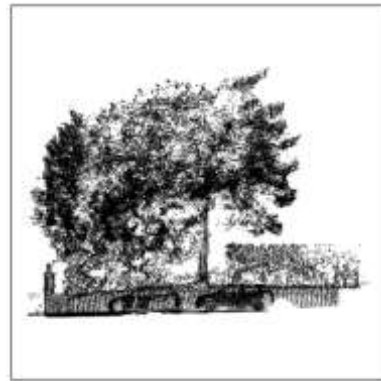
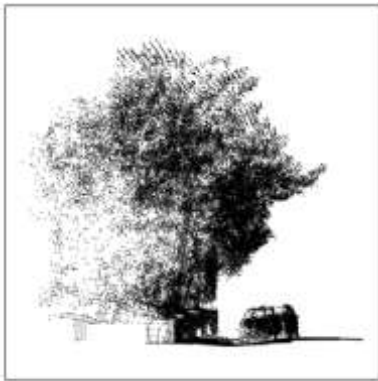


Figure 72: (A) Aerial image of a subset of the study area in Bournemouth containing the tree with ID 6; (B) the Thiessen polygons classified as tree crowns at the first scale, (C) second scale and (D) third scale; (E) points from the full-waveform data displayed in the x-z axis as viewed from the South and (F) in the

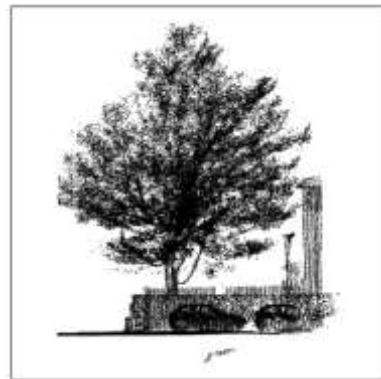
y-z axis as viewed from the East (G) the reference data from StreetMapper displayed in the x-z axis and (H) in the y-z axis. (Aerial image and StreetMapper data - Ordnance Survey © Crown Copyright. All Rights Reserved)



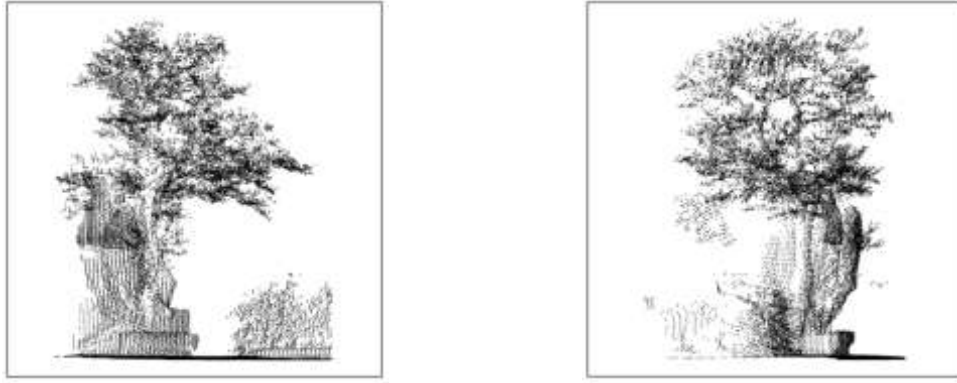
A



B



C



D

Figure 73: StreetMapper data for isolated single trees displayed in the x-z and y-z axes. Views from the South and East of trees with (A) ID 1, (B) ID 8, (C) ID 16 and (D) ID 19 (StreetMapper data - Ordnance Survey © Crown Copyright. All Rights Reserved)

7.5. Summary

This chapter looked at the three-dimensional attributes of vegetation that could be useful for a digital topographic database at different scales. Three scales – landscape, land parcel and single tree – were identified for analysis. A vector-based algorithm for tree crown delineation was used to detect the tree segments. The identified isolated single trees were compared with manually classified trees using an aerial photograph to assess the accuracy of detecting single trees. Information extracted from the full-waveform using commercial software seems to be quite useful in classifying the points and extracting information about vegetation. However, as seen from the literature review, more information could probably be extracted from the raw waveforms. The next chapter gives an overview of the contributions of this research to the classification of ALS data, and its representation in digital maps.

8. Conclusion

This study presented a method for classifying ALS point cloud data based on the attributes of individual points, and their spatial relationships. It also looked at how the attributes of vegetation can be represented within a digital topographic database. This chapter gives an overview of the contributions of this research.

8.1. Introduction

Different components of the urban landscape influence the functioning of urban systems. In addition to producing urban heat island effects, impermeable surfaces reduce the percolation of water to aquifers, and contribute to surface water runoff and urban flooding. This assumes a greater importance in the context of issues related to climate change. Urban drainage is likely to be overloaded as a result of wetter winters and heavier summer showers, predicted by climate models. In an independent review commissioned by the UK government, after the severe flooding in 2007, one of the recommendations was to bring under planning law the right of householders to pave over their front gardens. Mapping and quantification of urban vegetation could greatly contribute to the understanding of urban systems and judicious urban planning decisions (Ordnance Survey, 2008; ParliamentaryOfficeofScienceandTechnology, 2007).

Rapid urbanisation often occurs at the expense of green spaces. There is therefore a need to map existing natural resources to plan for their conservation and development. Digital topographic data, let alone detailed maps required for urban planning, are still unavailable in many parts of the world. ALS has the unique ability to provide geo-referenced data useful for the mapping of urban features. The three-dimensional attributes of features can be used for creating realistic 3D models of urban areas for urban planning applications, noise and air pollution modelling, flood risk assessment and modelling, and for estimating biomass (Muhar, 2001; Nowak et al., 2006; Thaiutsa et al., 2008; Wong and Yu, 2005).

This thesis examined the ability of full-waveform as well as discrete return ALS data to distinguish urban surface features, and the three-dimensional information extracted from vegetation was represented in maps at different scales. The objectives of the thesis were: (i) to explore different techniques for the classification of features in an urban environment using full-waveform ALS data; (ii) to determine whether the additional attributes from full-waveform data give a significant advantage over discrete return data with reference to the classification of urban features; (iii) to determine whether the method is transferable by applying it on full-waveform ALS data with a different scanning geometry ; and (iv) to identify the three-dimensional attributes of vegetation, for topographic mapping, using a vector-based approach for delineating tree crowns.

8.2. Contributions of this Research

ALS has an advantage over other remote sensing data for use in GIS as they are geo-referenced vector data that can be visualised and analysed in any GIS software. Decision tree is a classification method that is particularly suitable for GIS, as it can be converted to 'if-then' rules that can be implemented fully within a GIS environment. Although a decision tree can be data driven, the method works well with user-defined classes and carefully selected training data. In this study, Thiessen polygons were used to convert the point data to polygons representing the different categories. This study therefore developed a method to convert ALS point data to polygons representing urban features with three-dimensional attributes.

Elevation was initially considered the most important information obtained from ALS data. In recent years, there has been a growing interest in the use of attributes related to intensity – amplitude and echo width - and in the calibration of intensity from small-footprint full-waveform ALS data. Although the intensity information is available from discrete return data, it has been less explored as the method of derivation of intensity is not usually disclosed by the manufacturers of the scanners. The major difference between full-waveform and discrete return ALS is in the recording of data, as discrete return data are obtained by the real-time processing of full-waveform data. This study showed that the intensity information from discrete return data could be as useful as or better than amplitude information from full-waveform data at distinguishing urban features.

In addition to flying height and beam divergence angle, wavelength of the laser used in a sensor could have an influence on the intensity of the ALS echo. In this study, natural and artificial ground could be distinguished better using a sensor at a wavelength of 1064 nm than one at 1550 nm. Although a comparison was difficult between discrete return and full-waveform data collected in different seasons and from different flying heights, it is very likely that the differences in the intensities were brought about by the differences in the wavelengths. It might therefore be necessary to give due consideration to the wavelengths of lasers used in the scanners for particular applications.

Full-waveform data could be more useful than discrete return data for topographic mapping as intensity is a very useful attribute in classification, and calibration of intensity is currently possible only with full-waveform data. As the amplitude values are dependent on various factors such as flying height, scan angle and weather conditions, calibrated intensity might be necessary to make any classification method transferable.

Spatial relationships of points have been used for classification using discrete return ALS data. However, in many previous studies on classification using full-waveform data, the emphasis was on using the additional attributes such as echo width available only in full-waveform data. This study suggests that the attributes derived from elevation could improve the classification using full-waveform data.

Echo width from full-waveform data has been used for extracting vegetation points and for distinguishing terrain points from low vegetation points. However, echo width could be dependent on the method of decomposition of the return waveform, incidence angle and the footprint size of the laser beam. In this study, although echo width was useful for distinguishing trees from other features, it was less useful in separating natural and artificial ground.

The majority of existing studies on delineating trees from ALS are based on gridded data, typically using a higher point density ranging from 2.6 to 10 points m^{-2} . This study developed a vector-based approach to tree crown delineation using ALS point cloud at a point density of 1 point m^{-2} and TIN, instead of gridded data, which honour the data points. As the cost of acquiring ALS data increases with point density, this could be used for large area mapping of trees.

Similar to raster-based studies, the scales at which the seed points or local maxima, estimated to be treetops, were identified influenced the results. The finer scale gave a better description of the structure of the tree crown, especially in the case of broadleaf trees, where the crown surface is less compact, and was better at estimating tree cover, than the coarser scales. The coarser scale seemed to be better at identifying the number of trees, and their locations. The finer scale would therefore be more suitable for estimating biomass and canopy gaps, while the coarser scale would be more useful for modelling individual trees.

8.3. Future Work

The flying height and the divergence angle determine the size of the footprint of the laser beam, or the spatial resolution. This in turn has an influence on the acquired data, especially in the case of vegetation. Large footprints lead to a more generalised description of the vertical structure of vegetation, and small-footprint ALS has limitations in mapping and characterising vegetation on a global scale. However, small-footprint full-waveform ALS data can be used to validate large-footprint spaceborne data, as has been demonstrated by Duong (2009) in urban areas using data from ICESat-I. This method could be extended to understanding and relating

large-footprint waveform data to forest characteristics using small-footprint ALS data. Lidar is arguably the most promising remote sensing technology for estimating biomass, a useful predictor of carbon in terrestrial carbon pools. A few studies have looked at estimating forest biomass from ICESat-I data, which have a spatial resolution of approximately 70 m (Boudreau et al., 2008). The footprint of the laser beam most useful for estimating the three-dimensional structure of vegetation and biomass, for space missions, is still a topic of research (Report from the ICESat-II Workshop, 2007). Full-waveform ALS data acquired from different flying heights could be used to understand the effect of footprint on the collected data from vegetation.

The wavelengths of the full-waveform and the discrete return ALS data used in the study were 1550 nm and 1064 nm respectively. The classification using the discrete return data yielded better results than the one from the full-waveform data. As mentioned earlier, one reason for this could be the difference in wavelengths. This could be explored further using full-waveform data from other scanners. TopEye Mark II, Optech ALTM 3100 and Leica ALS60 provide full-waveform data at a wavelength of 1064 nm (Table 1).

The classifier developed in this study could be further improved based on the spatial relationships between the classified polygons, and including more feature classes. The major difficulty in the developed method was in the separation of trees and pitched roofs. Since the incorrect classification of buildings as trees is mainly at the edges, the spatial relationship between the classes could be used for refining the classification (de Almeida et al., 2007). For example, when Thiessen polygons are constructed around the classified points and merged based on class, a polygon that is classified as a shrub, and is surrounded on all sides by a long road polygon is likely to be a vehicle. A long and narrow tree polygon surrounding a building polygon has a high probability of being the building edge. Additional feature classes also need to be considered for generating a more refined classifier.

With these improvements, it should be possible to develop highly accurate classifiers for urban landscapes from full-waveform ALS data, which use a moderate point density such as 1 point m^{-2} , and are transferable between different locations.

Appendix 1

LAS FORMAT DESCRIPTION

(http://liblas.org/raw-attachment/wiki/WikiStart/asprs_las_format_v11.pdf)

Appendix 2

CONVERSION OF FULL WIDTH AT HALF MAXIMUM TO STANDARD DEVIATION

(<http://mathworld.wolfram.com/GaussianFunction.html>)

The Gaussian function can be written as:

$$f(x) = \frac{1}{s\sqrt{2\pi}} e^{\left[-\frac{(x-\mu)^2}{2s^2}\right]}$$

where s is the standard deviation and μ is the mean of the normal distribution.

The full width at half maximum (FWHM) for a Gaussian is found by solving:

$$e^{\left[-\frac{(x_0-\mu)^2}{2s^2}\right]} = \frac{1}{2} f(x_{max})$$

$f(x_{max})$ occurs at $x_{max} = \mu$. Therefore,

$$e^{\left[-\frac{(x_0-\mu)^2}{2s^2}\right]} = \frac{1}{2} f(\mu) = \frac{1}{2}$$

$$e^{\left[-\frac{(x_0-\mu)^2}{2s^2}\right]} = 2^{-1}$$

$$-\frac{(x_0 - \mu)^2}{2s^2} = -\ln 2$$

$$(x_0 - \mu)^2 = 2s^2 \ln 2$$

$$x_0 = \pm s \sqrt{2 \ln 2} + \mu$$

Therefore,

$$FWHM = x_+ - x_- = 2\sqrt{2 \ln 2} s$$

$$s = \frac{FWHM}{2\sqrt{2 \ln 2}}$$

Appendix 3

DECISION TREE USING AMPLITUDE

```
1  if ElevClass<2.5 then node 2 else node 3
2  if ElevClass<1.5 then node 4 else node 5
3  if AvSlope<45.395 then node 6 else node 7
4  if Amp<52.5 then node 8 else node 9
5  if HtVar<6.775 then node 10 else node 11
6  if HtVar<0.275 then node 12 else node 13
7  if Amp<67.5 then node 14 else node 15
8  if AvSlope<67.655 then node 16 else node 17
9  if AvSlope<60.105 then node 18 else node 19
10 class = Shrubs
11 class = Trees
12 class = F-Roof
13 if Width<4.65 then node 20 else node 21
14 class = Trees
15 if Amp<81.5 then node 22 else node 23
16 class = Road
17 class = Trees
18 class = Grass
19 class = Trees
20 class = P-Roof
21 if Width<4.95 then node 24 else node 25
22 if AvSlope<56.96 then node 26 else node 27
23 class = P-Roof
24 if SdSlope<16.045 then node 28 else node 29
25 class = Trees
26 if Width<4.55 then node 30 else node 31
27 class = Trees
28 class = P-Roof
29 class = Trees
30 class = P-Roof
31 class = Trees
```

DECISION TREE USING σ

```
1  if ElevClass<2.5 then node 2 else node 3
2  if Backscatter<0.356606 then node 4 else node 5
3  if AvSlope<45.395 then node 6 else node 7
4  if AvSlope<69.3 then node 8 else node 9
```

```

5  if ElevClass<1.5 then node 10 else node 11
6  if HtVar<0.275 then node 12 else node 13
7  if Backscatter<0.454847 then node 14 else node 15
8  if ElevClass<1.5 then node 16 else node 17
9  class = Trees
10 if AvSlope<55.255 then node 18 else node 19
11 if HtVar<7.41 then node 20 else node 21
12 class = F-Roof
13 if Width<4.65 then node 22 else node 23
14 class = Trees
15 if Width<4.55 then node 24 else node 25
16 class = Road
17 class = Shrubs
18 class = Grass
19 class = Trees
20 class = Shrubs
21 class = Trees
22 class = P-Roof
23 if Width<4.95 then node 26 else node 27
24 class = P-Roof
25 class = Trees
26 if Backscatter<0.447252 then node 28 else node 29
27 class = Trees
28 if SdAspect<40.23 then node 30 else node 31
29 class = P-Roof
30 class = P-Roof
31 class = Trees

```

DECISION TREE USING γ_{ci}

```

1  if ElevClass<2.5 then node 2 else node 3
2  if Backscatter c1<1.9093 then node 4 else node 5
3  if AvSlope<45.395 then node 6 else node 7
4  if AvSlope<70.005 then node 8 else node 9
5  if ElevClass<1.5 then node 10 else node 11
6  if HtVar<0.275 then node 12 else node 13
7  if Backscatter c1<2.74405 then node 14 else node 15
8  if ElevClass<1.5 then node 16 else node 17
9  class = Trees
10 if AvSlope<59.74 then node 18 else node 19
11 if HtVar<7.41 then node 20 else node 21

```

```

12 class = F-Roof
13 if Width<4.65 then node 22 else node 23
14 class = Trees
15 if Width<4.55 then node 24 else node 25
16 class = Road
17 class = Shrubs
18 class = Grass
19 class = Trees
20 class = Shrubs
21 class = Trees
22 class = P-Roof
23 if Width<4.95 then node 26 else node 27
24 class = P-Roof
25 class = Trees
26 if Backscatter c1<2.74622 then node 28 else node 29
27 class = Trees
28 if SdAspect<40.23 then node 30 else node 31
29 class = P-Roof
30 class = P-Roof
31 class = Trees

```

DECISION TREE USING γ_{cs}

```

1 if ElevClass<2.5 then node 2 else node 3
2 if Backscatter c2<1.9123 then node 4 else node 5
3 if AvSlope<45.395 then node 6 else node 7
4 if AvSlope<69.06 then node 8 else node 9
5 if ElevClass<1.5 then node 10 else node 11
6 if HtVar<0.275 then node 12 else node 13
7 if Backscatter c2<2.96957 then node 14 else node 15
8 class = Road
9 class = Trees
10 if AvSlope<59.74 then node 16 else node 17
11 if HtVar<7.015 then node 18 else node 19
12 class = F-Roof
13 if Width<4.65 then node 20 else node 21
14 class = Trees
15 if Width<4.55 then node 22 else node 23
16 class = Grass
17 class = Trees
18 class = Shrubs

```

```

19 class = Trees
20 class = P-Roof
21 if Width<4.95 then node 24 else node 25
22 class = P-Roof
23 class = Trees
24 if Backscatter c2<2.74622 then node 26 else node 27
25 class = Trees
26 if SdAspect<40.23 then node 28 else node 29
27 class = P-Roof
28 class = P-Roof
29 class = Trees

```

DECISION TREE USING γ_{ei}

```

1  if ElevClass<2.5 then node 2 else node 3
2  if Backscatter c3<1.18169 then node 4 else node 5
3  if AvSlope<45.395 then node 6 else node 7
4  if AvSlope<70.005 then node 8 else node 9
5  if ElevClass<1.5 then node 10 else node 11
6  if HtVar<0.275 then node 12 else node 13
7  if Backscatter c3<1.71485 then node 14 else node 15
8  if ElevClass<1.5 then node 16 else node 17
9  class = Trees
10 if AvSlope<59.74 then node 18 else node 19
11 if HtVar<7.41 then node 20 else node 21
12 class = F-Roof
13 if Width<4.65 then node 22 else node 23
14 class = Trees
15 if Width<4.55 then node 24 else node 25
16 class = Road
17 class = Shrubs
18 class = Grass
19 class = Trees
20 class = Shrubs
21 class = Trees
22 class = P-Roof
23 if Width<4.95 then node 26 else node 27
24 class = P-Roof
25 class = Trees
26 if Backscatter c3<1.82901 then node 28 else node 29
27 class = Trees

```

```
28 if SdAspect<40.23 then node 30 else node 31
29 class = P-Roof
30 class = P-Roof
31 class = Trees
```

DECISION TREE USING γ_{es}

```
1 if ElevClass<2.5 then node 2 else node 3
2 if Backscatter c4<1.17772 then node 4 else node 5
3 if AvSlope<45.395 then node 6 else node 7
4 if AvSlope<69.06 then node 8 else node 9
5 if ElevClass<1.5 then node 10 else node 11
6 if HtVar<0.275 then node 12 else node 13
7 if Backscatter c4<1.74916 then node 14 else node 15
8 class = Road
9 class = Trees
10 if AvSlope<59.74 then node 16 else node 17
11 if HtVar<7.015 then node 18 else node 19
12 class = F-Roof
13 if Width<4.65 then node 20 else node 21
14 class = Trees
15 if Width<4.65 then node 22 else node 23
16 class = Grass
17 class = Trees
18 class = Shrubs
19 class = Trees
20 class = P-Roof
21 if Width<4.95 then node 24 else node 25
22 if AvSlope<61.58 then node 26 else node 27
23 class = Trees
24 if Backscatter c4<1.82901 then node 28 else node 29
25 class = Trees
26 class = P-Roof
27 class = Trees
28 if SdAspect<40.23 then node 30 else node 31
29 class = P-Roof
30 class = P-Roof
31 class = Trees
```

References

- 3DLM, 2009. StreetMapper: Mobile Mapping Using LiDAR Technology. <http://www.streetmapper.net/streetmapper/overview.htm>, 2009(15.08).
- Ackermann, F., 1999. Airborne Laser Scanning - Present Status and Future Expectations. *ISPRS Journal of Photogrammetry and Remote Sensing*, 54: 64-67.
- Akel, N.A., Kremeike, K., Filin, S., Sester, M. and Doytsher, Y., 2005. Dense DTM Generalization Aided by Roads Extracted from LiDAR Data. *ISPRS WG III/3, III/4, V/3 Workshop "Laser scanning 2005"*, Enschede, the Netherlands: 54-59.
- Alexander, C., Smith-Voysey, S., Jarvis, C. and Tansey, K., 2009. Integrating Building Footprints and LiDAR Elevation Data to Classify Roof Structures and Visualise Buildings. *Computers, Environment and Urban Systems*, 33(4): 285-292.
- Alharthy, A. and Bethel, J., 2002. Heuristic Filtering and 3D Feature Extraction from Lidar Data. *International Archives of Photogrammetry and Remote Sensing*, 34-3A: A.29-A.35.
- Amable, G.S., Devereux, B.J., Cockerell, T. and Renshaw, G., 2004. Analysis of Interaction Patterns Between Vegetation Canopies and Small Footprint, High-density, Airborne Lidar. *Geo-Imagery Bridging Continents, XXth ISPRS Congress, Commission VII*: unpaginated.
- Andersen, H.-E. et al., 2003. A Comparison of Forest Canopy Models Derived from LiDAR and InSAR Data in a Pacific NorthWest Conifer Forest *ISPRS working group III/3 workshop '3-D reconstruction from airborne laserscanner and InSAR data'* Dresden, Germany.
- Anderson, J. et al., 2006. The use of Waveform Lidar to Measure Northern Temperate Mixed Conifer and Deciduous Forest Structure in New Hampshire. *Remote Sensing of Environment*, 105(3): 248-261.
- Antonarakis, A.S., Richards, K.S. and Brasington, J., 2008. Object-based Land Cover Classification using Airborne LiDAR. *Remote Sensing of Environment*, 112(6): 2988-2998.
- Aubrecht, C., Steinnocher, K., Hollaus, M. and Wagner, W., 2009. Integrating Earth Observation and GIScience for High Resolution Spatial and Functional Modeling of Urban Land Use. *Computers, Environment and Urban Systems*, 33(1): 15-25.
- Axelsson, P., 1999. Processing of Laser Scanner Data - Algorithms and Applications. *ISPRS Journal of Photogrammetry and Remote Sensing*, 54: 138-147.
- Baltsavias, E.P., 1999a. Airborne Laser Scanning: Basic Relations and Formulas. *ISPRS Journal of Photogrammetry & Remote Sensing*, 54: 199-214.
- Baltsavias, E.P., 1999b. A Comparison between Photogrammetry and Laser Scanning. *ISPRS Journal of Photogrammetry and Remote Sensing*, 54: 83-94.
- Balzter, H., Luckman, A., Skinner, L., Rowland, C. and Dawson, T., 2007. Observations of Forest Stand Top Height and Mean Height from Interferometric SAR and LiDAR over a Conifer Plantation at Thetford Forest, UK *International Journal of Remote Sensing*, 28(6): 1173 - 1197.
- Barber, C.B., David, P.D. and Hannu, H., 1996. The Quickhull Algorithm for Convex Hulls. *ACM Trans. Math. Softw.*, 22(4): 469-483.
- Blair, J.B., Rabine, D.L. and Hofton, M.A., 1999. The Laser Vegetation Imaging Sensor: a Medium-altitude, Digitisation-only, Airborne Laser Altimeter for Mapping Vegetation and Topography *ISPRS Journal of Photogrammetry and Remote Sensing*, 54: 115-122.

- Bork, E.W. and Su, J.G., 2007. Integrating LIDAR data and multispectral imagery for enhanced classification of rangeland vegetation: A meta analysis. *Remote Sensing of Environment*.
- Bortolot, Z.J. and Wynne, R.H., 2005. Estimating Forest Biomass using Small Footprint LiDAR Data: An Individual Tree-based Approach that Incorporates Training Data. *ISPRS Journal of Photogrammetry and Remote Sensing*, 59(6): 342-360.
- Boudreau, J. et al., 2008. Regional aboveground forest biomass using airborne and spaceborne LiDAR in Québec. *Remote Sensing of Environment*, 112(10): 3876-3890.
- Breiman, L., Friedman, J., Stone, C.J. and Olshen, R.A., 1984. *Classification and Regression Trees*. Chapman & Hall, New York.
- Brennan, R. and Webster, T.L., 2006. Object-oriented Land Cover Classification of Lidar-derived Surfaces. *Canadian Journal of Remote Sensing*, 32(2): 162-172.
- Bretar, F., Chauve, A., Mallet, C. and Jutzi, B., 2008. Managing Full Waveform LIDAR Data: A Challenging Task for the Forthcoming Years. *International Archives of Photogrammetry and Remote Sensing*, XXXVII: 415-420.
- Briese, C. et al., 2008. Calibration of Full-waveform Airborne Laser Scanning Data for Object Classification. *Proceedings of SPIE - The International Society for Optical Engineering*, 6950: 69500H.
- Burrough, P.A. and McDonnell, R.A., 1998. *Principles of Geographical Information Systems. Spatial Information Systems*. Oxford University Press, New York.
- Burtch, R., 2002. *Lidar Principles and Applications*. IMAGIN Conference: unpaginated.
- Charaniya, A., Manduchi, R. and Lodha, S., 2004. Supervised Parametric Classification of Aerial LiDAR data. 'Real-Time 3D Sensors and their use' Workshop, in conjunction with IEEE CVPR, Washington D.C., June 2004.: unpaginated.
- Chauve, A. et al., 2007. Processing Full-waveform Lidar Data: Modelling Raw Signals. *ISPRS Workshop on Laser Scanning*, Espoo, Finland: 102-107.
- Chen, Q., 2007. Airborne Lidar Data Processing and Information Extraction. *Photogrammetric Engineering and Remote Sensing*, 73(2): 109-112.
- Chilton, T.D., Jaafar, J. and Priestnall, G., *International Archives of ISPRS, Vol , 9 - 11 November 1999, La Jolla, California, , 1999. The use of Laser Scanner data for the extraction of building roof detail using standard elevation derived parameters. International Archives of Photogrammetry and Remote Sensing*, 32(3/W14): 137-143.
- Chust, G., Galparsoro, I., Borja, Á., Franco, J. and Uriarte, A., 2008. Coastal and Estuarine Habitat Mapping, using LIDAR Height and Intensity and Multi-spectral Imagery. *Estuarine, Coastal and Shelf Science*, 78(4): 633-643.
- Congalton, R.G. and Green, K., 1999. *Assessing the Accuracy of Remotely Sensed Data: Principles and Practices*. Lewis Publishers, Boca Raton.
- Coren, F. and Sterzai, P., 2006. Radiometric Correction in Laser Scanning. *International Journal of Remote Sensing*, 27(15): 3097-3104.
- Cunningham, D., Grebby, S., Tansey, K. and Gosar, A., 2006. Application of airborne LiDAR to mapping seismogenic faults in forested mountainous terrain, southeastern Alps, Slovenia. *Geophysical Research Letters*, 33.
- de Almeida, J.P., Morley, J.G. and Dowman, I.J., 2007. Graph Theory in Higher Order Topological Analysis of Urban Scenes. *Computers, Environment and Urban Systems*, 31(4): 426-440.

- Dubayah, R., Knox, R., Hofton, M.A., Blair, J., Bryan and Drake, J. (Editors), 2000. Land Surface Characterization using Lidar Remote Sensing. Spatial Information for Land Use Management. International Publishers Direct, Singapore.
- Dubayah, R.O. and Drake, J.B., 2000. Lidar Remote Sensing for Forestry. *Journal of Forestry*, 98(6): 44-52.
- Ducic, V., Hollaus, M., Ullrich, A., Wagner, W. and Melzer, T., 2006. 3D Vegetation Mapping and Classification Using Full-Waveform Laser Scanning. *Workshop on 3D Remote Sensing in Forestry*, Vienna: 211-217.
- Duong, H., Lindenbergh, R., Pfeifer, N. and Vosselman, G., 2009. ICESat Full-Waveform Altimetry Compared to Airborne Laser Scanning Altimetry Over The Netherlands. *IEEE Transactions on Geoscience and Remote Sensing*.
- Elmqvist, M., 2001. Ground Estimation of Laser Radar Data using Active Shape Models. *OEEPE Workshop on Airborne Laserscanning and Interferometric SAR for Detailed Digital Elevation Models*, Royal Institute of Technology, Department of Geodesy and Photogrammetry, Stockholm, Sweden: unpaginated.
- Evans, D.L., Roberts, S.D. and Parker, R.C., 2006. LiDAR - A New Tool for Forest Measurements? *The Forestry Chronicle*, 82(2): 211-218.
- Flood, M., 2001. Lidar Activities and Research Priorities in the Commercial Sector. *ISPRS Workshop on Land Surface Mapping and Characterization using Laser Altimetry*, XXXIV-3/W4: 3-7.
- Flood, M. and Gutelius, B., 1997. Commercial Implications of Topographic Terrain Mapping Using Scanning Airborne Laser Radar. *Photogrammetric Engineering and Remote Sensing*, 63(4): 327-366.
- Gutierrez, R., Neuenschwander, A. and Crawford, M.M., 2005. Development of Laser Waveform Digitization for Airborne LIDAR Topographic Mapping Instrumentation. *Geoscience and Remote Sensing Symposium, 2005. IGARSS apos;05. Proceedings. 2005 IEEE International*, 2: 1154-1157.
- Haala, N. and Brenner, C., 1999. Extraction of Buildings and Trees in Urban Environments. *ISPRS Journal of Photogrammetry and Remote Sensing*, 54: 130-137.
- Han, J. and Kamber, M., 2006. *Data Mining: Concepts and Techniques*. The Morgan Kaufmann Series in Data Management Systems. Morgan Kaufmann Publishers, San Francisco.
- Harding, D.J., Lefsky, M.A., Parker, G.G. and Blair, J.B., 2001. Laser Altimeter Canopy Height Profiles: Methods and Validation for Closed-canopy, Broadleaf Forests. *Remote Sensing of Environment*, 76(3): 283-297.
- Hecht, R., Meinel, G. and Buchroithner, M.F., 2008. Estimation of Urban Green Volume based on Single-pulse LiDAR Data. *IEEE Transactions on Geoscience and Remote Sensing*, 46(11): 3832-3840.
- Herold, M., Gardner, M.E. and Roberts, D.A., 2003. Spectral Resolution Requirements for Mapping Urban Areas. *IEEE Transactions on Geoscience and Remote Sensing*, 41(9 PART I): 1907-1919.
- Heurich, M., 2008. Automatic Recognition and Measurement of Single Trees based on Data from Airborne Laser Scanning over the Richly Structured Natural Forests of the Bavarian Forest National Park. *Forest Ecology and Management*, 255(7): 2416-2433.
- Hill, R.A., Smith, G.M., Fuller, R.M. and Veitch, N., 2002. Landscape Modelling using Integrated Airborne Multi-spectral and Elevation Data. *International Journal of Remote Sensing* 23: 2327-2334.

- Hill, R.A. and Thomson, A.G., 2005. Mapping Woodland Species Composition and Structure using Airborne Spectral and LiDAR Data. *International Journal of Remote Sensing*, 26(17): 3763-3779.
- Höfle, B., Hollaus, M., Lehner, H., Pfeifer, N. and Wagner, W., 2008. Area-based Parameterization of Forest Structure using Full-waveform Airborne Laser Scanning Data. *Silvilaser 2008: 8th international conference on LiDAR applications in forest assessment and inventory*, Edinburgh, Scotland: 227-235.
- Höfle, B. and Pfeifer, N., 2007. Correction of Laser Scanning Intensity Data: Data and Model-driven Approaches. *ISPRS Journal of Photogrammetry and Remote Sensing*, 62: 415-433.
- Hofton, M.A., Minster, J.B. and Blair, J.B., 2000. Decomposition of Laser Altimeter Waveforms. *IEEE Transactions on Geoscience and Remote Sensing*, 38(4): 1989-1996.
- Holland, D.A., Boyd, D.S. and Marshall, P., 2006. Updating Topographic Mapping in Great Britain using Imagery from High-resolution Satellite Sensors. *ISPRS Journal of Photogrammetry and Remote Sensing*, 60(3): 212-223.
- Hollaus, M., Wagner, W., Eberhöfer, C. and Karel, W., 2006. Accuracy of Large-scale Canopy Heights derived from LiDAR Data under Operational Constraints in a Complex Alpine Environment. *ISPRS Journal of Photogrammetry and Remote Sensing*, 60(5): 323-338.
- Holmgren, J. and Persson, A., 2004. Identifying Species of Individual Trees using Airborne Laser Scanner. *Remote Sensing of Environment*, 90: 415-423.
- Hug, C., Ullrich, A. and Grimm, A., 2004. LiteMapper-5600 - A Waveform-Digitizing LIDAR Terrain and Vegetation Mapping System. *International Archives of Photogrammetry and Remote Sensing*, 36(Part 8/W2): 24-29.
- Hyde, P. et al., 2005. Mapping Forest Structure for Wildlife Habitat Analysis using Waveform Lidar: Validation of Montane Ecosystems. *Remote Sensing of Environment*, 96: 427-437.
- Hyypä, J. et al., 2004. Algorithms and Methods of Airborne Laser Scanning for Forest Measurements. *International Archives Of Photogrammetry, Remote Sensing And Spatial Information Sciences. Proceedings of the ISPRS working group VIII/2 'Laser-Scanners for Forest and Landscape Assessment'*, Freiburg, Germany, XXXVI (8/W2): 82-89.
- Hyypä, J. et al., 2007. Improving Automation in Map Updating Based on National Laser Scanning, Classification Trees, Object-Based Change Detection and 3D Object Reconstruction. *Urban Remote Sensing Joint Event, 2007*: unpaginated.
- Hyypä, J., Pyysalo, U., Hyypä, H. and Samberg, A., 2000. Elevation Accuracy of Laser Scanning-derived Digital Terrain and Target Models in Forest Environment. *Proceedings of EARSeL-SIG-Workshop LIDAR, Dresden/FRG, June 16 – 17, 2000*: 139-147.
- Iovan, C., Boldo, D. and Cord, M., 2008. Detection, Characterization, and Modeling Vegetation in Urban Areas From High-Resolution Aerial Imagery. *IEEE Journal of Selected Topics in Applied Earth Observations and Remote Sensing*, 1(3): 206-213.
- Jelalian, A.V., 1991. *Laser Radar Systems*. Artech House Radar Library.
- Joffre, R. and Rambal, S., 1993. How Tree Cover Influences the Water Balance of Mediterranean Rangelands. *Ecology*, 74(2): 570-582.
- Kaasalainen, S., Ahokas, E., Hyypä, J. and Suomalainen, J., 2005. Study of Surface Brightness from Backscattered Laser Intensity: Calibration of Laser Data. *Geoscience and Remote Sensing Letters, IEEE*, 2(3): 255-259.

- Kager, H., 2006. The Importance of Exact Geo-referencing of Airborne LIDAR Data. GIS Development, http://www.gisdevelopment.net/magazine/years/2006/april/42_1.htm.
- Koetz, B., Morsdorf, F., van der Linden, S., Curt, T. and Allgöwer, B., 2008. Multi-source Land Cover Classification for Forest Fire Management based on Imaging Spectrometry and LiDAR Data. *Forest Ecology and Management*, 256(3): 263-271.
- Kotsiantis, S.B., 2007. Supervised Machine Learning: A Review of Classification Techniques. *Informatica*, 31: 249-268.
- Landis, J.R. and Koch, G.G., 1977. The Measurement of Observer Agreement for Categorical Data. *Biometrics*, 33(1): 159-174.
- Larose, D.T., 2004. *Discovering Knowledge in Data: An Introduction to Data Mining*. John Wiley & Sons, Inc., Hoboken, New Jersey.
- Leckie, D. et al., 2003. Combined High-density Lidar and Multispectral Imagery for Individual Tree Crown Analysis. *Canadian Journal of Remote Sensing*, 29(5): 633-649.
- Lefsky, M.A., 2002. Lidar Remote Sensing for Ecosystem Studies. *BioScience*, 52(1): 19-30.
- Liang, S., 2004. *Quantitative Remote Sensing of Land Surfaces*. John Wiley & Sons, Inc., Hoboken, New Jersey.
- Lillesand, T.M., Kiefer, R.W. and Chipman, J.W., 2004. *Remote Sensing and Image Interpretation*. Wiley & Sons, Chichester.
- Lim, K., Treitz, P., Wulder, M., St-Onge, B. and Flood, M., 2003. LiDAR Remote Sensing of Forest Structure. *Progress in Physical Geography*, 27: 88-106.
- Lohani, B., 2007. *Airborne Altimetric LiDAR: Principle, Data Collection, Processing and Applications*. http://home.iitk.ac.in/~blohani/LiDAR_Tutorial/Airborne_AltimetricLidar_Tutorial.htm, 2009(17.08).
- Mallet, C. and Bretar, F., 2009. Full-waveform Topographic Lidar: State-of-the-art. *ISPRS Journal of Photogrammetry and Remote Sensing*, 64(1): 1-16.
- Mallet, C., Soergel, U. and Bretar, F., 2008. Analysis of Full-Waveform LIDAR Data for an Accurate Classification of Urban Areas. *ISPRS Congress, Proceedings of Commission III, Beijing 2008*, 37-B3a: 85-91.
- Mathworks, 2008a. *Fuzzy Logic Toolbox™ User's Guide*.
- Mathworks, 2008b. *Statistics Toolbox™ User's Guide*.
- Matikainen, L., Kaartinen, H. and Hyyppä, J., 2007. Classification Tree based Building Detection from Laser Scanner and Aerial Image Data. *ISPRS Workshop on Laser Scanning 2007 and Silvilaser 2007, Espoo, Finland*: 280-287.
- Miliaresis, G. and Kokkas, N., 2007. Segmentation and Object-based Classification for the Extraction of the Building Class from LIDAR DEMs. *Computers & Geosciences*, 33(8): 1076-1087.
- Muhar, A., 2001. Three-dimensional modelling and visualisation of vegetation for landscape simulation. *Landscape and Urban Planning*, 54: 5-17.
- Nowak, D.J., Crane, D.E. and Stevens, J.C., 2006. Air Pollution Removal by Urban Trees and Shrubs in the United States. *Urban Forestry & Urban Greening*, 4(3-4): 115-123.
- Ordnance Survey, 2008. *Environmental Application of OS MasterMap®*, <http://www.ordnancesurvey.co.uk/oswebsite/products/osmastermap/Docs/D06341.pdf>.
- ParliamentaryOfficeofScienceandTechnology, 2007. *Urban Flooding. Postnote(289)*.

- Persson, A., Soderman, U., Topel, J. and Ahlberg, S., 2005. Visualization and Analysis of Full-waveform Airborne Laser Scanner Data. ISPRS WG III/3, III/4, V/3 Workshop "Laser Scanning 2005", Enschede, The Netherlands: 103-108.
- Peucker, T.K. and Chrisman, N., 1975. Cartographic Data Structures. *The American Cartographer*, 2(1): 55-69.
- Popescu, S.C., Wynne, R.H. and Nelson, R.E., 2003. Measuring Individual Tree Crown Diameter with Lidar and Assessing its Influence on Estimating Forest Volume and Biomass. *Canadian Journal of Remote Sensing*, 29(5): 564-577.
- Quest, G.S.L., 2009. 3D Datum Transformations for Great Britain and Ireland.
- Reitberger, J., Krzystek, P. and Stilla, U., 2006. Analysis of Full Waveform Lidar Data for Tree Species Classification. *Photogrammetric Computer Vision, Symposium of Commission III, ISPRS, Bonn, Germany*: unpaginated.
- Reitberger, J., Krzystek, P. and Stilla, U., 2008. Analysis of Full Waveform LIDAR Data for the Classification of Deciduous and Coniferous Trees. *International Journal of Remote Sensing*, 29(5): 1407-1431.
- RIEGL, 2007. Manual for RiAnalyze 560, LMS-Q560 Data Processing Software for Full Waveform Analysis.
- Rohrbach, A., 2007. Basics of Airborne LIDAR Sensing Technology, ISPRS Summer School on Theory and Application of Laser Scanning, Ljubljana, Slovenia.
- Rutzinger, M., Höfle, B., Hollaus, M. and Pfeifer, N., 2008. Object-based Point Cloud Analysis of Full-waveform Airborne Laser Scanning Data for Urban Vegetation Classification. *Sensors*, 8(8): 4505-4528
- Schanda, E., 1986. *Physical Fundamentals of Remote Sensing*. Springer Verlag.
- Schnadt, K. and Katzenbeisser, R., 2004. Unique Airborne Fiber Scanner Technique for Application-oriented Lidar Products. *International Archives of Photogrammetry, Remote Sensing and Spatial Information Sciences*, 36(8/W2): 19-23.
- Schreier, H., Loughheed, J., Tucker, C. and Leckie, D., 1985. Automated Measurements of Terrain Reflection and Height Variations using an Airborne Infrared Laser System. *International Journal of Remote Sensing*, 6(1): 101-113.
- Scurlock, J.M.O., Asner, G.P. and Gower, S.T., 2001. Worldwide Historical Estimates of Leaf Area Index, 1932–2000. Oak Ridge National Laboratory, Tennessee.
- Song, J.-H., Han, S.-H., Yu, K.-Y. and Kim, Y.-I., 2002. Assessing the Possibility of Land-Cover Classification Using Lidar Intensity Data. *Photogrammetric Computer Vision, ISPRS Commission III, Symposium 2002, Graz, Austria*: unpaginated.
- Spatial Resources, L., LP360: First of its Kind LIDAR Plug-in, for the ArcGIS Environment. <http://www.spatialresources.com/id78.html>(8.07.2009).
- St-Onge, B.A., 1999. Estimating Individual Tree Heights of the Boreal Forest using Airborne Laser Altimetry and Digital Videography. *ISPRS Workshop on Mapping Surface Structure and Topography by Airborne and Spaceborne Lasers, La Jolla, USA, November 1999*: unpaginated.
- Story, M. and Congalton, R.G., 1986. Accuracy Assessment: A User's Perspective. *Photogrammetric Engineering and Remote Sensing*, 52: 397–399.
- Straub, B.-M., 2003. Automatic Extraction of Trees from Aerial Images and Surface Models. *International Archives of Photogrammetry, Remote Sensing and Spatial Information Sciences*, XXXIV-3/W8: 157-164.

- Suárez, J.C., Ontiveros, C., Smith, S. and Snape, S., 2004. The use of airborne LiDAR and Aerial Photography in the estimation of individual tree heights in forestry, 7th AGILE Conference on Geographic Information Science, Heraklion, Greece.
- Thaiutsa, B., Puangchit, L., Kjellgren, R. and Arunpraparut, W., 2008. Urban Green Space, Street Tree and Heritage Large Tree Assessment in Bangkok, Thailand. *Urban Forestry & Urban Greening*, 7(3): 219-229.
- Tiede, D., Hochleitner, G. and Blaschke, T., 2005. A Full GIS-based Workflow for Tree Identification and Tree Crown Delineation using Laser Scanning. CMRT05. IAPRS, Vienna, Austria, 36-3/W/24: 9-14.
- Tiede, D. and Hoffmann, C., 2006. Process Oriented Object-based Algorithms for Single Tree Detection using Laser Scanning Data. EARSeL-Proceedings of the Workshop on 3D Remote Sensing in Forestry, Vienna: 162-167.
- Tooke, T.R.T., Coops, N.C., Goodwin, N.R. and Voogt, J.A., 2008. Extracting Urban Vegetation Characteristics using Spectral Mixture Analysis and Decision Tree Classifications. *Remote Sensing of Environment*, 113(2): 398-407.
- Toomay, J.C. and Hannen, P., 2004. *Radar Principles for the Non-Specialist*. Scitech Publishing Inc.
- Tovari, D. and Vogtle, T., 2004. Object Classification in Laser Scanning Data. Proceedings of the ISPRS working group VIII/2 on Laser-Scanners for Forest and Landscape Assessment, Freiburg, Germany: 45-49.
- Tukey, J.W., 1977. *Exploratory Data Analysis*. Addison-Wesley
- Ulaby, F.T., Moore, R.K. and Fung, A.K., 1982. *Microwave Remote Sensing, Active and Passive Vol. 2*. Artech House, Norwood, MA.
- Ullrich, A., 2006. Advantages of Echo Digitization and Subsequent Full Waveform Analysis in Laser Scanning. International LIDAR Mapping Forum 2006, Denver, Colorado.
- Van de Voorde, T., Vlaeminck, J. and Canters, F., 2008. Comparing Different Approaches for Mapping Urban Vegetation Cover from Landsat ETM+ Data: A Case Study on Brussels. *Sensors*, 8: 3880-3902.
- Vosselman, G., 2003. 3-D Reconstruction of Roads and Trees for City Modelling. *International Archives of Photogrammetry, Remote Sensing and Spatial Information Sciences*, Dresden, Germany, 34 (3/W13): 231-236.
- Vosselman, G. and Dijkman, S., 2001. 3D Building Model Reconstruction from Point Clouds and Ground Plans. *International Archives of Photogrammetry and Remote Sensing*, Annapolis, MD, 34(3/W4): 37-43.
- Wagner, W., Hollaus, M., Briese, C. and Ducic, V., 2008a. 3D Vegetation Mapping using Small-footprint Full-waveform Airborne Laser Scanners. *International Journal of Remote Sensing*, 29(5): 1433-1452.
- Wagner, W. et al., 2008b. Radiometric Calibration of Full-waveform Small-footprint Airborne Laser Scanners. *The International Archives of the Photogrammetry, Remote Sensing and Spatial Information Sciences*, XXXVII: 163-168.
- Wagner, W., Ullrich, A., Ducic, V., Melzer, T. and Studnicka, N., 2006. Gaussian Decomposition and Calibration of a Novel Small-footprint Full-waveform Digitising Airborne Laser Scanner. *ISPRS Journal of Photogrammetry and Remote Sensing*, 60: 100-112.
- Wagner, W., Ullrich, A., Melzer, T., Briese, C. and Kraus, K., 2004. From Single-pulse to Full-waveform Airborne Laser Scanners: Potential and Practical Challenges. *Geo-Imagery Bridging Continents*, XXth ISPRS Congress, Istanbul, Turkey, XXXV: unpaginated.
- Wehr, A., 2008. *LiDAR Systems and Calibration*. In: J. Shan and C.K. Toth (Editors), *Topographic Laser Ranging and Scanning: Principles and Processing*. CRC Press, Boca Raton.

- Wehr, A. and Lohr, U., 1999. Airborne Laser Scanning - An Introduction and Overview. *ISPRS Journal of Photogrammetry and Remote Sensing*, 54: 68-82.
- Weisstein, E.W., 2009. Full Width at Half Maximum. <http://mathworld.wolfram.com/FullWidthatHalfMaximum.html>, 2009(14-08).
- Wong, N.H. and Yu, C., 2005. Study of Green Areas and Urban Heat Island in a Tropical City. *Habitat International*, 29(3): 547-558.
- Woodhouse, I., 2006. *Introduction to Microwave Remote Sensing*. Taylor & Francis, New York.
- Yongwei, S., 2008. Quantifying the Size of a Lidar Footprint: A Set of Generalized Equations. *IEEE Geoscience and Remote Sensing Letters*, 5(3): 419-422.
- Zhao, K. and Popescu, S., 2007. Hierarchical Watershed Segmentation of Canopy Height Model for Multi-Scale Forest Inventory. *ISPRS Workshop on Laser Scanning 2007 and SilviLaser 2007*, Espoo, Finland: 436-441.
- Zhou, W. and Troy, A., 2008. An Object-oriented Approach for Analysing and Characterizing Urban Landscape at the Parcel Level. *International Journal of Remote Sensing*, 29(11): 3119 - 3135.